Abstract

LI, ZHENGMIN. Phase Behavior in Model Homopolymer/CO_2 and Surfactant/CO_2 Systems: Discontinuous Molecular Dynamics Simulations. (Under the direction of Carol K. Hall)

Discontinuous molecular dynamics simulation is used to explore phase behavior in homopolymer (P_n)/solvent and surfactant (H_mT_n)/solvent systems. This research provides insight into how homopolymer and surfactant geometry and intermolecular forces affect performance in supercritical CO_2 ($scCO_2$).

We first simulate surfactant/$scCO_2$ systems and explore the effect of the surfactant volume fraction, packing fraction and temperature on the phase behavior. We find a two-phase region, a micelle phase and a unimer phase with increasing packing fraction at fixed temperature or with increasing temperature at fixed packing fraction. The phase diagram for the surfactant/$scCO_2$ system in the surfactant volume fraction$-$packing fraction plane and the density dependence of the critical micelle concentration (CMC) are in qualitative agreement with experimental observations. Then we explore how the segment-segment, segment-solvent and solvent-solvent interaction parameters affect the types of phase behavior in homopolymer/$scCO_2$ systems. Increasing the packing fraction of homopolymers in both hard-sphere solvents and square-well solvents serves to increase the solvent's ability to dissolve homopolymers only when the segment-solvent interaction strength exceeds a critical value. For homopolymer/$scCO_2$ systems, we find that it is necessary to account for the solvent-solvent attraction to model lower critical solution temperature (LCST) behavior. Finally we explore how the head-head, head-solvent, tail-tail and tail-solvent interaction strengths affect phase behavior and micellization in surfactant/$scCO_2$ systems. We find that it is necessary to account for the interactions experienced by both the

head and tail blocks in order to capture the essential features of real surfactant/scCO$_2$ systems. The CMC increases with increasing packing fraction only when the head-solvent interaction strength exceeds a critical value. At strong head-solvent interaction strengths, the micelle $\rightarrow$ unimer transition occurs within the two-phase region. In that case we find a transition from a two-phase region with micelles in the polymer-rich phase to a two-phase region with unimers in the polymer-rich phase at low packing fraction, and a transition to a one-phase region with unimers at higher packing fraction. This is unexpected and is not observed experimentally.

Next we explore the physical conditions and parameters that give rise to the appearance of LCST behavior in homopolymer/supercritical solvent systems. In hard-sphere solvents, homopolymers always exhibit upper critical solution temperature (UCST) behavior for both solvent-phobic and solvent-philic homopolymers. The packing fraction and pressure required to dissolve homopolymers increase as homopolymer chain length increases. In square-well solvents, LCST behavior is observed at high solvent-solvent interaction strengths ($|\epsilon^*_{\rm SS}|$) but not at low ones. This indicates that the strong solvent-solvent attractions contribute to the appearance of LCST behavior in homopolymer/solvent systems. As $|\epsilon^*_{\rm SS}|$ increases, the packing fraction required to dissolve homopolymers increases while the pressure required to dissolve homopolymers decreases. Homopolymers exhibit LCST behavior at lower $|\epsilon^*_{\rm SS}|$ with increasing solvent-solvent interaction width, indicating that the solvent-solvent interaction range plays an important role in the appearance of LCST behavior in square-well solvents. Finally we find that by increasing the chain length for solvent-philic homopolymers, one can switch from UCST to LCST behavior in square-well solvents.

Phase Behavior in Model Homopolymer/CO_2 and Surfactant/CO_2 Systems: Discontinuous Molecular Dynamics Simulations

by

Zhengmin Li

A dissertation submitted to the Graduate Faculty
of North Carolina State University
in partial fulfillment of the
requirements for the Degree of
Doctor of Philosophy

Chemical Engineering

Raleigh, NC 27695

2004

APPROVED BY:

Carol K. Hall Chair of Advisory Committee	Keith E. Gubbins
Peter K. Kilpatrick	John H. van Zanten

Biography

The author was born in Leping, Jiangxi Province, P. R. China. She is the second daughter of Yiwen and Yueying Li and has one elder sister, Zhenggang, one younger sister, Guohong, and one younger brother, Zhengwei. In July, 1993, she received a B.S. degree in Chemical Engineering from Tianjin University in Tianjin, P. R. China. In July, 1999, she received an M.S. degree in Chemical Engineering from Tsinghua University in Beijing, P. R. China. On December 17, 1997, she married Jian Xu of Leping, Jiangxi Province, P. R. China. In August, 1999, she was admitted to North Carolina State University to pursue graduate studies in Chemical Engineering. In January, 2003, she received an M.S. degree in Chemical Engineering from North Carolina State University.

Acknowledgments

It is my pleasure to acknowledge the people who have contributed to the preparation of this thesis by supporting and encouraging me.

First, I would like to thank my advisor, Professor Carol Hall, for her guidance and patience in both academic and personal matters. Professor Hall is devoted to advising her graduate students and I am grateful to be one of them.

I thank the Science and Technology Center program of the National Science Foundation for funding under agreement No. CHE-9876674. Acknowledgment is made to the Office of Energy Research, Basic Sciences, Chemical Science Division of the U. S. Department of Energy for partial support of this work.

To the members of the Hall research group, past and present, I thank you for your friendship and encouragement. I would like to thank Brian Attwood, Andrew Schultz, Aysa Akad, Arthi Jayaraman and Alex Marchut for keeping the computers running smoothly. I feel especially indebted to Andrew Schultz as he has spent so much time discussing my research and explaining the simulation techniques.

To my family, especially my parents, I thank you for the love and encouragement that have sustained me during my study abroad. Even though my father was no longer living during this time, I felt his presence in my heart. Finally I thank my husband, Jian, for supporting me and making me happy in the past years. His love and encouragement have contributed immeasurably to this work.

Table of Contents

List of Tables

List of Figures

Page

CHAPTER 1

INTRODUCTION

Supercritical fluids (SCFs), especially supercritical carbon dioxide (scCO_2), are attractive alternatives to the organic solvents used for polymer manufacturing and processing. The structure, properties and phase behavior of SCFs are different from those in both gas and liquid states. Practical applications involving SCFs include polymer fractionation, impregnation and purification; polymer extrusion and foaming; dispersion and emulsion polymerization; and the formation of microemulsions and emulsions.

Supercritical CO_2 has received a great deal of scientific and industrial attention as a potential alternative to organic solvents because it is environmentally benign[1] and the temperature and pressure ranges for its operation are easily accessible ($T_c = 31^oC$, $P_c = 73.8$ bar). An additional attractive feature of scCO_2 as a solvent is that solute solubility can be controlled by varying pressure as well as temperature due to scCO_2's high compressibility. It is important to find atternatives to organic solvents since more than 30 billion pounds of organic and halogenated solvents are used worldwide each year, contaminating our enviroment.

Liquid and supercritical CO_2 are effective solvents for dissolving non-polar and slightly polar organic compounds. Unfortunately scCO_2 is a poor solvent for nonvolatile polar molecules and polymers due to its dipole moment of zero and weak van der Waals interactions[2]. The only

polymers that readily dissolve in $scCO_2$ are fluorinated or silicon-based.[3–8] This makes it necessary to use surfactants to assist in the solvation process. However, most commercial surfactants are designed and used in water/oil systems thus new surfactants are needed for water/$scCO_2$ or oil/$scCO_2$ systems. In order to design new surfactants for $scCO_2$-based technologies, it would be good to have a better understanding of the behavior of surfactants in compressible solvents. Through modeling and simulations of the phase behavior in surfactant/$scCO_2$ systems, we should be able to obtain enough insight into how intermolecular forces and geometry affect the performance of surfactants in $scCO_2$ to provide a useful set of guidelines for the design of new surfactants for specific applications in $scCO_2$.

Polymer/SCF systems are often characterized by LCST (lower critical solution temperature) behavior[9,10], that is they become miscible with decreasing temperature, as opposed to UCST (upper critical solution temperature) behavior, where they become miscible with increasing temperature. Examples of polymer/SCF systems that exhibit LCST behavior include polyethylene in n-pentane, polystyrene in various solvents and poly(vinyl acetate) in CO_2[11–13]. Miscibility of polymers in solvents can be affected by the temperature, pressure, polymer concentration, molecular weight and molecular weight distribution, the polymer type and the nature of the solvent under consideration. Unexpected phenomena can occur even with small changes in temperature, pressure or composition. By improving our insight into the phase behavior of SCF systems, we can avoid undesired phase behavior in SCF applications and develop novel SCF-based techniques.

1.1 Overview

This thesis describes our research into the phase behavior of homopolymer/solvent and surfactant/solvent systems via molecular simulation. In this section, we summarize the remaining chapters of this thesis. All chapters contain their own literature review and bibliography.

Chapter 2 describes parametric studies of the effect of varying the different interaction strengths on phase behavior in homopolymer/CO_2 and surfactant/CO_2 systems. We conduct simulations on systems modeled as a mixture of single-sphere solvent molecules and freely-jointed square-well chains composed of spheres. We first simulate homopolymer/scCO_2 systems of chain length n = 4, 8, 12 and 24 at various values of the segment-segment and segment-solvent interaction strengths. The interaction between solvent molecules is modeled using both a hard-sphere potential and a square-well potential in order to learn how the solvent-solvent interaction parameters affect the phase behavior, especially UCST versus LCST behavior. We then perform simulations on surfactant (H_4T_8)/scCO_2 systems and explore the effect of variations in the head-head, head-solvent, tail-tail and tail-solvent interaction strengths on the phase behavior and the micellization behavior. For homopolymers, it is necessary to account for the solvent-solvent attraction to model LCST behavior in scCO_2. We find that increasing the packing fraction of homopolymers in both hard-sphere solvents and in square-well solvents serves to increase the solvent's ability to dissolve homopolymers only when the segment-solvent interaction strength exceeds a critical value. For surfactants, it is necessary to account for the interactions experienced by both the head and tail blocks in order to capture the essential features of real surfactant/scCO_2 systems. In surfactant/scCO_2 systems, the critical micelle concentration (CMC) increases with increasing packing fraction only when the head-solvent interaction strength exceeds a critical

value. At strong head-solvent interaction strengths, the micelle $\rightarrow$ unimer transition occurs within the two-phase region. In that case we find a transition from a two-phase region with micelles in the polymer-rich phase to a two-phase region with unimers in the polymer-rich phase at low packing fraction, and a transition to a one-phase region with unimers at higher packing fraction. This is unexpected and is not observed experimentally.

Chapter 3 describes our investigation of the physical conditions and interaction parameters necessary to observe LCST behavior in homopolymer/solvent systems. We first simulate homopolymer/solvent systems with chain lengths $n = 8 - 24$ at various segment-segment ($|\epsilon^*_{\rm PP}|$) and segment-solvent ($|\epsilon^*_{\rm PS}|$) interaction strengths in hard-sphere solvents. Then we repeat the simulations at the same values of $|\epsilon^*_{\rm PP}|$ and $|\epsilon^*_{\rm PS}|$ but in square-well solvents at solvent-solvent interaction strengths ranging from $|\epsilon^*_{\rm SS}| = 0.1$ to $|\epsilon^*_{\rm SS}| = 0.5$ and interaction widths $\lambda = 0.75$ and 1.0. Both hard-sphere and square-well solvent-solvent potentials are considered in order to learn the influence of the solvent-solvent interactions on the appearance of UCST versus LCST behavior. We find that homopolymers always exhibit UCST behavior in hard-sphere solvents for both solvent-phobic and solvent-philic homopolymers at all chain lengths examined. In hard-sphere solvents, solvent-phobic homopolymers dissolve at high temperatures and high pressures only, but solvent-philic homopolymers can dissolve at low temperatures and low pressures. The solubility of solvent-phobic homopolymers is more strongly dependent on temperature than that of solvent-philic homopolymers. Strong solvent-solvent attractions promote the appearance of LCST behavior in homopolymer/solvent systems. As $|\epsilon^*_{\rm SS}|$ increases in square-well solvents, the packing fraction required to dissolve homopolymers increases while the pressure required to dissolve homopolymers decreases. Homopolymers exhibit LCST behavior at lower $|\epsilon^*_{\rm SS}|$ when

the solvent-solvent interaction width is increased, indicating that the solvent-solvent interaction range plays an important role in the appearance of LCST behavior. Finally we find that by increasing the chain length for solvent-philic homopolymers, one can switch from UCST to LCST behavior in square-well solvents.

For completeness, an earlier study on phase behavior in model homopolymer/CO_2 and surfactant/CO_2 systems has been included in Appendix A. This work was defended as part of my Master of Science research in January, 2003. In that research, we first simulate homopolymer/scCO_2 systems to establish the appropriate interaction parameters for a surfactant/scCO_2 system. Next we simulate surfactant/scCO_2 systems and explore the effect of the surfactant volume fraction, packing fraction and temperature on the phase behavior. Finally we investigate the influence of the variation in the surfactant head and tail chain length on the location of the two-phase $\rightarrow$ one-phase transition and the micelle $\rightarrow$ unimer transition. We find a two-phase region, a micelle phase and a unimer phase with increasing packing fraction at fixed temperature or with increasing temperature at fixed packing fraction. The phase diagram for the surfactant/scCO_2 system in the surfactant volume fraction$-$packing fraction plane and the density dependence of the CMC are in qualitative agreement with experimental observations[14].

Chapters 2 and 3 and Appendix A have been adapted from the following publications:

Chapter 2 Z. Li and C. K. Hall, "Parametric Studies of Interaction Strengths on Homopolymer/CO_2 and Surfactant/CO_2 Systems: Discontinuous Molecular Dynamics Simulations," (in preparation).

Chapter 3 Z. Li and C. K. Hall, "LCST/UCST Phase Behavior in Polymer/Supercritical Solvent Mixture: Discontinuous Molecular Dynamics Simulations," (in preparation).

Appendix A Z. Li and C. K. Hall, ”Phase Behavior in Model Homopolymer/CO_2 and Surfactant/CO_2 Systems: Discontinuous Molecular Dynamics Simulations,” Langmuir (accepted).

1.2 References

[1] C. A. Eckert, B. L. Knutson, and P. G. Debenedetti, "Supercritical fluids as solvents for chemical and materials processing," *Nature* **383**, 313 (1996).

[2] M. L. O'Neill, Q. Cao, M. Fang, and K. P. Johnston, "Solubility of homopolymers and copolymers in carbon dioxide," *Ind. Eng. Chem. Res.* **37**, 3067 (1998).

[3] M. K. McHugh and V. J. Krukonis, *Supercritical fluid extraction: principles and practice.* (Butterworth-Heinemann, Boston, MA, 1994).

[4] T. Hoefling, D. Stofesky, M. Reid, E. Beckman, and R. M. Enick, "The incorporation of a fluorinated ether functionalty into a polymer or surfactant to enhance CO_2-solubility," *J. Supercrit. Fluids* **5**, 237 (1992).

[5] J. M. Desimone, Z. Guan, and C. S. Elsbernd, "Synthesis of fluoropolymers in supercritical carbon-dioxide," *Science* **257**, 945 (1992).

[6] T. A. Hoefling, D. A. Newman, R. M. Enick, and E. J. Beckman, "Effect of structure on the cloud-point curves of silicone-based amphiphilies in supercritical carbon-dioxide," *J. Supercrit. Fluids* **6**, 165 (1993).

[7] Y. L. Hsiao, E. E. Maury, J. M. DeSimone, S. Mawson, and K. P. Johnston, "Dispersion polymerization of methyl-methacrylate stablized with poly(1,1-dihydroperfluorooctyl acrylate) in supercritical carbon-dioxide," *Macromolecules* **28**, 8159 (1995).

[8] Y. Xiong and E. Kiran, "Miscibility, density and viscosity of poly(dimethylsiloxane) in supercritical carbon-dioxide," *Polymer* **36**, 4817 (1995).

[9] M. A. Meilchen, B. M. Hasch, and M. A. Mchugh, "Effect of copolymer composition on the phase-behavior of mixtures of poly(ethylene-co-methyl acrylate) with propane and chlorodifluoromethane," *Macromolecules* **24**, 4974 (1991).

[10] S. Mawson, K. P. Johnston, J. R. Combes, and J. M. DeSimone, "Formation of poly(1,1,2,2-tetrahydroperfluorodecyl acrylate) submicron fibers and particles from supercritical carbon-dioxide solutions," *Macromolecules* **28**, 3182 (1995).

[11] S. J. Chen, I. G. Economou, and M. Radosz, "Density-tuned polyolefin phase equilibria. 2. Multicomponent solutions of alternating poly(ethylene-propylene) in subcritical and super-critical olefins. Experiment and SAFT model," *Macromolecules* **25**, 4987 (1992).

[12] A. C. Bae, S. M. Lambert, D. S. Soane, and J. M. Prausnitz, "Cloud-point curves of polymer-solutions from thermooptic measurements," *Macromolecules* **24**, 4403 (1991).

[13] F. Rindfleisch, T. P. DiNoia, and M. A. McHugh, "Solubility of polymers and copolymers in supercritical CO_2," *J. Phys. Chem.* **100**, 15581 (1996).

[14] E. Buhler, A. V. Dobrynin, J. M. DeSimone, and M. Rubinstein, "Light-scattering study of diblock copolymers in supercritical carbon dioxide: CO_2 density-induced micellization transition," *Macromolecules* **31**, 7347 (1998).

CHAPTER 2

PARAMETRIC STUDIES OF INTERACTION STRENGTHS ON POLYMER/CO_2 SYSTEMS: DISCONTINUOUS MOLECULAR DYNAMICS SIMULATIONS

2.1 Introduction

Supercritical CO_2 ($scCO_2$) is an attractive alternative for organic solvents in part because its solvation strength can be tuned by varying the density of the fluid phase. The addition of surfactants to $scCO_2$ has further enhanced its utility, allowing it to serve efficiently as a media for reactions, separations, and the synthesis of new materials. We have been engaged in a computational study aimed at gaining enough insight into how surfactant intermolecular forces and geometry affect the performance of surfactants in $scCO_2$ to provide a useful set of guidelines for the design of new surfactants for specific applications.

In a previous study[1] we performed discontinuous molecular dynamics simulations on surfactant (H_mT_n)/solvent systems modeled as a mixture of single-sphere solvent molecules and freely-jointed surfactant chains composed of m slightly solvent-philic head spheres (H) and n solvent-philic tail spheres (T), all of the same size. A square-well potential ac-

counted for the head-head, head-solvent, tail-tail and tail-solvent interactions and a hard-sphere potential accounted for the head-tail and solvent-solvent interactions. We first simulated homopolymer/scCO$_2$ systems to establish the appropriate interaction parameters for the surfactant/scCO$_2$ system. Next we simulated surfactant/scCO$_2$ systems and explored the effect of the surfactant volume fraction, packing fraction, temperature and surfactant architecture on the phase behavior. We found a two-phase region, a micelle phase and a unimer phase with increasing packing fraction at fixed temperature or with increasing temperature at fixed packing fraction. The phase diagram for the surfactant/scCO$_2$ system in the surfactant volume fraction$-$packing fraction plane and the density dependence of the critical micelle concentration (CMC) were in qualitative agreement with experimental observations[2] and the simulations by Scanu et al[3].

The study described above was limited in that we considered only one set of interaction parameters for the head-head, head-solvent, tail-tail and tail-solvent interactions and the solvent-solvent interaction was taken to be a hard-sphere potential. Our motivation for using a hard-sphere potential was to see whether such a simplified model would be able to represent polymer/scCO$_2$ systems and to take advantage of the computational efficiency afforded by using the hard-sphere potential. In addition the interaction between CO$_2$ molecules is relatively weak (quadrupolar) compared to other interactions in the polymer/scCO$_2$ systems, so the neglect of the solvent-solvent attraction compared to other interactions was not unreasonable. One weakness of our model for homopolymer/scCO$_2$ systems was that we observed only upper critical solution temperature (UCST) behavior for the homopolymers examined while many substances exhibit lower critical solution (LCST) temperature behavior in scCO$_2$.[4] We attributed this to our treatment of CO$_2$ molecules as hard-sphere molecules.

In this paper we explore how the values of the interaction parameters affect the types of phase behavior and micellization behavior observed. We first simulate homopolymer (P_n)/scCO$_2$ systems of chain length n = 4, 8, 12 and 24 at various values of the segment-segment and segment-solvent interaction strengths. The interaction between solvent molecules is modeled using both a hard-sphere potential and a square-well potential in order to learn how the solvent-solvent interaction parameters affect phase behavior, especially UCST/LCST behavior. We then perform simulations on surfactant (H_4T_8)/scCO$_2$ systems and explore the effect of variations in the head-head, head-solvent, tail-tail and tail-solvent interaction strengths on phase behavior.

The influence of the various factors that determine the solubility of homopolymers and surfactants in scCO$_2$ has been the subject of numerous investigations. Researchers have investigated the various interactions in the polymer/scCO$_2$ systems via experiments[5–8] and computer simulations[9–12], with special focus on the interactions between polymer molecules and CO$_2$ molecules.

Highlights of this paper are the following. Increasing the packing fraction serves to increase the solvent's ability to dissolve homopolymers in both hard-sphere solvents and square-well solvents but only when the segment-solvent interaction strength exceeds a critical value. Although only UCST behavior is observed for homopolymers in hard-sphere solvents, both UCST and LCST behavior are observed for homopolymers in square-well solvents, depending upon the interaction strengths and chain length. This indicates that it is necessary to account for the solvent-solvent attraction to observe LCST behavior in scCO$_2$. Our simulation results on surfactant/solvent systems with square-well potentials acounting for the head-head, head-solvent, tail-tail and tail-solvent interactions agree with experimental observations[2] qualitatively; in con-

trast our simulation results on surfactant/solvent systems with a square-well potential accounting solely for the head-head interaction disagree with experimental observations[2]. This indicates that it is necessary to model the interactions experienced by both the head and the tail blocks in order to capture the essential features of real surfactant/scCO_2 systems. In surfactant/solvent systems the CMC increases with increasing packing fraction only when the head-solvent interaction strength exceeds a critical value. At strong head-solvent interaction strengths, the micelle $\rightarrow$ unimer transition occurs within the two-phase region. In that case we find a transition from a two-phase region with micelles in the polymer-rich phase to a two-phase region with unimers in the polymer-rich phase at low packing fraction, and a transition to a one-phase region with unimers at higher packing fraction. This is unexpected and is not observed experimentally. The tail-solvent interaction strength impacts the packing fraction of the unimer $\rightarrow$ micelle transition more strongly at low η than at high η. The head-solvent interaction strength affects the packing fraction of the micelle $\rightarrow$ unimer transition strongly but the packing fraction of the two-phase $\rightarrow$ one-phase transition only slightly; the tail-tail interaction strength affects the packing fraction of the two-phase $\rightarrow$ one-phase transition strongly but the packing fraction of the micelle $\rightarrow$ unimer transition only slightly.

2.2 Molecular Models and Simulation Methods

For the homopolymer/solvent and surfactant/solvent systems, the solvent is modeled as a single sphere. The homopolymer (P_n) and surfactant (H_mT_n) molecules are modeled respectively as a freely-jointed chain composed of n polymer spheres (P), and as a freely-jointed chain composed of m slightly solvent-philic head spheres (H) and n solvent-philic tail spheres (T).

All spheres are of the same size. The segment-segment and segment-solvent interactions are modeled using square-well potentials. Solvent-solvent interactions in the homopolymer/solvent systems are modeled in two ways: (1) as a hard-sphere potential as was the case in our previous study[1], and (2) as a square-well potential. The latter has the advantage that it is more realistic and allows us to investigate how the solvent-solvent interactions influence the types of phase behavior observed − LCST versus UCST behavior. For the surfactant/solvent systems, the head-head, head-solvent, tail-tail and tail-solvent interactions are modeled using square-well potentials. A hard-sphere potential is used for the head-tail interactions since the miscibility of real polymers comprised of the surfactant head segments and surfactant tail segments is generally low. Solvent-solvent interactions in the surfactant/solvent systems are modeled as a hard-sphere potential as was the case in our previous study[1].

The variables in our simulations are defined as the following. The homopolymer P_n volume fraction is defined to be $\phi_{\mathrm{P}_n} \equiv nN_{\mathrm{P}_n}/(nN_{\mathrm{P}_n} + N_{\mathrm{CO}_2})$ and the surfactant $\mathrm{H}_m\mathrm{T}_n$ volume fraction is defined to be $\phi_{\mathrm{H}_m\mathrm{T}_n} \equiv (m+n)N_{\mathrm{H}_m\mathrm{T}_n}/[(m+n)N_{\mathrm{H}_m\mathrm{T}_n} + N_{\mathrm{CO}_2}]$, where N_i is the number of molecules of species i. The homopolymer P_n mole fraction is defined to be $X_{\mathrm{P}_n} \equiv N_{\mathrm{P}_n}/(N_{\mathrm{P}_n} + N_{\mathrm{CO}_2})$ and the surfactant $\mathrm{H}_m\mathrm{T}_n$ mole fraction is defined to be $X_{\mathrm{H}_m\mathrm{T}_n} \equiv N_{\mathrm{H}_m\mathrm{T}_n}/(N_{\mathrm{H}_m\mathrm{T}_n} + N_{\mathrm{CO}_2})$. The system packing fraction is defined to be $\eta \equiv \pi N_{\mathrm{b}}\sigma^3/6V$, where V is the box volume and N_{b} is the number of beads in the system. In this paper, $|\epsilon_{\mathrm{PP}}|$ and $|\epsilon_{\mathrm{PS}}|$ are the segment-segment and segment-solvent interaction strengths in homopolymer/scCO$_2$ system and $|\epsilon_{\mathrm{HH}}|$, $|\epsilon_{\mathrm{HS}}|$, $|\epsilon_{\mathrm{TT}}|$ and $|\epsilon_{\mathrm{TS}}|$ are the head-head, head-solvent, tail-tail and tail-solvent interaction strengths in surfactant/scCO$_2$ systems. We choose a reference interaction strength $|\epsilon^*|$ and refer to reduced parameters for the interaction strengths as $|\epsilon^*_{\mathrm{PP}}|$ =

$|\epsilon_{\rm PP}|/|\epsilon^*|$, $|\epsilon^*_{\rm PS}|$ = $|\epsilon_{\rm PS}|/|\epsilon^*|$, $|\epsilon^*_{\rm HH}|$ = $|\epsilon_{\rm HH}|/|\epsilon^*|$, $|\epsilon^*_{\rm HS}|$ = $|\epsilon_{\rm HS}|/|\epsilon^*|$, $|\epsilon^*_{\rm TT}|$ = $|\epsilon_{\rm TT}|/|\epsilon^*|$ and $|\epsilon^*_{\rm TS}|$ = $|\epsilon_{\rm TS}|/|\epsilon^*|$. The reduced temperature is defined to be $T^* \equiv {\rm k_B T}/|\epsilon^*|$, where $\rm k_B$ is Boltzmann's constant, T is the temperature.

We limit our study to packing fractions η between 0.2 and 0.5 so as to keep the solvent packing fraction greater than the critical packing fraction for a square-well fluid of width $\lambda = 0.75$ ($\eta_{\rm c} \approx 0.126$) and less than the packing fraction at which a hard-sphere fluid would undergo a transition to a solid phase. This serves to limit our study to model CO_2 densities that are in the supercritical or liquid regime.[1] Since solvent, homopolymer segments and surfactant segments all have the same diameter in our model, the solvent reduced density in our simulations can be simply calculated from ${\rho_{\rm CO_2}}^* = \phi_{\rm CO_2}\rho^*$, where $\rho^* \equiv N_{\rm b}\sigma^3/V = 6\eta/\pi$ is the overall reduced density, and $\phi_{\rm CO_2}$, the solvent volume fraction, is obtained from $\phi_{\rm CO_2} = 1 - \phi_{\rm P_{\it n}}$ for homopolymer ($\rm P_{\it n}$)/solvent systems or $\phi_{\rm CO_2} = 1 - \phi_{\rm H_{\it m}T_{\it n}}$ for surfactant ($\rm H_{\it m}T_{\it n}$)/solvent systems.

We choose the following interaction parameters for the homopolymer/solvent and surfactant/solvent systems. For the square-well solvent-solvent interactions in homopolymer/solvent systems, the square-well depth, $|\epsilon^*_{\rm SS}|$, is 0.15 and the square-well widths, $\lambda_{\rm SS}$, are 0.75 or 1.0. These parameters are a reasonable choice since the interactions between CO_2 molecules are relatively weak (quadrapolar) compared to other interactions in the system. For the segment-segment and segment-solvent interactions in homopolymer/solvent systems and the head-head, head-solvent, tail-tail and tail-solvent interactions in surfactant/solvent systems, the square-well depths, $|\epsilon^*_{\rm PP}|$, $|\epsilon^*_{\rm PS}|$, $|\epsilon^*_{\rm HH}|$, $|\epsilon^*_{\rm HS}|$, $|\epsilon^*_{\rm TT}|$ and $|\epsilon^*_{\rm TS}|$, are varied between 0 and 2.0, in order to investigate their influence on the phase behavior; the square-well widths, $\lambda_{\rm PP}$, $\lambda_{\rm PS}$, $\lambda_{\rm HH}$, $\lambda_{\rm HS}$,

λ_{TT} and λ_{TS}, are 0.75. We also limit our study on the phase behavior in square-well solvents to reduced temperatures, T^*, between 0.95 and 1.05 so as to keep the temperature above the critical reduced temperature for a square-well fluid of width $\lambda = 1.0$ ($T_{\mathrm{c}}^* \approx 0.9$) but not so high as to become gas-like. This serves to limit our study to CO_2 temperatures that are in the supercritical regime.

In a discontinuous molecular dynamics (DMD) simulation, particles collide when they arrive at a discontinuity in the potential, i.e. the hard-sphere diameter or the square-well width. Between collisions, particles move with linear trajectories, making DMD simulations much faster than traditional molecular dynamics simulations with continuous potentials which require a small integration time step. The post-collision velocities of particles in DMD are found by solving the collision dynamics equations analytically. To simulate chains of spheres effectively, Rapaport introduced bonds between spheres by limiting the distance between adjacent beads to be between σ and $\sigma(1+\delta)$, where δ is the bond extension parameter.[13] Later Bellemans modified this model so that the distance between adjacent spheres must lie between $\sigma(1-\delta/2)$ and $\sigma(1+\delta/2)$ which makes the average bond length equal to σ.[14] The value of δ in our simulations is 0.3.

Since we are interested in simulating at constant temperature, we use discontinuous canonical molecular dynamics (DCMD),[15–18] an adaptation of the standard microcanonical ensemble DMD technique. The DCMD technique is based on Anderson's stochastic collision method[16] and involves stochastic interaction of the system particles with imaginary constant-temperature heat bath particles. We assume that the system is immersed in a constant-temperature heat bath containing imaginary "ghost" particles. The ghost particles stabilize the system temperature by colliding with the system particles, resulting in the reassignment of particle velocities accord-

ing to a Maxwell-Boltzmann distribution about the required temperature. Details of the DCMD method have been described by Gulati et al.[15] and by Zhou et al.[18]

Our DMD code was originally developed by Smith and coworkers[19] to treat entangled polymer melts. More recently, it was extended by Schultz et al.[20] to the treatment of any mixture of monomers, polymers, and/or copolymers and optimized to allow for the efficient simulation of large multicomponent systems.

The reduced pressure, P^*, in our simulations is calculated using the virial theorem

$$P^* \equiv \frac{P\sigma^3}{\mathrm{k_B}T} = \frac{N_\mathrm{b}\sigma^3}{V} - \frac{\sigma^3 m \sum_{\mathrm{coll}} \vec{r}_{ij}\Delta\vec{v}_j}{3V\mathrm{k_B}Tt} \tag{2.1}$$

where $\mathrm{k_B}$ is Boltzmann's constant, T is the temperature, N_b is the number of beads, V is the volume, m is the mass of each segment, $\vec{r}_{ij}$ is the distance between colliding particles i and j, $\Delta\vec{v}_j = -\Delta\vec{v}_i$ is the velocity change for the particle j, $\sum_{\mathrm{coll}}$ refers to a sum over all collisions, and t is the elapsed simulation time.

Several different types of transitions occur in the homopolymer/solvent and surfactant/solvent systems considered here. As the packing fraction or temperature increases, a two-phase $\rightarrow$ one-phase transition occurs as a phase-separated homopolymer/solvent or surfactant/solvent system turns into a one-phase system. In the one-phase region for the homopolymer/solvent system, the chains are evenly distributed throughout the solvent either as homopolymer aggregates or as unimers. In the one-phase region for the surfactant/solvent system, the chains are evenly distributed throughout the solvent. If the surfactant/solvent system two-phase $\rightarrow$ one-phase transition results in the formation of micelles, then an additional transition, the micelle $\rightarrow$ unimer transition, can occur in which the micelles turn into unimers as the pack-

ing fraction or temperature increases. The surfactant chains are distributed evenly as unimers throughout the solvent in the unimer phase. The phase transitions in the homopolymer/solvent and surfactant/solvent systems are located using the procedure described in our previous paper[1]. The two-phase $\rightarrow$ one-phase transition is located using snapshots of the configuration of an equilibrated system and the calculated contrast structure factor. The calculated aggregate size distribution is used to locate the micelle $\rightarrow$ unimer transition in the surfactant/solvent systems.

Discontinuous molecular dynamics simulations are performed in the canonical ensemble (constant N, V, T) on the homopolymer/solvent or surfactant/solvent systems. In order to investigate phase separation it is necessary to consider large systems. In the interests of computational efficiency, we begin by equilibrating a small system with a random initial configuration and then enlarge the now-equilibrated small system to re-equilibrate. The small system contains 2000 solvent molecules and $18 - 54$ chains at the desired packing fraction, reduced temperature and polymer volume fraction. We first run the simulation for $20-30$ minutes (CPU time) to calculate the initial aggregate or micelle size distribution; we then continue running the simulation and re-calculating the size distribution several times. Once the system is equilibrated, as indicated by a lack of variation in the peak positions of the aggregate or micelle size distribution, the simulation box is replicated two times in every direction yielding 16000 solvent molecules and $144 - 432$ chains. The simulation is then continued on the large system until equilibrium is reached, as indicated by a lack of variation in the peak position for the contrast structure factor and in the aggregate or micelle size distribution. The size distribution and the contrast structure factor calculated for the large system are used to determine the phase transitions. (The small system size distribution only serves to indicate whether the small system is equilibrated.) Finally, to ensure

that the system size does not influence the nature of the location of the various phase transtions, we double the size of the large system and run simulations. We find that the location of the phase transition stays the same even when the size of the large system is doubled, indicating that the large system is big enough for the calculation of phase transitions.

The average CPU time needed on our 600 MHz Alpha 21164 for each state point is 2h for equilibration of the small systems, and 30h for equilibration of the large systems. At the end of this process, a snapshot of the large system displaying the distribution of chains in the solvent is taken, and the contrast structure factor or aggregate size distribution is calculated to determine which phase the system was in. Phase transitions are assumed to be located at the mid-point between two different phases and are determined as a function of homopolymer or surfactant volume fraction or mole fraction, system packing fraction and reduced temperature. The error bars in these calculations are based on the closest state points in the two different regions. In this paper, the error bars are shown in the figures unless they are smaller than the symbols.

2.3 Results and Discussion

2.3.1 Homopolymer

A. Hard-sphere Solvent

In this section we describe our results for homopolymer/solvent systems in which the solvent-solvent interaction is modeled as a hard-sphere potential. We investigate the dependence of the phase transition on the segment-segment interaction strength $|\epsilon^*_{\rm PP}|$ and the segment-solvent interaction strength $|\epsilon^*_{\rm PS}|$ to learn how this is affected by the value of the packing fraction, η. Fi-

nally we explore the temperature dependence of the phase transition for homopolymers with different interaction parameters and chain lengths.

To investigate the influence of interaction parameters on the phase behavior of homopolymer/solvent systems, we locate the one-phase $\rightarrow$ two-phase transition at various values of $|\epsilon^*_{\mathrm{PP}}|$ and $|\epsilon^*_{\mathrm{PS}}|$. Figure 2.1 displays the location of the one-phase $\rightarrow$ two-phase transition for homopolymers (a) P_4 and (b) P_8 in the space spanned by the segment-segment interaction strength ($|\epsilon^*_{\mathrm{PP}}|$) and segment-solvent interaction strength ($|\epsilon^*_{\mathrm{PS}}|$) at $\phi_{\mathrm{P}} = 0.178$, $\eta = 0.2$ and 0.4, and $T^* = 1.0$. For both P_4 and P_8 we see the following. At low packing fraction ($\eta = 0.2$) we find a one-phase $\rightarrow$ two-phase transition as $|\epsilon^*_{\mathrm{PP}}|$ increases for all $|\epsilon^*_{\mathrm{PS}}|$ values considered. We also find a two-phase $\rightarrow$ one-phase transition as $|\epsilon^*_{\mathrm{PS}}|$ increases at low values ($|\epsilon^*_{\mathrm{PS}}| < 0.5$) and a one-phase $\rightarrow$ two-phase transition as $|\epsilon^*_{\mathrm{PS}}|$ increases at high values ($|\epsilon^*_{\mathrm{PS}}| > 0.5$). The precipitation of homopolymers as $|\epsilon^*_{\mathrm{PP}}|$ increases is expected because homopolymers with strong segment-segment attractions are more likely to attract other polymer molecules than to attract solvent molecules. The occurence of two different transitions as $|\epsilon^*_{\mathrm{PS}}|$ increases at fixed $|\epsilon^*_{\mathrm{PP}}|$ is unexpected; it can be explained in the following fashion. As $|\epsilon^*_{\mathrm{PS}}|$ increases at low values ($|\epsilon^*_{\mathrm{PS}}| < 0.5$), homopolymers with stronger segment-solvent attractions become more likely to attract solvent molecules, increasing the miscibility of the polymer and solvent molecules and causing a two-phase $\rightarrow$ one-phase transition to occur. As $|\epsilon^*_{\mathrm{PS}}|$ increases at high values ($|\epsilon^*_{\mathrm{PS}}| > 0.5$), homopolymers with very strong segment-solvent attractions are even more likely to attract solvent molecules. However, in this case, the solvent molecules act as bridges between homopolymer molecules since the segment-solvent attraction is much stronger than the segment-segment attraction. This causes the homopolymers with solvent bridges to precipitate, thereby

yielding a one-phase $\rightarrow$ two-phase transition. Evidence for this idea come from the following. In the polymer-rich phase for P_8 at ($|\epsilon^*_{PP}|$, $|\epsilon^*_{PS}|$) = (0.3, 0.9) and $\eta = 0.2$, 41 percent of the total solvent molecules reside in the attractive wells of neighbouring polymer segments. However, in the polymer-rich phase for P_8 at ($|\epsilon^*_{PP}|$, $|\epsilon^*_{PS}|$) = (0.3, 0.1) and $\eta = 0.2$, only 16 percent of the total solvent molecules reside in the attractive wells of neighbouring polymer segments. This indicates that many of the solvent molecules act as bridges between homopolymer molecules at very strong segment-solvent attractions.

Figure 2.1 also shows that the location of the one-phase $\rightarrow$ two-phase transition at high η is different from that at low η. At $\eta = 0.4$ we find a one-phase $\rightarrow$ two-phase transition as $|\epsilon^*_{PP}|$ increases and a two-phase $\rightarrow$ one-phase transition as $|\epsilon^*_{PS}|$ increases as we did at $\eta = 0.2$, but no one-phase $\rightarrow$ two-phase transition as $|\epsilon^*_{PS}|$ increases at high values of $|\epsilon^*_{PS}|$. As η increases from 0.2 to 0.4, the two-phase $\rightarrow$ one-phase transition moves to higher $|\epsilon^*_{PP}|$ for all $|\epsilon^*_{PS}|$ except very low values. The phase transition lines at $\eta = 0.2$ and 0.4 intersect at a single point at very low values of $|\epsilon^*_{PP}|$ and $|\epsilon^*_{PS}|$ for both P_4 and P_8. The intersections are located at $(\epsilon^*_{PP}|, |\epsilon^*_{PS}|) = (0.3, 0.05)$ for P_4 and $(0.25, 0.1)$ for P_8.

The intersection point marks a boundary between polymers whose solubility increases with increasing solvent density and polymers that precipate with increasing solvent density. At $|\epsilon^*_{PS}|$ greater than the value at the intersection point, the one-phase region extends to higher $|\epsilon^*_{PP}|$ as η increases, indicating that by increasing η one can dissolve a homopolymer with stronger $|\epsilon^*_{PP}|$ at fixed $|\epsilon^*_{PS}|$. This is because the solvent density around each homopolymer molecule increases as η increases, establishing more polymer/solvent attractions which are strong enough to screen the segment-segment attractions. Thus the solvent's ability to dissolve homopolymers

increases as η increases and homopolymers with stronger $|\epsilon^*_{\rm PP}|$ can be dissolved by raising η. At $|\epsilon^*_{\rm PS}|$ lower than that at the intersection point, the one-phase region moves to lower $|\epsilon^*_{\rm PP}|$ as η increases, indicating that by increasing η one cannot dissolve a homopolymer with stronger $|\epsilon^*_{\rm PP}|$ at fixed $|\epsilon^*_{\rm PS}|$. Although the solvent density around each homopolymer molecule increases as η increases, establishing more segment-solvent attractions between the polymer and solvent molecules, the segment-solvent interaction is too weak to screen out the attraction between polymer molecules. Thus the solvent's ability to dissolve homopolymers decreases as η increases causing homopolymer molecules to precipate.

The intersection of the phase transition lines at $\eta = 0.2$ and 0.4 in Figure 2.1 tells us that the tunability of scCO$_2$ (sensitive dependence of solvation strength on solvent density) depends critically on the value of $|\epsilon^*_{\rm PS}|$. If $|\epsilon^*_{\rm PS}|$ is below the value at the intersection point, a homopolymer whose interaction strengths lie between the two phase transition lines dissolves at low η but not at high η. Thus increasing η will result in a phase separation in the homopolymer/solvent systems with very weak $|\epsilon^*_{\rm PS}|$. If $|\epsilon^*_{\rm PS}|$ is above the value at the intersection point, a homopolymer whose interaction strengths lie between the two phase transition lines will not dissolve at low η but will dissolve at high η. Thus increasing η will increase the solubility of homopolymers with moderate or strong $|\epsilon^*_{\rm PS}|$.

The shape of the region between the phase transition lines at η = 0.2 and 0.4 tells us that whether or not increasing η will be a big factor in dissolving homopolymer depends critically on the value of $|\epsilon^*_{\rm PS}|$. The region between the phase transition lines at $\eta = 0.2$ and 0.4 becomes wider as $|\epsilon^*_{\rm PS}|$ increases above the value of $|\epsilon^*_{\rm PS}|$ at the intersection point, indicating that increasing η becomes a more and more effective tool to dissolve homopolymers with strong $|\epsilon^*_{\rm PP}|$ as

$|\epsilon^*_{\rm PS}|$ increases. In other words, in the narrow region between the two phase transition lines, increasing η is not a big factor in dissolving polymer but in the much wider region between the two phase transition lines, it is.

To illustrate the case in which increasing η causes homopolymer molecules to precipate in the solvent, we consider a homopolymer with interaction strengths located between the two phase transition lines at very weak $|\epsilon^*_{\rm PS}|$ (lower than that at the intersection point) in Figure 2.1. Figure 2.2 shows the one-phase $\rightarrow$ two-phase transition in the polymer volume fraction ($\phi_{\rm P}$)$-$packing fraction (η) plane for homopolymer P_4 at $T^* = 1.0$ with $(|\epsilon^*_{\rm PP}|, |\epsilon^*_{\rm PS}|) = (0.25, 0)$, which is to the left of and slightly below the intersection point $(0.3, 0.05)$ on Figure 2.1a. At $(|\epsilon^*_{\rm PP}|, |\epsilon^*_{\rm PS}|) = (0.25, 0)$ the homopolymer dissolves at low η and phase-separates at high η, thus causing a one-phase $\rightarrow$ two-phase transition as η increases. This result is the opposite of that found for homopolymers whose interaction parameters are located between the two phase transition lines at $|\epsilon^*_{\rm PS}|$ above the value of the intersection point, e. g. at $(|\epsilon^*_{\rm PP}|, |\epsilon^*_{\rm PS}|) = (0.9, 0.6)$, $(1.0, 0.6)$ and $(1.0, 0.55)$[1]. We found in our previous paper[1] that the latter systems phase-separate at low η and dissolve at high η, causing the homopolymer solubility to increase with increasing η.

To investigate the temperature dependence of the phase transition at various interaction parameters ($|\epsilon^*_{\rm PP}|$, $|\epsilon^*_{\rm PS}|$) and chain lengths, we simulate homopolymer (P_8 and P_{24})/solvent systems with ($|\epsilon^*_{\rm PP}|$, $|\epsilon^*_{\rm PS}|$) = (0.5, 0.5) and (0.5, 1.0). Figure 2.3 displays the two-phase $\rightarrow$ one-phase transition in the (a) packing fraction (η) $-$ reduced temperature (T^*) plane and (b) reduced pressure (P^*) $-$ reduced temperature (T^*) plane at $\phi_{\rm P} = 0.067$ for homopolymers P_8 and P_{24} with $(|\epsilon^*_{\rm PP}|, |\epsilon^*_{\rm PS}|) = (0.5, 0.5)$ and (0.5, 1.0). Figure 2.3 shows that the packing fraction and

pressure required to dissolve the homopolymers decreases with increasing temperature for all the homopolymers examined. (Recall that a homopolymer exhibits UCST behavior if a single phase is obtained as temperature increases isobarically and exhibits LCST behavior if phase separtion occurs as temperature increases isobarically.) It can be seen that the homopolymers P_8 and P_{24} with $(|\epsilon^*_{PP}|, |\epsilon^*_{PS}|) = (0.5, 0.5)$ and (0.5, 1.0) exhibit UCST behavior in hard-sphere solvents. The packing fraction and pressure required to dissolve homopolymer P_{24} are higher than those for homopolymer P_8 since the solubility of long chains is lower than that of short chains.

B. Square-well Solvent

To investigate whether or not the trends in homopolymer phase behavior with $|\epsilon^*_{PP}|$ and $|\epsilon^*_{PS}|$ are affected by how the solvent-solvent interaction is modeled, we consider the case in which a square-well potential is used to model the interaction between solvent molecules. Simulations are performed on homopolymers in square-well solvents at various values of $|\epsilon^*_{PP}|$ and $|\epsilon^*_{PS}|$. Figure 2.4 displays the location of the two-phase $\rightarrow$ one-phase transition for homopolymers (a) P_8 and (b) P_{12} in the space spanned by the segment-segment interaction strength ($|\epsilon^*_{PP}|$) and segment-solvent interaction strength ($|\epsilon^*_{PS}|$) at $\phi_P = 0.067$, $\eta = 0.2$ and 0.4, and $T^* = 1.0$ in CO_2 solvents with $|\epsilon^*_{SS}| = 0.15$ and $\lambda_{SS} = 0.75$. For both homopolymers at η = 0.2 and 0.4, we find a one-phase $\rightarrow$ two-phase transition as $|\epsilon^*_{PP}|$ increases at fixed $|\epsilon^*_{PS}|$ and a two-phase $\rightarrow$ one-phase transition as $|\epsilon^*_{PS}|$ increases at low values at fixed $|\epsilon^*_{PP}|$. The phase transition lines at η = 0.2 and 0.4 intersect at low values of $|\epsilon^*_{PP}|$ and $|\epsilon^*_{PS}|$ for both P_8 and P_{12}. Figure 2.4 also shows that a phase precipitation occurs at $\eta = 0.2$ as $|\epsilon^*_{PS}|$ increases at high values ($|\epsilon^*_{PS}| > 0.6$) for homopolymers P_8 and P_{12}.

A comparison between Figure 2.4 and Figure 2.1 tells us that the effect of varying $|\epsilon^*_{\mathrm{PP}}|$ and $|\epsilon^*_{\mathrm{PS}}|$ on the two-phase $\rightarrow$ one-phase transition in a square-well solvent is qualitatively similiar to that in a hard-sphere solvent. This indicates that modeling the solvent-solvent interaction with a hard-sphere potential is as good as modeling it with a square-well potential if we wish to learn the trends in the phase behavior of homopolymer/solvent systems with variations in $|\epsilon^*_{\mathrm{PP}}|$ and $|\epsilon^*_{\mathrm{PS}}|$.

Figure 2.4 can be used to get an idea of the solubility of homopolymers with different interaction parameters. For example, consider the interaction parameters chosen by Scanu et al.[3] for their lattice surfactant H_4T_5 in $scCO_2$: $\epsilon_{\mathrm{SS}} = -\epsilon$, $\epsilon_{\mathrm{TT}} = -\epsilon$, $\epsilon_{\mathrm{HH}} = -3\epsilon$, $\epsilon_{\mathrm{TS}} = -3\epsilon$, $\epsilon_{\mathrm{HS}} = -\epsilon$ and $\epsilon_{\mathrm{HT}} = -\epsilon$. We can locate their tail block interaction parameters on Figure 2.4 as follows. Since the solvent-solvent interaction strength ($|\epsilon^*_{\mathrm{SS}}|$) in Figure 2.4 is 0.15, the interaction strengths for the Scanu et al. tail block is $|\epsilon^*_{\mathrm{TT}}| = 0.15$ and hence $|\epsilon^*_{\mathrm{TS}}| = 0.45$. Figure 2.4 shows that $(|\epsilon^*_{\mathrm{TT}}|, |\epsilon^*_{\mathrm{TS}}|) = (0.15, 0.45)$ for P_8 is located far below the two-phase $\rightarrow$ one-phase transition line at $\eta = 0.2$, indicating that a homopolymer P_8 with $(|\epsilon^*_{\mathrm{TT}}|, |\epsilon^*_{\mathrm{TS}}|) = (0.15, 0.45)$ dissolves in $scCO_2$ at very low packing fraction. Homopolymer P_5 with the same interaction parameters as the tail block in the surfactant H_4T_5 would dissolve at an even lower packing fraction than P_8 since it is shorter. Although we cannot locate the interaction parameters for the head block with $(|\epsilon^*_{\mathrm{HH}}|, |\epsilon^*_{\mathrm{HS}}|) = (0.45, 0.15)$ in Figure 2.4, we could estimate the packing fraction required to dissolve homopolymer P_4 by performing simulations to draw a similiar phase diagram for homopolymer P_4 as Figure 2.4.

The interaction parameters of the model systems considered in the literature have been obtained by various methods. Lisal et al.[21] obtained the contact energies between like molecular

units by matching the critical temperatures of the model fluids with the critical temperatures of the real fluids. Cece et al.[9] obtained their computed binding energies for the CO_2-C_2F_6 cluster and CO_2-C_2H_6 cluster via Hartree-Fock calculations. Raveendran et al.[22] determined the dissociation engeries for CO_2 with CH_4, CH_3F, CH_2F_2, CHF_3 and CF_4 by using ab initio calculations and the "supermolecule" method[23]. Colina[24] showed how to obtain the scCO_2 and polymer parameters for the SAFT (Statistical Associating Fluid Theory) equation of state by regressing various properties, such as saturated vapor pressures, saturated liquid densities, the critical properties of CO_2, pure liquid molar volumes of polymers and binary phase equilibrium data[25–27], etc.

To determine whether modeling the solvent-solvent interaction with a hard-sphere potential prevents us from observing LCST behavior in homopolymer/solvent systems, we simulate the phase behavior of homopolymer/solvent systems when the solvent-solvent interaction, $|\epsilon^*_{\rm SS}|$, is modeled using a square-well potential. Figure 2.5 displays the two-phase $\rightarrow$ one-phase transition in the (a) packing fraction (η) $-$ reduced temperature (T^*) plane and (b) reduced pressure (P^*) $-$ reduced temperature (T^*) plane at $\phi_{\rm P} = 0.067$ for homopolymers P_8 and P_{24} with $(|\epsilon^*_{\rm PP}|, |\epsilon^*_{\rm PS}|) = (0.5, 0.5)$ and (0.5, 1.0) in square-well solvents. Figure 2.5a shows that the packing fraction required to dissolve the homopolymer decreases with increasing temperature for all the homopolymers examined. Figure 2.5b shows that the pressure required to dissolve homopolymer P_8 decreases with increasing temperature but that the pressure required to dissolve homopolymer P_{24} both increases and decreases with increasing temperature, depending upon the temperature range considered. Homopolymers P_8 with $(|\epsilon^*_{\rm PP}|, |\epsilon^*_{\rm PS}|) = (0.5, 0.5)$ and (0.5, 1.0) exhibit UCST behavior since a single phase phase is obtained as temperature increases

isobarically. Homopolymers P_{24} with $(|\epsilon^*_{PP}|, |\epsilon^*_{PS}|) = (0.5, 0.5)$ and (0.5, 1.0) exhibit UCST behavior at $T^* = 0.95 - 1.0$ since a single phase phase is obtained as temperature increases isobarically and exhibit LCST behaivor at $T^* = 1.0 - 1.05$ since a phase separation occurs as temperature increases isobarically. A comparison between Figure 2.5 and Figure 2.3 shows that it is necessary to model the solvent-solvent interaction with a square-well potential in order to observe LCST behavior in homopolymer/solvent systems. In addition, the chain length and the interaction parameters of the homopolymers can affect the temperature dependence of the phase transition in square-well solvents. This will be described in more detail in a future publication.

2.3.2 Surfactant

In this section we consider how the phase behavior of surfactant/solvent systems is affected by variation in the parameters associated with the head-head, head-solvent, tail-tail and tail-solvent interactions when the solvent-solvent interactions are modeled with a hard-sphere potential. However, before doing this it is interesting to see whether or not a model that includes a square-well potential for the head-head attractions only, the approach taken in modeling the micellization of model surfactant in aqueous systems,[28–30] can be applied to compressible surfactant/scCO$_2$ systems. Figure 2.6a shows the phase transition in the surfactant volume fraction $-$ packing fraction plane for surfactant H_4T_8 with $(|\epsilon^*_{HH}|, |\epsilon^*_{HS}|, |\epsilon^*_{TT}|, |\epsilon^*_{TS}|) = (0.5, 0, 0, 0)$. Figure 2.6b shows the simulation results from our previous study[1] on the phase behavior for surfactant H_4T_8 at $(|\epsilon^*_{HH}|, |\epsilon^*_{HS}|, |\epsilon^*_{TT}|, |\epsilon^*_{TS}|) = (1.0, 0.525, 0.45, 0.4)$. The phase behaviors for these two systems are completely different. In the phase diagram for H_4T_8 at $(|\epsilon^*_{HH}|, |\epsilon^*_{HS}|, |\epsilon^*_{TT}|, |\epsilon^*_{TS}|) = (0.5, 0, 0, 0)$, there are two regions (a unimer phase at low η and

a micelle phase at high η) and a single phase transition (a unimer $\rightarrow$ micelle transition as η increases). In the phase diagram of H_4T_8 at $(|\epsilon^*_{HH}|, |\epsilon^*_{HS}|, |\epsilon^*_{TT}|, |\epsilon^*_{TS}|) = (1.0, 0.525, 0.45, 0.4)$, there are three regions (a two-phase region at low η, a micelle phase at intermediate η and a unimer phase at high η) and two phase transitions (a two-phase $\rightarrow$ one-phase transition and a micelle $\rightarrow$ unimer transition as η increases). These differences can be explained in the following way. For the case when $(|\epsilon^*_{HH}|, |\epsilon^*_{HS}|, |\epsilon^*_{TT}|, |\epsilon^*_{TS}|) = (1.0, 0.525, 0.45, 0.4)$, as described in our previous study[1] the head and tail blocks of surfactant H_4T_8 have different solubilities in the solvent since the head and tail blocks dissolve at high η and very low η, respectively. Surfactants precipitate at very low η since neither the head nor the tail block can dissolve in the solvent, form micelles at intermediate η since the tail block can dissolve but the head block cannot, and dissolve as unimers at high η since both the head and tail blocks can be dissolved. For the case when $(|\epsilon^*_{HH}|, |\epsilon^*_{HS}|, |\epsilon^*_{TT}|, |\epsilon^*_{TS}|) = (0.5, 0, 0, 0)$, no two-phase region is found since the tail block dissolves completely in the solvent. Even though there are no attractions between tail block and solvent molecule ($|\epsilon^*_{TT}| = |\epsilon^*_{TS}| = |\epsilon^*_{SS}| = 0$), the entropy encourages their miscibility. The surfactant phase behavior in this case depends only on the solubility of the head block in the solvent. Surfactants dissolve as unimers at low η and form micelles at high η meaning that a unimer $\rightarrow$ micelle transition occurs as η increases, which is the opposite of the trend found in the simulation results for surfactants[1,3] and in experimental observations[2]. The solubility of a surfactant head block with $|\epsilon^*_{PS}| = 0$ decreases as η increases as can be seen by referring to the simulation results on the solubility of a homopolymer with $|\epsilon^*_{PS}| = 0$ shown in Figure 2.2. Surfactants form micelles as η increases since the surfactant head blocks can dissolve at low η and precipate at high η.

Figure 2.6 shows that the highly simplified model with $|\epsilon^*_{\rm HH}| \neq 0, |\epsilon^*_{\rm HS}| = |\epsilon^*_{\rm TT}| = |\epsilon^*_{\rm TS}| = |\epsilon^*_{\rm SS}| = |\epsilon^*_{\rm HT}| = 0$ used to describe incompressible model surfactant systems[28–30] is not suitable for compressible model surfactant systems because variations in the solvent density only affect the solubility of the surfactant head block and lead to the wrong trend, i. e. that surfactants dissolve as unimers at low η and form micelles at high η. In experiments, however, the solvent density affects the solubility of both surfactant head and tail blocks. Figure 2.6 also explains the discrepancy between the simulation results of Lisal et al.[21] showing that the CMC decreases as CO_2 density increases and experimental results on surfactant (PVAc-*b*-PTAN)/scCO_2[2] showing that the CMC increases as CO_2 density increases. The head-solvent interaction strength in the simulations by Lisal et al.[21] was zero; thus the solubility of the CO_2-phobic block decreased as the CO_2 density increased and a unimer $\rightarrow$ micelle transition occurred as the CO_2 density increased.

Next we consider how the phase behavior of surfactant/solvent systems is affected by variations in the strengths of the head-head, head-solvent, tail-tail and tail-solvent square-well attractions. First we look at the influence of $|\epsilon^*_{\rm HH}|$ and $|\epsilon^*_{\rm HS}|$ on the unimer $\rightarrow$ micelle transition. Figure 2.7 displays the location of the unimer $\rightarrow$ micelle transition for surfactant H_4T_8 with ($|\epsilon^*_{\rm TT}|$, $|\epsilon^*_{\rm TS}|$) = (0.3, 0.4) in the space spanned by the head-head attraction strength ($|\epsilon^*_{\rm HH}|$) and head-solvent attraction strength ($|\epsilon^*_{\rm HS}|$) at $\phi_{\rm P}$ = 0.178, η = 0.2, 0.3 and 0.4, and T^* = 1.0. It can be seen that surfactants form micelles at high values of $|\epsilon^*_{\rm HH}|$ and a unimer $\rightarrow$ micelle transition occurs as $|\epsilon^*_{\rm HH}|$ increases at all values of the packing fraction. This is because surfactants with strong head-head attractions are highly likely to attract other surfactant molecules, forming micelles. We also see that micelles dissolve as unimers at high values of $|\epsilon^*_{\rm HS}|$ and a micelle $\rightarrow$

unimer transition occurs as $|\epsilon^*_{\mathrm{HS}}|$ increases. This is because surfactants with strong head-solvent attractions are more likely to attract solvent molecules than surfactants with weak head-solvent attractions. Increasing $|\epsilon^*_{\mathrm{HS}}|$ increases the miscibility of the head block and solvent molecules, causing more solvent molecules to permeate into the head cores of micelles until they break the micelles, causing a micelle $\rightarrow$ unimer transition to occur.

Figure 2.7 also shows that the location of the unimer $\rightarrow$ micelle transition at high η is different from that at low η. As η increases, the unimer $\rightarrow$ micelle transition moves to higher $|\epsilon^*_{\mathrm{HH}}|$ for all $|\epsilon^*_{\mathrm{HS}}|$ except very low values. The unimer $\rightarrow$ micelle transition lines at η = 0.2, 0.3 and 0.4 intersect at a single point: ($|\epsilon^*_{\mathrm{HH}}|$, $|\epsilon^*_{\mathrm{HS}}|$) = (0.7, 0.2). At $|\epsilon^*_{\mathrm{HS}}|$ values greater than that at the intersection point, the unimer region extends to higher $|\epsilon^*_{\mathrm{HH}}|$ as η increases, indicating that by increasing η one can dissolve a surfactant with strong head-head attraction at fixed head-solvent attraction as a unimer. This is because the solvent density around the head block of each surfactant molecule increases as η increases, establishing more head-solvent attractions which can screen the stronger head-head attractions. Thus the solvent's ability to dissolve surfactants as unimers increases as η increases and surfactants with stronger head-head attractions can be dissolved by raising η. At $|\epsilon^*_{\mathrm{HS}}|$ values lower than that at intersection point, the unimer region moves to lower $|\epsilon^*_{\mathrm{HH}}|$ as η increases, indicating that by increasing η one cannot dissolve a surfactant with stronger head-head attractions at fixed head-solvent attraction. In this case, although the solvent density around the head block of each surfactant molecule increases as η increases, establishing more head-solvent attractions between head block and solvenet molecules, the head-solvent interaction is too weak to screen the head-head attractions. In addition, it is difficult for solvent molecules to insert themselves into the solvent-phobic head core of micelles at very weak

$|\epsilon^*_{\mathrm{HS}}|$. Thus at very weak $|\epsilon^*_{\mathrm{HS}}|$, the solvent's ability to dissolve surfactants as unimers decreases as η increases.

The intersection of the unimer $\rightarrow$ micelle transition lines at η = 0.2, 0.3 and 0.4 in Figure 2.7 and the shape of the region between them tell us that the value of $|\epsilon^*_{\mathrm{HS}}|$ determines whether increasing η will help dissolve surfactants as unimer and, if so, how big a factor this will be in dissolving surfactants as unimers. We find that increasing η results in micellization at very weak $|\epsilon^*_{\mathrm{HS}}|$ and solubilization of surfactants as unimers at moderate to strong $|\epsilon^*_{\mathrm{HS}}|$. Increasing η becomes a more and more effective tool to dissolve surfactants as unimers for surfactants with strong $|\epsilon^*_{\mathrm{HH}}|$ as $|\epsilon^*_{\mathrm{HS}}|$ increases. The location of the intersection of the phase transition lines at different η is relatively independent of η since the effect of η on the unimer $\rightarrow$ micelle transition is very small at weak $|\epsilon^*_{\mathrm{HS}}|$.

We also look at the influence of $|\epsilon^*_{\mathrm{TS}}|$ on the unimer $\rightarrow$ micelle transition of the surfactant/solvent systems. Figure 2.8 compares the location of the unimer $\rightarrow$ micelle transition for the surfactants H_4T_8 with ($|\epsilon^*_{\mathrm{TT}}|$, $|\epsilon^*_{\mathrm{TS}}|$) = (0.3, 0.4) and (0.3, 0.8) in the space spanned by the head-head attraction strength ($|\epsilon^*_{\mathrm{HH}}|$) and head-solvent attraction strength ($|\epsilon^*_{\mathrm{HS}}|$) at ϕ_{P} = 0.178, η = 0.2 and 0.4, and T^* = 1.0. Figure 2.8 shows that the unimer $\rightarrow$ micelle transition line moves to lower $|\epsilon^*_{\mathrm{HH}}|$ as $|\epsilon^*_{\mathrm{TS}}|$ increases from 0.4 to 0.8 at η = 0.20 but stays the same at η = 0.40, indicating that the tail-solvent interaction impacts the unimer $\rightarrow$ micelle transition much more strongly at low η than at high η.

To more fully explore the influence of $|\epsilon^*_{\mathrm{HS}}|$ on the phase transition of surfactant/solvent systems, we locate the two-phase $\rightarrow$ one-phase transition and the micelle $\rightarrow$ unimer transition at various values of $|\epsilon^*_{\mathrm{HS}}|$. Figure 2.9 shows the phase behavior of surfactant H_4T_8 in the $\eta - |\epsilon^*_{\mathrm{HS}}|$

plane at $(|\epsilon^*_{\mathrm{HH}}|, |\epsilon^*_{\mathrm{TT}}|, |\epsilon^*_{\mathrm{TS}}|) = (1.0, 0.45, 0.4)$ at fixed $\phi_{\mathrm{H_4T_8}} = 0.178$ and $T^* = 1.0$. The effect of varying $|\epsilon^*_{\mathrm{HS}}|$ on the location of the two-phase $\rightarrow$ one-phase transition is different from that on the micelle $\rightarrow$ unimer transition. The two-phase $\rightarrow$ one-phase transition is not sensitive to the value of $|\epsilon^*_{\mathrm{HS}}|$ since the packing fraction at which the two-phase $\rightarrow$ one-phase transition occurs does not vary much as $|\epsilon^*_{\mathrm{HS}}|$ increases. In contrast, the packing fraction at which the micelle $\rightarrow$ unimer transition occurs decreases dramatically as $|\epsilon^*_{\mathrm{HS}}|$ increases from 0.4 to 0.55. We also find that the micelles cannot dissolve as unimers for surfactant with $|\epsilon^*_{\mathrm{HS}}| \leq 0.4$ even at the highest packing fraction ($\eta \approx 0.5$). At $|\epsilon^*_{\mathrm{HS}}| \approx 0.55$ the two-phase $\rightarrow$ one-phase transition and micelle $\rightarrow$ unimer transition merge and no micelle region is found.

An interesting phenomenon is observed in our simulations for the surfactants with strong head-solvent attractions. At high values of $|\epsilon^*_{\mathrm{HS}}|$ ($|\epsilon^*_{\mathrm{HS}}| > 0.55$) in Figure 2.9, the micelle $\rightarrow$ unimer transition (solid line) is at lower η than the two-phase $\rightarrow$ one-phase transition (dashed line). This is unusual as can be seen by comparing Figure 2.9 with Figure 2.6b. In this case, at low η the surfactant molecules form micelles in the polymer-rich phase. As η increases the micelles in the polymer-rich phase break into unimers even before the surfactant molecules dissolve in the solvent, thus a 'micelle $\rightarrow$ unimer' transition is observed within the two-phase region. As η continues to increase, surfactant molecules dissolve in the solvent and the two-phase $\rightarrow$ one-phase transition occurs. In other words, as η increases we find two phase transitions: a transition at low η from a two-phase region with micelles in the polymer-rich phase to a two-phase region with unimers in the polymer-rich phase, and then a transition at higher η to a one-phase region with unimers. This can be explained in the following way. At low η, the solubility of both surfactant head and tail is low, causing the surfactant molecules to precipitate; in addi-

tion, the surfactant head is solvent-phobic and the surfactant tail is solvent-philic thus surfactant molecules form micelles within the polymer-rich phase. As η increases, the strong attractions between head segments and solvent molecules allow the solvent molecules to insert themselves into the head cores of the micelles, causing the micelles in the polymer-rich phase to break into unimers even before the surfactants dissolve completely in the solvent. This causes a micelle $\rightarrow$ unimer transition within the two-phase region. At high η, the surfactant solubility increases and surfactant molecules dissolve as unimers in the solvent directly, thus a two-phase $\rightarrow$ one-phase transition occurs. Thus we see that at high $|\epsilon^*_{\mathrm{HS}}|$ no micelles are formed when the two-phase $\rightarrow$ one-phase transition is crossed but that at low $|\epsilon^*_{\mathrm{HS}}|$ micelles are formed when the two-phase $\rightarrow$ one-phase transition is crossed.

We also investigate the influence of $|\epsilon^*_{\mathrm{TT}}|$ on the phase transitions of surfactant/solvent systems. Figure 2.10 shows the phase behavior in the $\eta - |\epsilon^*_{\mathrm{TT}}|$ plane for surfactant $\mathrm{H_4T_8}$ with $(|\epsilon^*_{\mathrm{HH}}|, |\epsilon^*_{\mathrm{HS}}|) = (1.0, 0.5)$ and $|\epsilon^*_{\mathrm{TS}}| = (\mathrm{a})0.4$ and (b) 0.8 at fixed $\phi_{\mathrm{H_4T_8}} = 0.178$ and $T^* = 1.0$. As in the analysis of the effect of $|\epsilon^*_{\mathrm{HS}}|$ on the phase transitions in Figure 2.9, we find that the value of $|\epsilon^*_{\mathrm{TT}}|$ plays an important role in determining the location of the two-phase $\rightarrow$ one-phase transition (dashed line), but affects the location of the micelle $\rightarrow$ unimer transition (solid line) only slightly. The two-phase $\rightarrow$ one-phase transition and micelle $\rightarrow$ unimer transition merge at high $|\epsilon^*_{\mathrm{TT}}|$; beyond this no single phase micelle region is found as η increases. We also find that higher η is needed to dissolve the surfactant with higher $|\epsilon^*_{\mathrm{TS}}|$, which can be explained by the "bridge" effect discussed in Figure 2.1. The solvent molecules are more likely to act as bridges between surfactant tails at $|\epsilon^*_{\mathrm{TS}}|$ = 0.8 rather than at $|\epsilon^*_{\mathrm{TS}}|$ = 0.4, causing the surfactant molecules with solvent bridges to precipitate. Recall that homopolymer $\mathrm{P_8}$ with $|\epsilon^*_{\mathrm{PP}}|$ lower than 0.5 and

$|\epsilon^*_{\mathrm{PS}}|$ greater than 0.5 precipates with the solvent bridges at η = 0.2, as shown in Figure 2.1b. Figure 2.10 shows that surfactants H_4T_8 with $|\epsilon^*_{\mathrm{TT}}|$ lower than 0.4 and $|\epsilon^*_{\mathrm{TS}}|$ =0.4 and 0.8 dissolve in the η range of 0.25-0.30, which is close to η = 0.2. In addition, surfactant H_4T_8 is longer than homopolymer P_8 and the surfactant head is more CO_2-phobic than the surfactant tail, so higher η is needed to dissolve surfactant H_4T_8 than homopolymer P_8.

2.4 Summary and Discussion

In this study, we investigated the influence of interaction strengths on the phase behavior of homopolymer/solvent and surfactant/solvent systems using the simple model developed in our previous study[1]. Phase diagrams were constructed for homopolymers in both hard-sphere and square-well solvents and for surfactants in hard-sphere solvents. For homopolymers in both hard-sphere and square-well solvents, the value of $|\epsilon^*_{\mathrm{PS}}|$ has a profound effect on the homopolymer solubility. Increasing η serves to increase the solvent's ability to dissolve homopolymers only when the segment-solvent interaction strength exceeds a critical value. Increasing η is not a big factor in dissolving homopolymers with weak segment-solvent attractions but is a big factor in dissolving homopolymers with strong segment-solvent attractions. In addition, we find that homopolymers precipate in hard-sphere solvents as $|\epsilon^*_{\mathrm{PS}}|$ increases at high values when η is low. Although only UCST behavior is observed for homopolymers in hard-sphere solvents, both UCST and LCST behavior are observed for homopolymers in square-well solvents, depending upon the interaction strengths and chain length. This indicates that it is necessary to account for the solvent-solvent attraction to investigate LCST versus UCST behavior in scCO_2.

Our simulation results on different models of surfactant/solvent systems show that it is

necessary to model the interactions experienced by both the surfactant head and tail blocks in order to capture the essential features of real surfactant/scCO_2 systems. The CMC increases with increasing η as it does in most experiments only when the head-solvent interaction strength exceeds a critical value. At strong head-solvent interaction strengths, the micelle $\rightarrow$ unimer transition occurs within the two-phase region. In that case we find a transition from a two-phase region with micelles in the polymer-rich phase to a two-phase region with unimers in the polymer-rich phase at low packing fraction, and a transition to a one-phase region with unimers at higher packing fraction. This is unexpected and is not observed experimentally. The tail-solvent interaction impacts the location of the unimer $\rightarrow$ micelle transition much more strongly at low η than at high η. The head-solvent interaction affects the location of the micelle $\rightarrow$ unimer transition strongly but affects the location of the two-phase $\rightarrow$ one-phase transition only slightly; the tail-tail interaction affects the location of the two-phase $\rightarrow$ one-phase transition strongly but affects the location of the micelle $\rightarrow$ unimer transition only slightly.

2.5 Acknowledgements

The material is based upon work supported by the STC Program of the National Science Foundation under Agreement No. CHE-9876674. Acknowledgment is made to the Office of Energy Research, Basic Sciences, Chemical Science Division of the U. S. Department of Energy under Contract No. DE-FG05-91ER14181 for partial support of this work. Z. Li thanks A. J. Schultz for fruitful discussions and many valuable suggestions.

2.6 References

[1] Z. Li and C. K. Hall, "Phase behavior in model homopolymer/CO_2 and surfactant/CO_2 systems: discontinuous molecular dynamics simulations," *Langmuir* .

[2] E. Buhler, A. V. Dobrynin, J. M. DeSimone, and M. Rubinstein, "Light-scattering study of diblock copolymers in supercritical carbon dioxide: CO_2 density-induced micellization transition," *Macromolecules* **31**, 7347 (1998).

[3] L. F. Scanu, K. E. Gubbins, and C. K. Hall, "Lattice Monte Carlo simulations of phase separation and micellization in supercritical CO_2/surfactant systems: Effect of CO_2 density," *Langmuir* **20**, 514 (2004).

[4] Z. Shen, M. A. McHugh, J. Xu, J. Belardi, S. Kilic, A. Mesiano, S. Bane, C. Karnikas, E. Beckman, and R. Enick, "CO_2-solubility of oligomers and polymers that contain the carbonyl group," *Polymer* **44**, 1491 (2003).

[5] V. M. Shah, B. J. Hardy, and S. A. Stern, "Solubility of carbon-dioxide, methane, and propane in silicone polymers - effect of polymer backbone chains," *J. Polym. Sci. Pol. Phys.* **31**, 313 (1993).

[6] J. C. Merdith, K. P. Johnston, J. M. Seminario, S. G. Kazarian, and C. A. Eckert, "Quantitative equilibrium constants between CO_2 and Lewis bases from FTIR spectroscopy," *J. Phys. Chem.* **100**, 10837 (1996).

[7] A. Dardin, J. M. DeSimone, and E. T. Samulski, "Fluorocarbons dissolved in supercritical

carbon dioxide. NMR evidence for specific solute-solvent interactions," *J. Phys. Chem. B* **102**, 1775 (1998).

[8] C. R. Yonker and B. J. Palmer, "Investigation of CO_2/fluorine interactions through the intermolecular effects on the H-1 and F-19 shielding of CH_3F and CHF_3 at various temperatures and pressures," *J. Phys. Chem. A* **105**, 308 (2001).

[9] A. Cece, S. H. Jureller, J. L. Kerschner, and K. F. Moschner, "Molecular modeling approach for contrasting the interaction of ethane and hexafluoroethane with carbon dioxide," *J. Phys. Chem.* **100**, 7435 (1996).

[10] Y. K. Han and H. Y. Jeong, "Molecular modeling approach for contrasting the interaction of ethane and hexafluoroethane with carbon dioxide - Comment," *J. Phys. Chem. A* **101**, 5604 (1997).

[11] P. Diep, K. D. Jordan, J. K. Johnson, and E. J. Beekman, "CO_2-fluorocarbon and CO_2-hydrocarbon interactions from first-principles calculations," *J. Phys. Chem. A* **102**, 2231 (1998).

[12] M. Lisal and I. NeZbeda, "Conformations of attractive, repulsive, and amphiphilic polymer chains in a simple supercritical solvent: Molecular simulation study," *J. Chem. Phys.* **119**, 4026 (2003).

[13] D. C. Rapaport, "Molecular dynamics study of a polymer chain," *J. Chem. Phys.* **71**, 3299 (1979).

[14] A. Bellemans, J. Orban, and D. V. Belle, "Molecular dynamics of rigid and non-rigid necklaces of hard disks," *Mol. Phys.* **39**, 781 (1980).

[15] H. S. Gulati and C. K. Hall, "Fluids and fluid mixtures containing square-well diatomics: Equations of state and canonical molecular dynamics simulation," *J. Chem. Phys.* **107**, 3930 (1997).

[16] H. C. Anderson, "Molecular-dynamics simulations at constant pressure and-or temperature," *J. Chem. Phys.* **72**, 2384 (1980).

[17] Y. Zhou, C. K. Hall, and M. Karplus, "First-order disorder-to-order transition in an isolated homopolymer model," *Phys. Rev. Lett.* **77**, 2822 (1996).

[18] Y. Zhou, M. Karplus, J. M. Wichert, and C. K. Hall, "Equilibrium thermodynamics of homopolymers and clusters: Molecular dynamics and Monte Carlo simulations of systems with square-well interactions," *J. Chem. Phys.* **107**, 10691 (1997).

[19] S. W. Smith, B. D. Freeman, and C. K. Hall, "Discontinuous molecular dynamics for polymeric fluids.," *J. Comput. Phys.* **134**, 16 (1997).

[20] A. J. Schultz, C. K. Hall, and J. Genzer, "Computer simulation of copolymer phase behavior," *J. Chem. Phys.* **117**, 10329 (2002).

[21] M. Lisal, C. K. Hall, K. E. Gubbins, and A. Z. Panagiotopoulos, "Self-assembly of surfactants in a supercritical solvent from lattice Monte Carlo simulations," *J. Chem. Phys.* **116**, 1171 (2002).

[22] P. Raveendran and S. L. Wallen, "Exploring CO_2-philicity: effects of stepwise fluorination," *J. Phys. Chem. B* **107**, 1473 (2003).

[23] K. Morokuma and K. Kitaura, *Molecular interactions* (Wiley, New York, 1980), p. 21.

[24] C. M. Colina, PhD dissertation, North Carolina State University, Dept. of Chem. Eng., 2004.

[25] C. F. Kirby and M. A. McHugh, "Phase behavior of polymers in supercritical fluid solvents," *Chem. Rev.* **99**, 565 (1999).

[26] S. Takishima, M. L. ONeill, and K. P. Johnston, "Solubility of block copolymer surfactants in compressed CO2 using a lattice fluid hydrogen-bonding model," *Ind. Eng. Chem. Res.* **36**, 2821 (1997).

[27] M. Lora, F. Rindfleisch, and M. A. McHugh, "Influence of the alkyl tail on the solubility of poly(alkyl acrylates) in ethylene and CO2 at high pressures: Experiments and modeling," *J. Appl. Poly. Sci.* **73**, 1979 (1999).

[28] M. A. Floriano, E. Caponetti, and A. Z. Panagiotopoulos, "Micellization in model surfactant systems," *Langmuir* **15**, 3143 (1999).

[29] A. Z. Panagiotopoulos, M. A. Floriano, and S. K. Kumar, "Micellization and phase separation of diblock and triblock model surfactants," *Langmuir* **18**, 2940 (2002).

[30] S. Salaniwal, S. K. Kumar, and A. Z. Panagiotopoulos, "Competing ranges of attractive and repulsive interactions in the micellization of model surfactants," *Langmuir* **19**, 5164 (2003).

2.7 Figures

Page

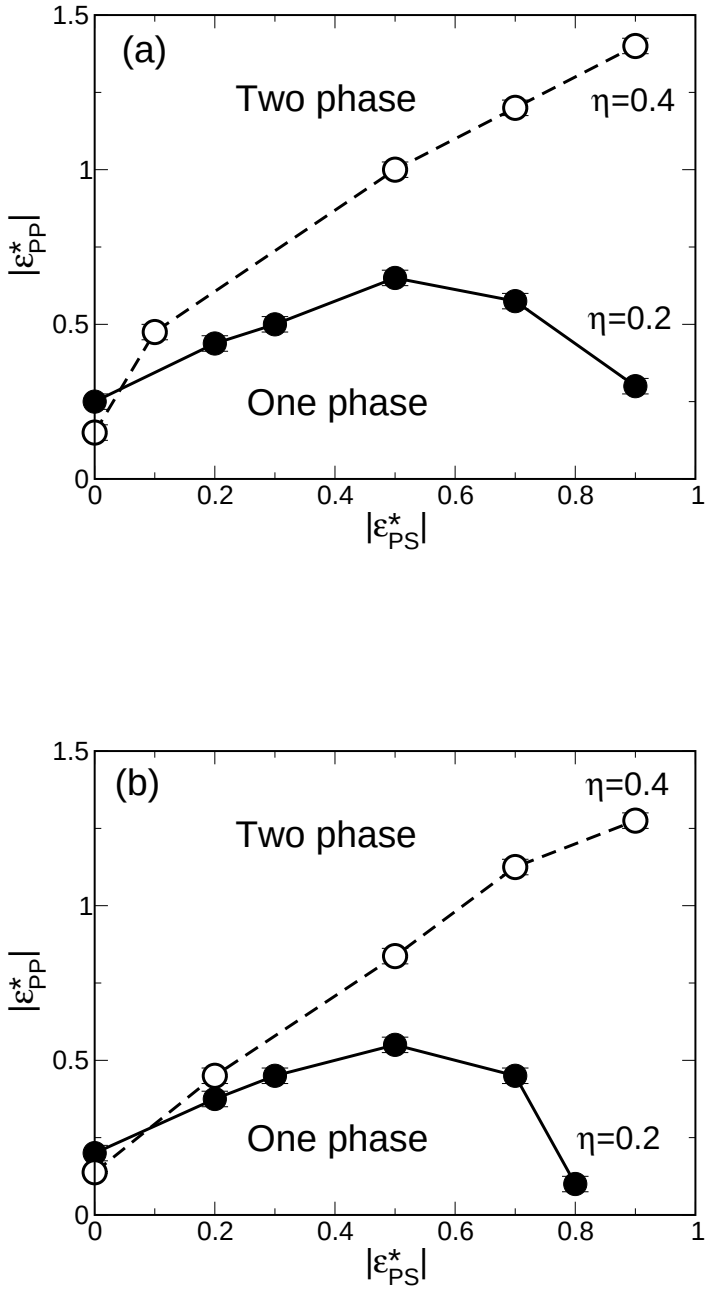

Figure 2.1: Phase transition in the $|\epsilon^*_{\rm PP}| - |\epsilon^*_{\rm PS}|$ plane for homopolymers (a) P_4 and (b) P_8 in hard-sphere solvents when $\phi_{\rm P} = 0.178$, $T^* = 1.0$ at $\eta = 0.2$ (solid line) and 0.4 (dashed line).

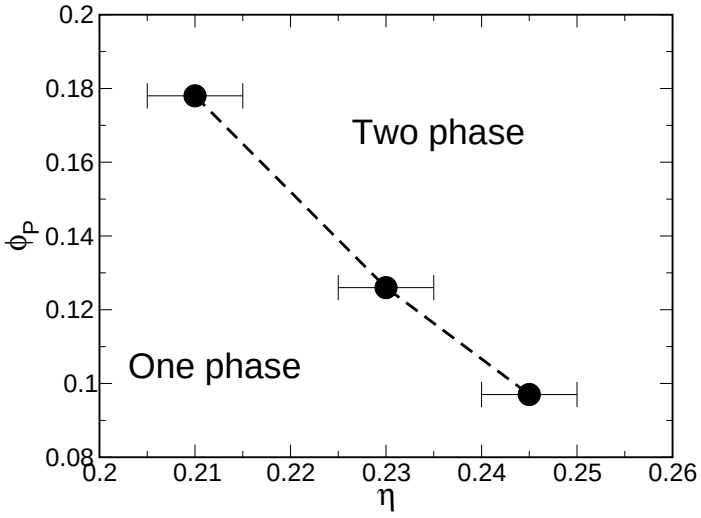

Figure 2.2: Phase transition in the polymer volume fraction (ϕ_{P}) $-$ packing fraction (η) plane for homopolymer P_4 in hard-sphere solvents when$(|\epsilon^*_{\mathrm{PP}}|, |\epsilon^*_{\mathrm{PS}}|) = (0.25, 0)$ and $T^* = 1.0$.

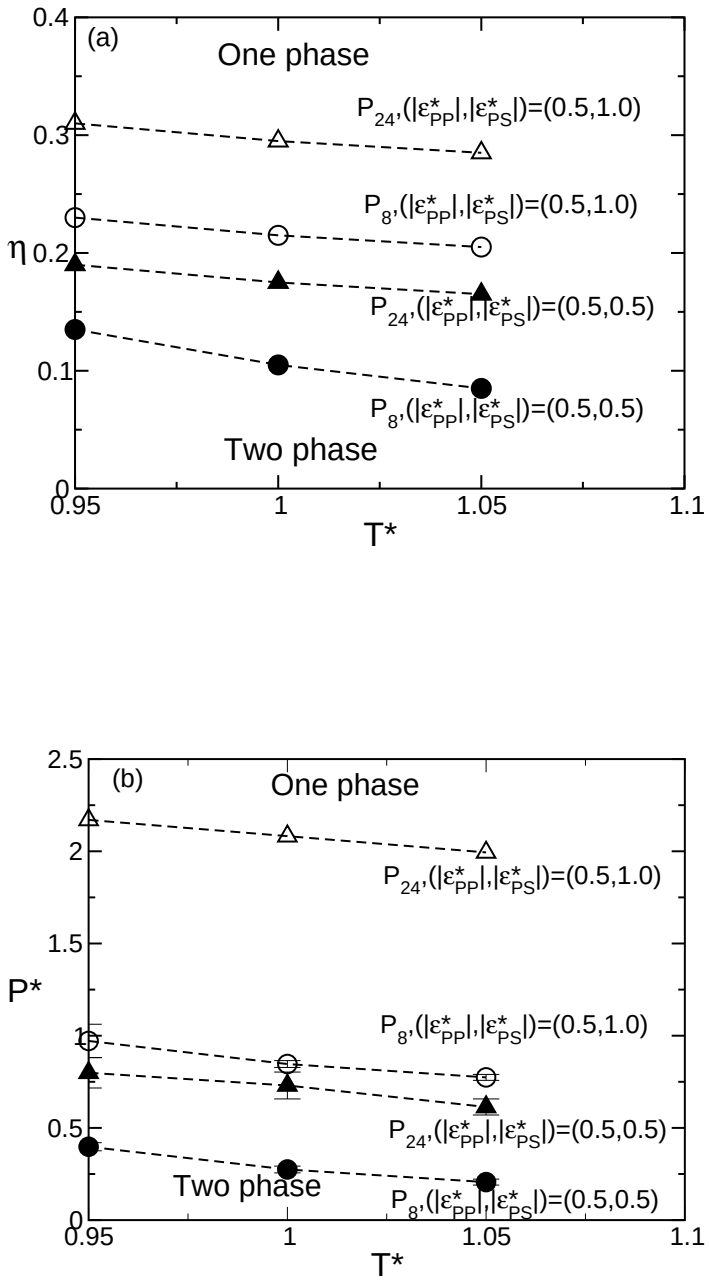

Figure 2.3: Phase transition in the (a) packing fraction (η) - reduced temperature (T^*) plane and (b) reduced pressure (P^*) - reduced temperature (T^*) plane for homopolymers P_8 and P_{24} in hard-sphere solvents when $(|\epsilon^*_{\rm PP}|, |\epsilon^*_{\rm PS}|) = (0.5, 0.5)$ and (0.5, 1.0) and $\phi_{\rm P} = 0.067$.

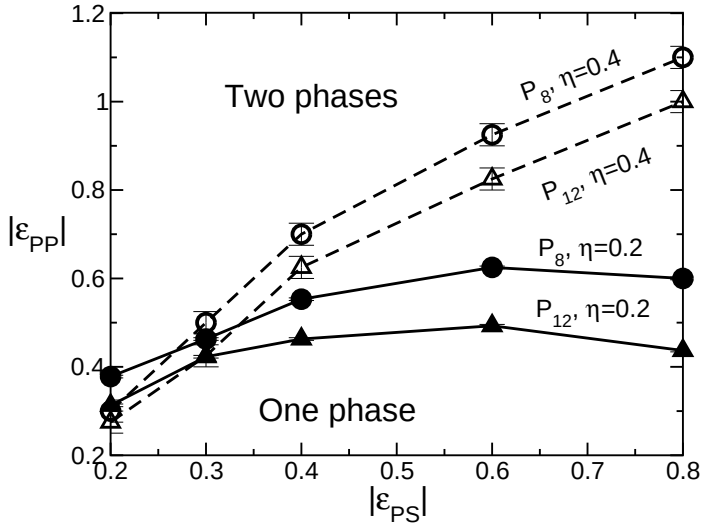

Figure 2.4: Phase transition in the $|\epsilon^*_{\rm PP}| - |\epsilon^*_{\rm PS}|$ plane for homopolymers P_8 and P_{12} in square-well solvents when $|\epsilon^*_{\rm SS}| = 0.15$, $\lambda_{\rm SS} = 0.75$, $\phi_{\rm P} = 0.067$, $T^* = 1.0$ at $\eta = 0.2$ (solid line) and 0.4 (dashed line).

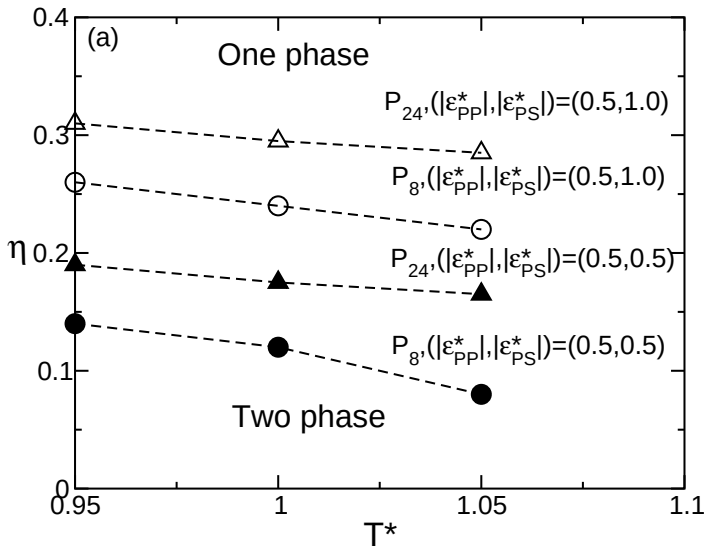

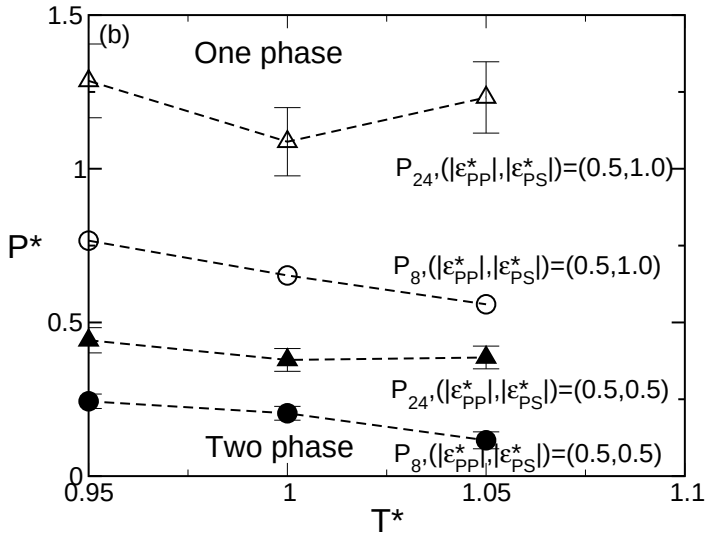

Figure 2.5: Phase transition in the (a) packing fraction (η) - reduced temperature (T^*) plane and (b) reduced pressure (P^*) - reduced temperature (T^*) plane for homopolymers P_8 and P_{24} in square-well solvents when $(|\epsilon^*_{\rm PP}|, |\epsilon^*_{\rm PS}|) = (0.5, 0.5)$ and (0.5, 1.0), $|\epsilon^*_{\rm SS}| = 0.15$, $\lambda_{\rm SS} = 1.0$, and $\phi_{\rm P} = 0.067$.

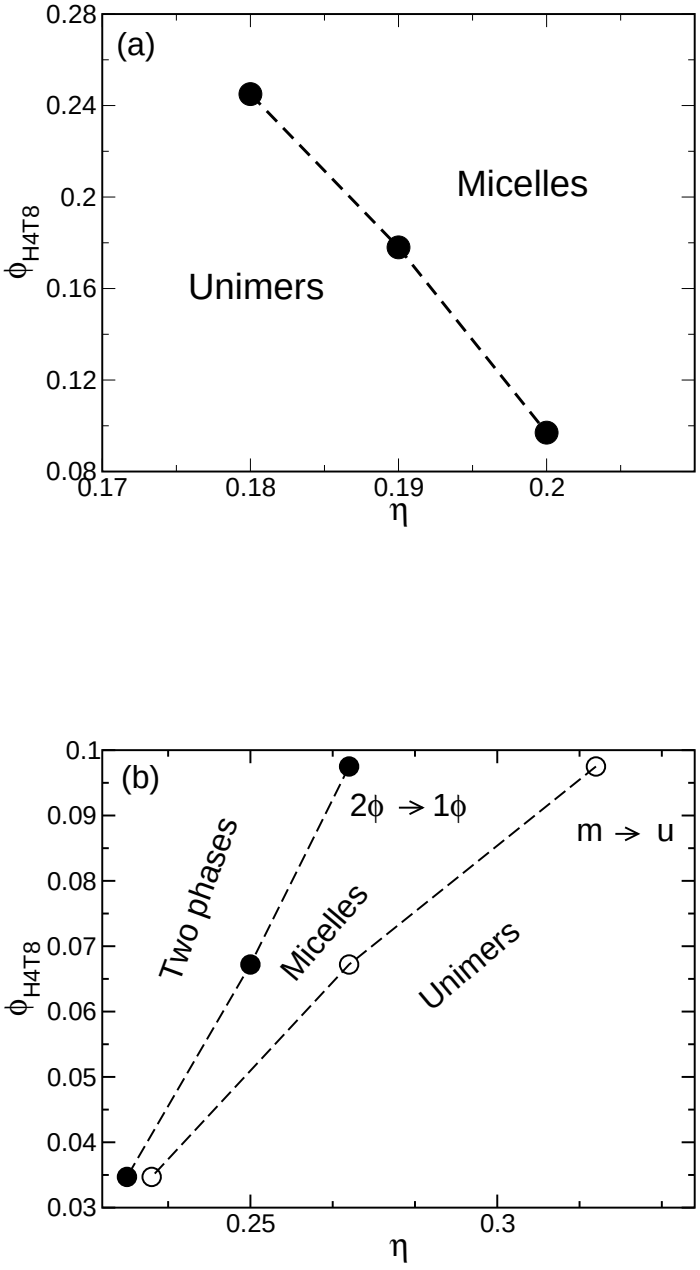

Figure 2.6: Phase transition in the surfactant volume fraction (ϕ_{H4T8}) $-$ packing fraction (η) plane for surfactant H_4T_8 in hard-sphere solvents when $(|\epsilon^*_{\mathrm{HH}}|, |\epsilon^*_{\mathrm{HS}}|, |\epsilon^*_{\mathrm{TT}}|, |\epsilon^*_{\mathrm{TS}}|)$ = (a) (0.5, 0, 0, 0) and (b) (1.0, 0.525, 0.45, 0.4), and $T^* = 1.0$.

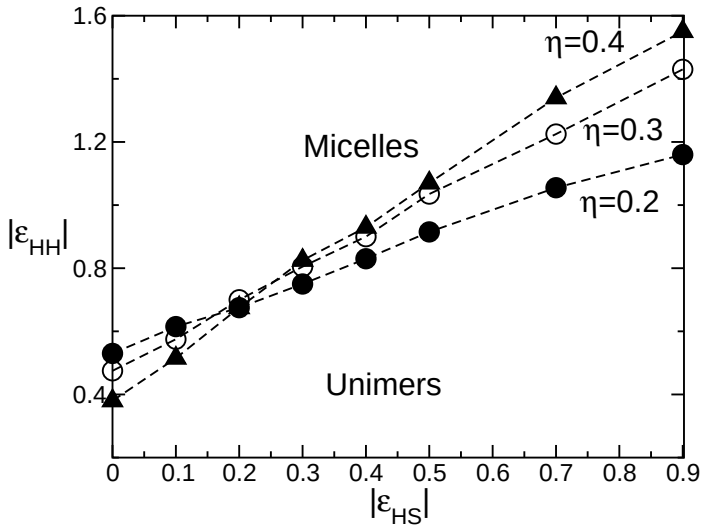

Figure 2.7: Phase transition in the $|\epsilon^*_{\rm HH}| - |\epsilon^*_{\rm HS}|$ plane for surfactant H_4T_8 in hard-sphere solvents when $(|\epsilon^*_{\rm TT}|, |\epsilon^*_{\rm TS}|) = (0.3, 0.4)$, $\phi_{\rm H_4T_8} = 0.178$, $T^* = 1.0$, at $\eta = 0.2, 0.3$ and 0.4.

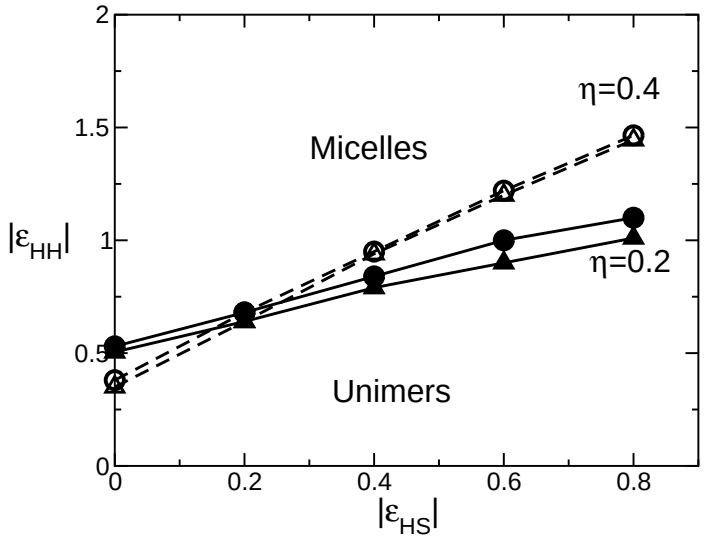

Figure 2.8: Phase transition in the $|\epsilon^*_{\rm HH}| - |\epsilon^*_{\rm HS}|$ plane for for surfactant H_4T_8 in hard-sphere solvents when $(\epsilon_{\rm TS}, \epsilon_{\rm TS}) = (0.3, 0.4)$ (circle) and $(\epsilon_{\rm TS}, \epsilon_{\rm TS}) = (0.3, 0.8)$ (triangle), $\phi_{\rm H_4T_8} = 0.178$, $T^* = 1.0$, at $\eta = 0.2$ (solid line) and 0.4 (dashed line).

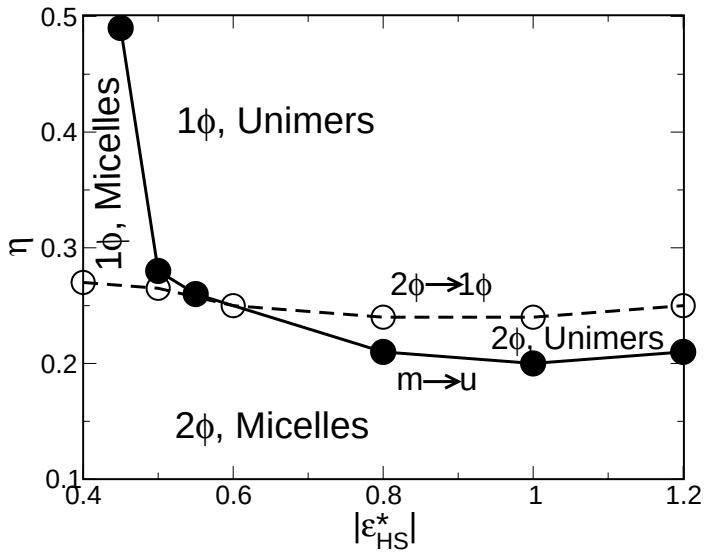

Figure 2.9: Two-phase $\rightarrow$ one-phase transition (dashed line) and micelle $\rightarrow$ unimer transition (solid line) in the packing fraction (η) $-$ head-solvent interaction strength ($|\epsilon^*_{\rm HS}|$) plane for surfactant H_4T_8 in hard-sphere solvents when $(|\epsilon^*_{\rm HH}|, |\epsilon^*_{\rm TT}|, |\epsilon^*_{\rm TS}|) = (1.0, 0.45, 0.4)$, $\phi_{\rm P} = 0.178$ and $T^* = 1.0$.

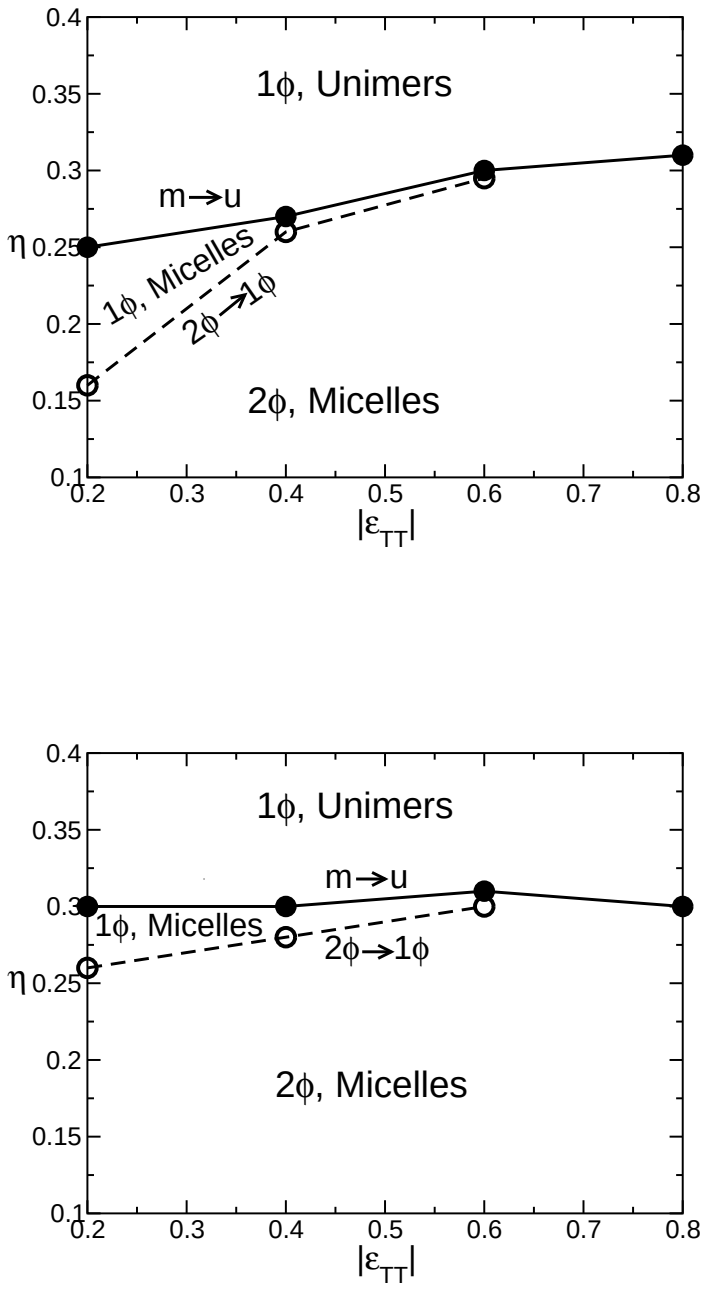

Figure 2.10: Two-phase $\rightarrow$ one-phase transition (dashed line) and micelle $\rightarrow$ unimer transition (solid line) in the packing fraction (η) $-$ tail-tail interaction strength ($|\epsilon^*_{\rm TT}|$) plane for surfactant H_4T_8 in hard-sphere solvents when $(|\epsilon^*_{\rm HH}|, |\epsilon^*_{\rm HS}|, |\epsilon^*_{\rm TS}|)$ = (a) (1.0, 0.5, 0.4) and (b) $(1.0, 0.5, 0.8)$, $\phi_{\rm P} = 0.178$ and $T^* = 1.0$.

CHAPTER 3

LCST/UCST PHASE BEHAVIOR IN POLYMER/SUPERCRITICAL SOLVENT MIXTURES: DISCONTINUOUS MOLECULAR DYNAMICS SIMULATIONS

3.1 Introduction

A supercritical fluid (SCF) is a substance at a pressure and temperature above the liquid-vapor critical point, the point at which coexisting liquid and vapor phases become indistinguishable. SCFs, especially supercritical carbon dioxide ($scCO_2$) are attractive alternatives to the organic solvents used for polymer manufacturing and processing. Practical applications involving SCFs include polymer fractionation, impregnation and purification; polymer extrusion and foaming; dispersion and emulsion polymerization; and the formation of microemulsions and emulsions. Polymer/SCF systems are often characterized by LCST (lower critical solution temperature) behavior[1,2], that is they become miscible with decreasing temperature, as opposed to UCST (upper critical solution temperature) behavior where they become miscible with in-

creasing temperature. Examples of polymer/SCF systems that exhibit LCST behavior include polyethylene in n-pentane, polystyrene in various solvents and poly(vinyl acetate) in CO_2[3–5]. Miscibility of polymers in solvents depends on the temperature, pressure, polymer concentration, molecular weight and molecular weight distribution, the polymer type and the nature of the solvent under consideration. This paper is aimed at exploring the physical conditions and parameters that give rise to the appearance of LCST phase behavior in polymer-SCF systems via computer simulations.

LCST behavior in polymer/solvent systems was first observed by Malcolm and Rowlinson[6] in 1957 in aqueous solutions of polyethylene oxide. This was explained by appealing to the high possibility of hydrogen bonding interactions between the components. Strong directional attractive interactions at temperatures below the LCST give rise to favourable heats of solutions, causing the polymer and solvent to become miscible. At temperatures above the LCST, the hydrogen bonds break, causing the solution to become unstable and to phase-separate.

A few years later in 1960, Freeman and Rowlinson[7] observed LCST behavior in solutions of hydrocarbon polymers in a hydrocarbon solvent. Extensive liquid-liquid separation was observed when the polymer and solvent were very dissimiliar in either their molecular weights or their interactions. The thermodynamic contributions that lead to LCST behaviors in mixtures of polymers and non-hydrogen bonding solvents are very different from those that give rise to LCST behaviors in mixtures of hydrogen-bonding molecules and polymers. LCST behavior in mixtures of polymers and non-hydrogen bonding solvents is a consequence of compressibility (density changes)[8–10]. As the temperature increases towards the critical point of the solvent, the solvent expands more rapidly than the polymers thus the polymer solubility decreases until phase

separation occurs.

Modeling and simulation approaches can help enhance our theoretical understanding of LCST behaviors in polymer/SCF systems. A number of equation-of-state-based theories have been used to model the phase behavior of polymers in supercritical fluids. For example, the Sanchez-Lacombe equation of state[11–13] for chain-like fluids, a compressible version of the Flory-Huggins lattice model that incorporates volume effects via vacant lattice sites, exhibits both LCST and UCST behavior, depending on the values of the segment-segment, segment-solvent and solvent-solvent interactions.

Paricaud et al.[14] used the Wertheim first-order thermodynamic perturbation theory (TPT1)[15,16] to describe the phase equilibria of model polymer/solvent systems composed of hard spheres and hard-sphere chains where the diameter of the solvent and the polymeric segments are the same (symmetrical system). The relevant thermodynamic contributions that give rise to the liquid phase instability were examined for mixtures of polymers in solvents with hydrogen-bonding interactions and for mixtures without hydrogen-bonding interactions. For the mixtures without hydrogen-bonding interactions, they studied first a purely repulsive (athermal) system and then a simple system with mean-field attractions incorporated such that the solvent-solvent, solvent-segment, and segment-segment interaction energies were all the same. No fluid-fluid phase separation (UCST or LCST) was found for the athermal systems, regardless of the polymer chain length. LCST behavior was found for the system with attractions when the 'polymer' chain length was seven segments or greater. This indicates that attractive interactions are essential in describing the liquid-liquid phase separation. They found an increase in the solvent density upon addition of small amounts of polymer leading to an unfavourable (negative) en-

tropy of mixing, which is the driving force of the phase instability. For the the mixtures with hydrogen-bonding interactions, the thermodynamic properties of mixing for a system of spherical molecules of the same size with directional interactions were determined and they found LCST and closed-loop behavior. As expected the mechanism of LCST phase separation in a system of spherical molecules of the same size with directional interactions is very different from that in polymer solutions without hydrogen-bonding interactions.

LunaBarcenas et al.[17] investigated the connection between polymer conformation and phase behavior in supercritical fluids via continuous-space Monte Carlo simulations. The polymer/SCF systems were modeled as mixtures of freely-jointed Lennard-Jones chains (component 1) in a Lennard-Jones monomeric solvent (component 2) with symmetric interactions where $\epsilon_{11} = \epsilon_{22} = \epsilon_{12}$ and $\sigma_{11} = \sigma_{22} = \sigma_{12}$. They found that the polymer conformation is a strong function of solvent quality. They observed chain collapse at low densities, suggesting that solvent quality diminishes as the solvent density decreases. This is the opposite of that observed in systems without attractive interactions[18–20]. In purely repulsive systems, chain collapse is observed at high densities, indicating that the solvent quality decreases with increasing solvent density (or equivalently, increasing pressure). The driving force for chain collapse in the absence of attractive interactions is a chain-solvent excluded volume effect. In contrast, attractive interactions seem to dominate over any excluded volume effects and completely change the dependence of solvent quality on density. LunaBarcenas et al. also found that changing the solvent density changes the amount of solvent screening the attractions between chains (i.e., segment-segment attractions). The denser the solvent, the more effective it is in screening attractive intrachain forces.

Gromov et al.[21] investigated phase equilibria in polymer-supercritical solvent mixtures via expanded Gibbs ensemble simulations. The polymer-SCF system was modeled as freely-jointed, Lennard-Jones chains (component 1, n = 16 - 64) in a Lennard-Jones monomeric solvent (component 2) with symmetric energetics, $\epsilon_{11} = \epsilon_{22} = \epsilon_{12}$, and sizes, $\sigma_{11} = \sigma_{22} = \sigma_{12}$. Both LCST and UCST behavior were observed and a closed-loop phase diagram was also observed in the supercritical regime of the solvent. Their simulations results agree with experimental observations on homopolymers in supercritical solvents.

As part of a previous study[22], we performed discontinuous molecular dynamics simulations on homopolymer/solvent systems modeled as a mixture of single-sphere solvent molecules and freely-jointed homopolymer chains (P_n) composed of n spheres (P), all of the same size. A square-well potential accounted for the segment-segment and segment-solvent interactions and both a hard-sphere potential and a square-well potential were considered for the solvent-solvent interactions. Simulations on the temperature dependence of the phase transition in homopolymer/scCO_2 systems revealed UCST behavior only in hard-sphere solvents and both UCST and LCST behavior in square-well solvents, depending upon the homopolymer chain length and the parameters of the segment-segment, segment-solvent and solvent-solvent interactions.

In this paper we explore the physical conditions and interaction parameters necessary to observe LCST behavior in homopolymer/solvent systems in more depth. We calculate the packing fraction and pressure required to dissolve homopolymers in supercritical solvents at various temperatures. We ascertain whether LCST or UCST behavior occurs by noting whether a single phase is obtained as temperature increases isobarically (UCST behavior) or phase separation

occurs as temperature increases isobarically (LCST behavior). We first simulate homopolymer/solvent systems with chain lengths $n = 8$ and 24 at various segment-segment ($|\epsilon^*_{\rm PP}|$) and segment-solvent ($|\epsilon^*_{\rm PS}|$) interaction strengths $(|\epsilon^*_{\rm PP}|, |\epsilon^*_{\rm PS}|) = (0.5, 0.25), (0.5, 0.5), (0.5, 1.0)$ and (1.0, 0.5) in hard-sphere solvents. Then we repeat the simulations at the same values of $|\epsilon^*_{\rm PP}|$ and $|\epsilon^*_{\rm PS}|$ but in square-well solvents at solvent-solvent interaction strengths ranging from $|\epsilon^*_{\rm SS}| = 0.1$ to $|\epsilon^*_{\rm SS}| = 0.5$ and interaction widths $\lambda = 0.75$ and 1.0. Both hard-sphere and square-well solvent-solvent potentials are considered in order to learn the influence of the solvent-solvent interactions on the appearance of UCST versus LCST behavior.

Highlights of our results are the following. Homopolymers always exhibit UCST behavior in hard-sphere solvents for both solvent-phobic and solvent-philic homopolymers at all chain lengths examined. In hard-sphere solvents, solvent-phobic homopolymers dissolve at high temperatures and high pressures only, but solvent-philic homopolymers dissolve at low temperatures and low pressures. Here by solvent-philic we mean homopolymers for which the segment-segment attractions are relatively weak compared to the segment-solvent attractions and by solvent-phobic we mean homopolymers for which the segment-segment attractions are relatively strong compared to the segment-solvent attractions. The pressure required to dissolve solvent-phobic homopolymers decreases with increasing temperature much faster than the pressure required to dissolve solvent-philic homopolymers, indicating that the solubility of solvent-phobic homopolymers is more strongly dependent on temperature than that of solvent-philic homopolymers. In square-well solvents, both UCST and LCST behavior are observed at strong solvent-solvent attractions but only UCST behavior is observed at weak solvent-solvent attractions in the supercritical temperature range examined. This indicates that the strong solvent-solvent at-

tractions promote the appearance of LCST behavior in homopolymer/solvent systems. As $|\epsilon^*_{\rm SS}|$ increases in square-well solvents, the packing fraction required to dissolve homopolymers increases while the pressure required to dissolve homopolymers decreases since the solvent compressibility is different at different $|\epsilon^*_{\rm SS}|$. As the solvent-solvent interaction width increases, the solvent-solvent interaction strength at which LCST behavior begins to appear decreases. Therefore the range of the interactions between solvent molecules plays an important role in the appearance of LCST behavior in homopolymer/solvent systems. Finally we find that by increasing chain length for solvent-philic homopolymers, one can switch from UCST to LCST behavior in square-well solvents.

3.2 Molecular Models and Simulation Methods

The solvent and homopolymer (P_n) molecules are modeled, respectively, as a single sphere and as a freely-jointed chain composed of n polymer spheres (P). The segment-segment and segment-solvent interactions are modeled using square-well potentials. Solvent-solvent interactions are modeled in two ways: (1) as a hard-sphere potential, as was the case in our previous study[23], and (2) as a square-well potential. The latter has the advantage that it is more realistic and allows us to investigate how the solvent-solvent interactions influence the types of phase behavior observed $-$ LCST versus UCST behavior.

The variables in our simulations are defined in the following way. The homopolymer P_n mole fraction is defined to be $X_{\mathrm{P}_n} \equiv N_{\mathrm{P}_n}/(N_{\mathrm{P}_n} + N_{\mathrm{CO}_2})$ and the homopolymer P_n volume fraction is defined to be $\phi_{\mathrm{P}_n} \equiv nN_{\mathrm{P}_n}/(nN_{\mathrm{P}_n} + N_{\mathrm{CO}_2})$, where N_i is the number of molecules of species i. The system packing fraction is defined to be $\eta \equiv \pi N_{\rm b}\sigma^3/6V$, where V is the

box volume and $N_{\rm b}$ is the number of beads in the system. In this paper, $|\epsilon_{\rm PP}|$ and $|\epsilon_{\rm PS}|$ are the segment-segment and segment-solvent interaction strengths. We choose a reference interaction strength $|\epsilon^*|$ and refer to reduced parameters for the interaction strengths as $|\epsilon^*_{\rm PP}|$ = $|\epsilon_{\rm PP}|/|\epsilon^*|$ and $|\epsilon^*_{\rm PS}|$ = $|\epsilon_{\rm PS}|/|\epsilon^*|$. The reduced temperature is defined to be $T^* \equiv {\rm k_B T}/|\epsilon^*|$, where $\rm k_B$ is Boltzmann's constant and T is the temperature.

We limit our study to packing fractions η between 0.2 and 0.5 so as to keep the solvent packing fraction greater than the critical packing fraction for a square-well fluid of width $\lambda = 0.75$ ($\eta_{\rm c} \approx 0.126$) and less than the packing fraction at which a hard-sphere fluid would undergo a transition to a solid phase. This serves to limit our study to model solvent densities that are in the supercritical or liquid regime.[23] Since solvent and homopolymer segments all have the same diameter in our model, the solvent reduced density in our simulations can be simply calculated from ${\rho_{\rm S}}^* = \phi_{\rm S}\rho^*$, where $\rho^* \equiv N_{\rm b}\sigma^3/V = 6\eta/\pi$ is the overall reduced density, and $\phi_{\rm S}$, the solvent volume fraction, is obtained from $\phi_{\rm S} = 1 - \phi_{{\rm P}_n}$.

We choose the following interaction parameters for homopolymer/solvent systems. For the square-well solvent-solvent interactions, the square-well depth, $|\epsilon^*_{\rm SS}|$, is between 0 and 0.5 and the square-well widths, $\lambda_{\rm SS}$, are 0.75 or 1.0. For the segment-segment and segment-solvent interactions, the square-well depths, $|\epsilon^*_{\rm PP}|$ and $|\epsilon^*_{\rm PS}|$, are varied between 0.25 and 1.0, in order to investigate their influence on the phase behavior; the square-well widths, $\lambda_{\rm PP}$ and $\lambda_{\rm PS}$, are 0.75. We also limit our study on the phase behavior in square-well solvents to reduced temperatures, T^*, between 0.95 and 1.05 so as to keep the temperature above the critical reduced temperature for a square-well fluid of width $\lambda = 1.0$ ($T^*_{\rm c} \approx 0.9$) but not so high as to become gas-like. This serves to limit our study to temperatures that are in the supercritical regime.

In a discontinuous molecular dynamics (DMD) simulation, particles collide when they arrive at a discontinuity in the potential, i.e. the hard-sphere diameter or the square-well width. Between collisions, particles move with linear trajectories, making DMD simulations much faster than traditional molecular dynamics simulations with continuous potentials which require a small integration time step. The post-collision velocities of particles in DMD are found by solving the collision dynamics equations analytically. To simulate chains of spheres effectively, Rapaport introduced bonds between spheres by limiting the distance between adjacent beads to be between σ and $\sigma(1+\delta)$, where δ is the bond extension parameter.[24] Later Bellemans modified this model so that the distance between adjacent spheres must lie between $\sigma(1-\delta/2)$ and $\sigma(1+\delta/2)$ which makes the average bond length equal to σ.[25] The value of δ in our simulations is 0.3.

Since we are interested in simulating at constant temperature, we use discontinuous canonical molecular dynamics (DCMD),[26–29] an adaptation of the standard microcanonical ensemble DMD technique. The DCMD technique is based on Anderson's stochastic collision method[27] and involves stochastic interaction of the system particles with imaginary constant-temperature heat bath particles. We assume that the system is immersed in a constant-temperature heat bath containing imaginary "ghost" particles. The ghost particles stabilize the system temperature by colliding with the system particles, resulting in the reassignment of particle velocities according to a Maxwell-Boltzmann distribution about the required temperature. Details of the DCMD method have been described by Gulati et al.[26] and by Zhou et al.[29]

Our DMD code was originally developed by Smith and coworkers[30] to treat entangled polymer melts. More recently, it was extended by Schultz et al.[31] to the treatment of any mixture of monomers, polymers, and/or copolymers and optimized to allow for the efficient simulation of

large multicomponent systems.

The reduced pressure, P^*, in our simulations is calculated using the virial theorem

$$P^* \equiv \frac{P\sigma^3}{\mathrm{k_B}T} = \frac{N_\mathrm{b}\sigma^3}{V} - \frac{\sigma^3 m \sum_{\mathrm{coll}} \vec{r}_{ij}\Delta\vec{v}_j}{3V\mathrm{k_B}Tt} \tag{3.1}$$

where $\mathrm{k_B}$ is Boltzmann's constant, T is the temperature, N_b is the number of beads, V is the volume, m is the mass of each segment, $\vec{r}_{ij}$ is the distance between colliding particles i and j, $\Delta\vec{v}_j = -\Delta\vec{v}_i$ is the velocity change for the particle j, $\sum_{\mathrm{coll}}$ refers to a sum over all collisions, and t is the elapsed simulation time.

A phase transition between a one-phase region and two-phase region occurs in the homopolymer/solvent systems as the packing fraction or temperature increases. In the one-phase region, the chains are evenly distributed throughout the solvent. In the two-phase region, most chains stay in the polymer-rich phase with very few chains in the solvent. The two-phase $\rightarrow$ one-phase transition in the homopolymer/solvent systems is located using snapshots of the configuration of an equilibrated system and the calculated contrast structure factors as described in our previous paper[23].

Discontinuous molecular dynamics simulations are performed in the canonical ensemble (constant N, V, T) on the homopolymer/solvent systems. In order to investigate phase separation it is necessary to consider large systems. In the interests of computational efficiency, we begin by equilibrating a small system with a random initial configuration and then enlarge the now-equilibrated small system to re-equilibrate. The small system contains 2000 solvent molecules and $18 - 54$ chains at the desired packing fraction, reduced temperature and polymer volume fraction. We first run the simulation for $20 - 30$ minutes (CPU time) to calculate the initial

aggregate size distribution; we then continue running the simulation and recalculating the size distribution several times. Once the system is equilibrated, as indicated by a lack of variation in the peak positions of the aggregate size distribution, the simulation box is replicated two times in every direction yielding 16000 solvent molecules and $144 - 432$ chains. The simulation is then continued on the large system until equilibrium is reached, as indicated by a lack of variation in the peak position for the contrast structure factor. The contrast structure factors calculated for the large system are used to determine the phase transitions. (The small system size distribution only serves to indicate whether the small system is equilibrated.) Finally, to ensure that the system size does not influence the nature of the location of the various phase transitions, we double the size of the large system and run simulations. We find that the location of the phase transition stays the same even when the size of the large system is doubled, indicating that the large system is big enough for the calculation of phase transitions.

The average CPU time needed on our 600 MHz Alpha 21164 for each state point is 2h for equilibration of the small systems, and 30h for equilibration of the large systems. At the end of this process, a snapshot of the large system displaying the distribution of chains in the solvent is taken, and the contrast structure factor is calculated to determine which phase the system is in. Phase transitions are assumed to be located at the mid-point between two different phases and are determined as a function of homopolymer volume fraction or mole fraction, system packing fraction and reduced temperature. The error bars in these calculations are based on the closest state points in the two different regions. In this paper, the error bars are shown in the figures unless they are smaller than the symbols.

3.3 Results and Discussion

3.3.1 Hard-sphere Solvent

In this section we describe our simulation results for homopolymer/solvent systems when the solvent-solvent interaction is modeled as a hard-sphere potential. The two-phase $\rightarrow$ one-phase transition is located by calculating the packing fraction and pressure required to dissolve homopolymers. This is done at different interaction parameter sets and chain lengths for various temperatures to see whether LCST behavior occurs in hard-sphere solvents.

To understand how the homopolymer interaction parameters influence the UCST versus LCST behavior in hard-sphere solvents, we locate the two-phase $\rightarrow$ one phase transition at various temperatures for several sets of interaction strengths. Figure 3.1 displays the two-phase $\rightarrow$ one-phase transition in the (a) packing fraction (η) $-$ reduced temperature (T^*) plane and (b) reduced pressure (P^*) $-$ reduced temperature (T^*) plane for homopolymer P_8 in hard-sphere solvents when $(|\epsilon^*_{PP}|, |\epsilon^*_{PS}|) = (0.5, 0.25)$, (0.5, 0.5), (0.5, 1.0) and (1.0, 0.5) at $\phi_P = 0.067$. Figure 3.1a and Figure 3.1b show that the packing fraction and pressure required to dissolve homopolymers in hard-sphere solvents always decrease with increasing temperature for the different interaction parameter sets examined. Homopolymers P_8 with $(|\epsilon^*_{PP}|, |\epsilon^*_{PS}|) = (0.5, 0.25)$, (0.5, 0.5), (0.5, 1.0) and (1.0, 0.5) exhibit UCST behavior in hard-sphere solvents since a single phase is obtained as temperature increases isobarically.

The packing fraction and pressure required to dissolve homopolymer P_8 with $(|\epsilon^*_{PP}|, |\epsilon^*_{PS}|) = (0.5, 0.25)$ are higher than those for homopolymer P_8 with $(|\epsilon^*_{PP}|, |\epsilon^*_{PS}|) = (0.5, 0.5)$, indicating that the solubility of the former homopolymer is lower than that of the latter homopolymer. It is expected that the homopolymer solubility increases as $|\epsilon^*_{PS}|$ increases.

We also find that the packing fraction and pressure required to dissolve homopolymer P_8 with $(|\epsilon^*_{PP}|, |\epsilon^*_{PS}|) = (0.5, 1.0)$ are higher than those for homopolymer P_8 with $(|\epsilon^*_{PP}|, |\epsilon^*_{PS}|) = (0.5, 0.5)$, indicating that the solubility of the former homopolymer is lower than that of the latter homopolymer. This was initially unexpected since homopolymer solubility normally increases not decreases as $|\epsilon^*_{PS}|$ increases. These two results can be understood, however, by referring to the simulation results found in our previous study[22]. Homopolymer solubility increases with increasing $|\epsilon^*_{PS}|$ when $|\epsilon^*_{PS}|$ is not too strong. However when $|\epsilon^*_{PS}|$ is very strong, solvent molecules can act as bridges between homopolymer molecules causing homopolymer molecules with solvent bridges to precipate and thereby decreasing homopolymer solubility. The segment-solvent attraction for homopolymer P_8 with $(|\epsilon^*_{PP}|, |\epsilon^*_{PS}|) = (0.5, 1.0)$ is very strong and those for $(|\epsilon^*_{PP}|, |\epsilon^*_{PS}|) = (0.5, 0.25)$ and (0.5, 0.5) are not. Thus the homopolymer solubility increases as $|\epsilon^*_{PS}|$ increases from 0.25 to 0.5 but decreases as $|\epsilon^*_{PS}|$ increases from 0.5 to 1.0.

Much higher temperatures are required to dissolve homopolymer P_8 with $(|\epsilon^*_{PP}|, |\epsilon^*_{PS}|) = (1.0, 0.5)$ in hard-sphere solvents than homopolymers with $(|\epsilon^*_{PP}|, |\epsilon^*_{PS}|) = (0.5, 0.25)$, (0.5, 0.5) and (0.5, 1.0). Homopolymer P_8 with $(|\epsilon^*_{PP}|, |\epsilon^*_{PS}|) = (1.0, 0.5)$ cannot dissolve in hard-sphere solvents at low temperatures, $T^* = (0.95 - 1.05)$, even at the highest packing fractions considered ($\eta \approx 0.5$). In contrast homopolymers P_8 with $(|\epsilon^*_{PP}|, |\epsilon^*_{PS}|) = (0.5, 0.25)$ (0.5, 0.5) and (0.5, 1.0) can dissolve at low packing fractions and low pressures. This is because the segment-segment interaction for P_8 with $(|\epsilon^*_{PP}|, |\epsilon^*_{PS}|) = (1.0, 0.5)$ is much stronger than that for $(|\epsilon^*_{PP}|, |\epsilon^*_{PS}|) = (0.5, 0.25)$, (0.5, 0.5) and (0.5, 1.0), making the former homopolymer much more solvent-phobic than the latter homopolymers. Thus higher temperatures and packing fractions or pressures are required to render the homopolymer and solvent molecules miscible.

Figure 3.1b shows that the pressures required to dissolve homopolymers P_8 with $(|\epsilon^*_{PP}|, |\epsilon^*_{PS}|) = (0.5, 0.25)$ and (1.0, 0.5) decrease with increasing temperature much faster than the pressures required to dissolve homopolymers P_8 with $(|\epsilon^*_{PP}|, |\epsilon^*_{PS}|) = (0.5, 0.5)$ and (0.5, 1.0). The former homopolymers are solvent-phobic since they require high η and P^* to dissolve and the latter homopolymers are solvent-philic since they dissolve in low η and P^*. Thus we see that solvent-phobic homopolymers exhibit much stronger temperature dependence in their solubility than solvent-philic homopolymers. The slopes of the P^* versus T^* curves for homopolymer P_8 with $(|\epsilon^*_{PP}|, |\epsilon^*_{PS}|) = (0.5, 0.25)$ and (1.0, 0.5), which are large and negative, tell us that it would be very difficult to switch the slopes from negative to positive, meaning to switch the phase behaviors from UCST to LCST, by varying the solvent-solvent interaction parameters. However the slopes of the P^* versus T^* curves for homopolymers P_8 with $(|\epsilon^*_{PP}|, |\epsilon^*_{PS}|) = (0.5, 0.5)$ and (0.5, 1.0) are small and negative, indicating that it might be possible to switch the slopes of the P^* versus T^* curves from negative to positive, causing LCST behavior instead of UCST behavior. These two interaction parameter sets are chosen for further investigation on how to promote LCST behaviors for homopolymers in both hard-sphere and square-well solvents.

Next we investigate whether increasing chain length can switch UCST behavior to LCST behavior for homopolymers in hard-sphere solvents. Figure 3.2 shows the two-phase $\rightarrow$ one-phase transition in the (a) packing fraction (η) $-$ reduced temperature (T^*) plane and (b) reduced pressure (P^*) $-$ reduced temperature (T^*) plane for homopolymers P_8 and P_{24} in hard-sphere solvents when $(|\epsilon^*_{PP}|, |\epsilon^*_{PS}|) = (0.5, 0.5)$ at $\phi_P = 0.067$. The interaction parameter set $(|\epsilon^*_{PP}|, |\epsilon^*_{PS}|) = (0.5, 0.5)$ was chosen because, as described above, we thought it would be possible to switch the slope of the P^* versus T^* curve from negative to positive (causing LCST

behavior instead of UCST behavior) by changing a parameter, in this case the chain length. We see that both homopolymers P_8 and P_{24} exhibit UCST behavior and that the slopes of P^* versus T^* for homopolymers P_8 and P_{24} are quite similiar, indicating that the temperature dependence of the phase transition for homopolymers P_8 and P_{24} is similiar. We also find that the packing fraction and pressure required to dissolve homopolymer P_{24} are higher than those for homopolymer P_8. This is because the solubility of a long chain is lower than that of a short chain, as discussed in our previous study[23].

Finally we look at how the packing fraction and pressure required to dissolve homopolymers at fixed temperature vary as homopolymer chain length increases. Figure 3.3 displays the two-phase $\rightarrow$ one-phase transition in the (a) packing fraction (η) $-$ chain length (n) plane and (b) reduced pressure (P^*) $-$ chain length (n) plane for homopolymers P_8, P_{12}, P_{16} and P_{24} in hard-sphere solvents when $(|\epsilon^*_{\rm PP}|, |\epsilon^*_{\rm PS}|) = (0.5, 0.5)$ at $\phi_{\rm P} = 0.067$ and $T^* = 1.0$. We find that the pressure required to dissolve homopolymers is sensitive to homopolymer chain length. This is in qualitative agreement with the simulation results by Gromov et al.[21] on the dependence of the demixing pressure on chain length in homopolymer/supercritical solvents systems modeled with Lennard-Jones potentials. It is also consistent with experimental observations for the the dependence of the demixing pressure on polymer molecular weight for poly(ethylene-propylene) in butene when the molecular weight is below 20000.[3]

3.3.2 Square-well Solvent

In this section, we investigate how the values of the solvent-solvent interaction parameters influence the UCST versus LCST behavior in square-well solvents. We locate the two-phase $\rightarrow$

one-phase transition at various temperatures in square-well solvents with various solvent-solvent interaction parameters, including interaction strength and interaction width. In this way, we can find when and where LCST behavior occurs in square-well solvents.

To determine whether homopolymers exhibit LCST behavior in square-well solvents, we measure the packing fraction and pressure of the phase transition at various temperatures for homopolymers in square-well solvents with different values of $|\epsilon^*_{\rm SS}|$. Figure 3.4 displays the two-phase $\rightarrow$ one-phase transition in the (a) packing fraction (η) $-$ reduced temperature (T^*) plane and (b) reduced pressure (P^*) $-$ reduced temperature (T^*) plane for homopolymer P_8 with $(|\epsilon^*_{\rm PP}|, |\epsilon^*_{\rm PS}|) = (0.5, 0.5)$ in hard-sphere solvents ($|\epsilon^*_{\rm SS}| = 0$) and in square-well solvents at $|\epsilon^*_{\rm SS}|$ ranging from 0.2 to 0.5, $\lambda_{\rm SS}$ = 0.75 and $\phi_{\rm P} = 0.067$.

Figure 3.4a shows that the packing fraction required to dissolve homopolymers decreases with increasing temperature in all of the solvents examined. Figure 3.4b shows that the pressure required to dissolve the homopolymer decreases with increasing temperature in hard-sphere solvents and in square-well solvents with $|\epsilon^*_{\rm SS}| = 0.2$ and 0.4, and both increases and decreases (depending upon the temperature range considered) in square-well solvents with $|\epsilon^*_{\rm SS}| = 0.5$. In the hard-sphere solvent and the square-well solvents with $|\epsilon^*_{\rm SS}| = 0.2$ and 0.4, homopolymer P_8 exhibits UCST behavior for all temperatures examined ($T^* = 0.8 - 1.05$) since a single phase is obtained as temperature increases isobarically. In the square-well solvent with $|\epsilon^*_{\rm SS}| = 0.5$, homopolymer P_8 exhibits LCST behavior for $T^* = 0.85 - 1.0$, since a phase separation occurs as temperature increases isobarically, and exhibits UCST behavior at $T^* = 1.0 - 1.05$, since a single phase is obtained as temperature increases isobarically. Thus we find closed loop phase behavior for homopolymer P_8 with $(|\epsilon^*_{\rm PP}|, |\epsilon^*_{\rm PS}|) = (0.5, 0.5)$ in square-well solvents when $|\epsilon^*_{\rm SS}| = 0.5$

since LCST and UCST behavior occur at low and high temperatures, respectively. This is in qualitative agreement with the simulation results by Gromov et al[21] on the polymer-SCF system modeled as a mixture of freely-jointed Lennard-Jones chains (n = 16) and Lennard-Jones monomeric solvents with symmetric energetics ($|\epsilon^*_{11}| = |\epsilon^*_{22}| = |\epsilon^*_{12}|$ and $\sigma_{11} = \sigma_{22} = \sigma_{12}$).

Figure 3.4 also shows that LCST behavior is observed in square-well solvents with strong solvent-solvent attractions but not in the square-well solvents with weak solvent-solvent attractions. This indicates that the strong solvent-solvent interaction strengths promote the appearance of LCST behavior in homopolymer/solvent systems.

An interesting phenomenon is found by comparing Figure 3.4a and Figure 3.4b. As $|\epsilon^*_{\rm SS}|$ increases from 0.2 to 0.5, the packing fraction required to dissolve homopolymers increases but the pressure required to dissolve homopolymers decreases. This can be explained in the following way. The miscibility between homopolymer molecules and solvent molecules decreases as $|\epsilon^*_{\rm SS}|$ increases. As discussed in our previous study[23], increasing the packing fraction serves to increasing the solvent's ability to dissolve homopolymers in square-well solvents when $|\epsilon^*_{\rm PS}|$ is not too low. Thus higher packing fractions are needed to increase the miscibility between homopolymer molecules and solvent molecules as $|\epsilon^*_{\rm SS}|$ increases. It is known that the pressure of square-well solvents with strong solvent-solvent attractions is lower than that with weak solvent-solvent attractions when the packing fractions of these square-well solvents are the same. In other words, lower pressure is needed to compress the solvent with strong $|\epsilon^*_{\rm SS}|$ to the same packing fraction as that with weak $|\epsilon^*_{\rm SS}|$. Thus at strong $|\epsilon^*_{\rm SS}|$ homopolymers can dissolve in the solvent when the pressure is lower than that at weak $|\epsilon^*_{\rm SS}|$ if the packing fractions at weak $|\epsilon^*_{\rm SS}|$ and strong $|\epsilon^*_{\rm SS}|$ are the same.

The packing fraction required to dissolve homopolymers in hard-sphere solvents is the same as that required to dissolve homopolymers in square-well solvents with $|\epsilon^*_{\rm SS}|$ = 0.2, but the pressures are different over the temperature range $T^* = 0.9 - 1.0$. This indicates that the pressure required to dissolve homopolymers is more sensitive to the solvent-solvent interaction strength than the packing fraction is when the attraction between solvent molecules is weak or zero.

We can also look at how the range of the square-well potential, $\lambda_{\rm SS}$, affects the LCST versus UCST behavior in homopolymer/solvent systems. Figure 3.5 displays the two-phase $\rightarrow$ one-phase transition in the (a) packing fraction (η) $-$ reduced temperature (T^*) plane and (b) reduced pressure (P^*) $-$ reduced temperature (T^*) plane for homopolymer P_8 with $(|\epsilon^*_{\rm PP}|, |\epsilon^*_{\rm PS}|) = (0.5, 0.5)$ in square-well solvents with various $|\epsilon^*_{\rm SS}|$ = 0.1, 0.2 and 0.3 when $\lambda_{\rm SS}$ = 1.0 at $\phi_{\rm P} = 0.067$. There is no data for $|\epsilon^*_{\rm SS}|$ = 0.4 and 0.5 shown in Figure 3.5 since homopolymers cannot dissolve in the solvent at those $|\epsilon^*_{\rm SS}|$ values, even at the highest packing fraction considered ($\eta \approx 0.5$) at $\lambda_{\rm SS} = 1.0$.

A comparison between Figure 3.5 (at $\lambda_{\rm SS}$ = 1.0) and Figure 3.4 (at $\lambda_{\rm SS}$ = 0.75) shows that LCST behavior occurs in square-well solvents at lower values of $|\epsilon^*_{\rm SS}|$ as $\lambda_{\rm SS}$ increases ($|\epsilon^*_{\rm SS}|$ = 0.3 at $\lambda_{\rm SS}$ =1.0 and $|\epsilon^*_{\rm SS}|$ = 0.5 at $\lambda_{\rm SS}$ = 0.75), indicating that a homopolymer can exhibit LCST behavior in square-well solvents with weaker $|\epsilon^*_{\rm SS}|$ if the solvent-solvent interaction range is larger. Increasing the interaction range at fixed interaction strength results in a stronger attraction beween molecules. Therefore the interaction range of solvent-solvent attractions also contributes to the appearance of LCST behavior.

Finally we explore how the LCST versus UCST behavior in square-well solvents varies for homopolymers with different chain lengths and interaction parameters $(|\epsilon^*_{\rm PP}|, |\epsilon^*_{\rm PS}|)$, as we

have done for homopolymers in hard-sphere solvents. Figure 3.6 displays the two-phase $\rightarrow$ one-phase transition in the (a) packing fraction (η) $-$ reduced temperature (T^*) plane and (b) reduced pressure (P^*) $-$ reduced temperature (T^*) plane for homopolymers P_8 in square-well solvents when $(|\epsilon^*_{PP}|, |\epsilon^*_{PS}|) = (0.5, 0.5)$ and (0.5, 1.0), $|\epsilon^*_{SS}|$ = 0.15 and λ_{SS} = 1.0 at $\phi_P = 0.067$. Figure 3.7 displays the simulation results for homopolymer P_{24} at the same conditions as in Figure 3.6.

Figure 3.6b shows that homopolymers P_8 with $(|\epsilon^*_{PP}|, |\epsilon^*_{PS}|) = (0.5, 0.5)$ and (0.5, 1.0) exhibit only UCST behavior in square-well solvents since a single phase is obtained as temperature increases isobarically. Homopolymers P_{24} with $(|\epsilon^*_{PP}|, |\epsilon^*_{PS}|) = (0.5, 0.5)$ and (0.5, 1.0) exhibit UCST behavior in square-well solvents at $T^* = 0.95 - 1.0$ since a single phase is obtained as temperature increases isobarically and exhibit LCST behavior in square-well solvents at $T^* = 1.0 - 1.05$ since a phase separation occurs as temperature increases isobarically. In this case, we do not find closed loop behavior. Instead we see UCST behavior at low temperatures and LCST behavior at high temperatures.

A comparison between Figure 3.7 and Figure 3.6 shows that homopolymer P_8 exhibits UCST behavior only, and in contrast, homopolymer P_{24} exhibits both LCST and UCST behavior (depending upon the temperature range considered) when $(|\epsilon^*_{PP}|, |\epsilon^*_{PS}|) = (0.5, 0.5)$ and (0.5, 1.0). These homopolymers with the above interaction parameter sets are solvent-philic since their segment-segment attractions are not strong compared to the segment-solvent attractions. Thus we see that one can switch from UCST to LCST behavior by increasing the chain length for solvent-philic homopolymers.

3.4 Summary and Discussion

In this study, we performed DMD simulations for homopolymer/solvent systems to explore the physical conditions and parameters that give rise to the appearance of LCST behavior in polymer-SCF systems. We investigated the dependence of the two-phase $\rightarrow$ one-phase transition on the packing fraction, temperature and pressure for homopolymers in hard-sphere solvents and in square-well solvents by using the simple model developed in our previous study[22,23]. Phase diagrams were constructed for homopolymers with various interaction strengths and chain lengths in hard-sphere solvents and square-well solvents with various solvent-solvent interaction strengths and interaction widths. The appearance of LCST behavior depends upon the homopolymer interaction strengths, chain length and solvent-solvent interaction parameters.

In hard-sphere solvents, homopolymers always exhibit UCST behavior for both solvent-phobic homopolymers and solvent-philic homopolymers at all chain lengths examined. Solvent-phobic homopolymers dissolve at high temperatures and high pressures only, but solvent-philic homopolymers can dissolve at low temperatures and low pressures. Here by solvent-philic we mean homopolymers for which the segment-segment attractions are relatively weak compared to the segment-solvent attractions and by solvent-phobic we mean homopolymers for which the segment-segment attractions are relatively strong compared to the segment-solvent attractions. The pressure required to dissolve solvent-phobic homopolymers decreases with increasing temperature much faster than the pressure required to dissolve solvent-philic homopolymers, indicating that the solubility of solvent-phobic homopolymers is more strongly dependent on temperature than that of solvent-philic homopolymers. The packing fraction and pressure required to dissolve homopolymers in hard-sphere solvents increase as homopolymer chain length

increases and are sensitive to homopolymer chain length, in qualitative agreement with the simulation results on the dependence of the demixing pressure on polymer chain length by Gromov et al.[21] and experimental observations for the demixing pressure dependence on polymer molecular weight for poly(ethylene-propylene) in butene[3].

In square-well solvents, homopolymers can exhibit LCST behavior depending upon the solvent-solvent interaction parameters, homopolymer chain length and interaction strengths, and the temperature range considered. LCST behavior is observed at strong solvent-solvent attractions but not at weak solvent-solvent attractions. This indicates that strong solvent-solvent attractions promote the appearance of LCST behavior in homopolymer/solvent systems. LCST and UCST behavior at low and high temperature are observed, indicating that closed-loop behavior occurs for homopolymer P_8 with $|\epsilon^*_{\rm PP}|, |\epsilon^*_{\rm PS}|$ = (0.5, 0.5) when $|\epsilon^*_{\rm SS}|$ = 0.5 and $|\lambda_{\rm SS}|$ = 0.75. This is in qualitative agreement with the simulation results on the phase behavior of polymer-SCF systems by Gromov et al[21]. Homopolymers exhibit LCST behavior at weaker solvent-solvent interaction strengths as the solvent-solvent interaction width is increased. Increasing the interaction range at fixed interaction strength results in a stronger attraction between solvent molecules. Therefore the interaction range between solvent molecules plays an important role in the appearance of LCST behavior in homopolymer/solvent systems. Finally we find that by increasing chain length for solvent-philic homopolymers, one can switch from UCST to LCST behavior in square-well solvents.

3.5 Acknowledgements

The material is based upon work supported by the STC Program of the National Science Foundation under Agreement No. CHE-9876674. Acknowledgment is made to the Office of Energy Research, Basic Sciences, Chemical Science Division of the U. S. Department of Energy under Contract No. DE-FG05-91ER14181 for partial support of this work. Z. Li thanks A. J. Schultz for fruitful discussions and many valuable suggestions.

3.6 References

[1] M. A. Meilchen, B. M. Hasch, and M. A. Mchugh, “Effect of copolymer composition on the phase-behavior of mixtures of poly(ethylene-co-methyl acrylate) with propane and chlorodifluoromethane,” *Macromolecules* **24**, 4974 (1991).

[2] S. Mawson, K. P. Johnston, J. R. Combes, and J. M. DeSimone, “Formation of poly(1,1,2,2-tetrahydroperfluorodecyl acrylate) submicron fibers and particles from supercritical carbon-dioxide solutions,” *Macromolecules* **28**, 3182 (1995).

[3] S. J. Chen, I. G. Economou, and M. Radosz, “Density-tuned polyolefin phase equilibria. 2. Multicomponent solutions of alternating poly(ethylene-propylene) in subcritical and super-critical olefins. Experiment and SAFT model,” *Macromolecules* **25**, 4987 (1992).

[4] A. C. Bae, S. M. Lambert, D. S. Soane, and J. M. Prausnitz, “Cloud-point curves of polymer-solutions from thermooptic measurements,” *Macromolecules* **24**, 4403 (1991).

[5] F. Rindfleisch, T. P. DiNoia, and M. A. McHugh, “Solubility of polymers and copolymers in supercritical CO_2,” *J. Phys. Chem.* **100**, 15581 (1996).

[6] G. N. Malcolm and J. S. Rowlinson, “The thermodynamic properties of aqueous solutions of polyethylene glycol, polypropylene glycol and dioxane,” *Trans. Faraday Soc.* **53**, 921 (1957).

[7] P. J. Freeman and J. S. Rowlinson, “Lower critical points in polymer solutions,” *Polymer* **1**, 20 (1960).

[8] D. Patterson, “Free volume and polymer solubility. a qualitative view,” *Macromolecules* **2**, 672 (1969).

[9] L. P. McMaster, “Aspects of polymer-polymer thermodynamics,” *Macromolecules* **6**, 760 (1973).

[10] D. Patterson, “Polymer compatibility with and without a solvent,” *Polym. Eng. Sci.* **22**, 64 (1982).

[11] S. M. Lambert, Y. Song, and J. M. Prausnitz, *Equations of state for fluids and fluid mixtures, Vol. 2* (Elsevier, Amsterdam, 2000).

[12] I. C. Sanchez and R. H. Lacombe, “Elementary molecular theory of classical fluids - pure fluids,” *J. Phys. Chem.* **80**, 2352 (1976).

[13] I. C. Sanchez and R. H. Lacombe, “Statistical thermodynamics of polymer-solutions,” *Macromolecules* **11**, 1145 (1978).

[14] P. Paricaud, A. Galindo, and G. Jackson, “Understanding liquid-liquid immiscibility and LCST behaviour in polymer solutions with a Wertheim TPT1 description,” *Mol. Phys.* **101**, 2575 (2003).

[15] M. S. Wertheim, “Thermodynamic perturbation-theory of polymerization,” *J. Chem. Phys.* **87**, 7323 (1987).

[16] W. G. Chapman, G. Jackson, and K. E. Gubbins, “Phase-equilibria of associating fluids chain molecules with multiple bonding sites,” *Mol. Phys.* **65**, 1057 (1988).

[17] G. LunaBarcenas, D. G. Gromov, J. C. Meredith, I. C. Sanchez, J. J. dePable, and K. P. Johnston, "Polymer chain collapse near the lower critical solution temperature," *Chem. Phys. Lett.* **278**, 302 (1997).

[18] M. Dijkstra, D. Frenkel, and J. P. Hansen, "Phase-separation in binary hard-core mixtures," *J. Chem. Phys.* **101**, 3179 (1994).

[19] G. LunaBarcenas, G. E. Bennett, I. C. Sanchez, and K. P. Johnston, "Monte Carlo simulation of polymer chain collapse in athermal solvents," *J. Chem. Phys.* **104**, 9971 (1996).

[20] J. K. C. Suen, F. A. Escobedo, and J. J. dePablo, "Monte Carlo simulation of polymer chain collapse in an athermal solvent," *J. Chem. Phys.* **106**, 1288 (1977).

[21] D. G. Gromov, J. J. de Pablo, G. Luna-Barcenas, I. C. Sanchez, and K. P. Johnston, "Simulation of phase eequilibria for polymer-supercritical solvent mixtures," *J. Chem. Phys.* **108**, 4647 (1998).

[22] Z. Li and C. K. Hall, "Parametric studies of interaction strengths on polymer/CO_2 systems: discontinuous molecular dynamics simulations," *In preparation* .

[23] Z. Li and C. K. Hall, "Phase behavior in model homopolymer/CO_2 and surfactant/CO_2 systems: discontinuous molecular dynamics simulations," *Langmuir* .

[24] D. C. Rapaport, "Molecular dynamics study of a polymer chain," *J. Chem. Phys.* **71**, 3299 (1979).

[25] A. Bellemans, J. Orban, and D. V. Belle, "Molecular dynamics of rigid and non-rigid necklaces of hard disks," *Mol. Phys.* **39**, 781 (1980).

[26] H. S. Gulati and C. K. Hall, “Fluids and fluid mixtures containing square-well diatomics: Equations of state and canonical molecular dynamics simulation,” *J. Chem. Phys.* **107**, 3930 (1997).

[27] H. C. Anderson, “Molecular-dynamics simulations at constant pressure and-or temperature,” *J. Chem. Phys.* **72**, 2384 (1980).

[28] Y. Zhou, C. K. Hall, and M. Karplus, “First-order disorder-to-order transition in an isolated homopolymer model,” *Phys. Rev. Lett.* **77**, 2822 (1996).

[29] Y. Zhou, M. Karplus, J. M. Wichert, and C. K. Hall, “Equilibrium thermodynamics of homopolymers and clusters: Molecular dynamics and Monte Carlo simulations of systems with square-well interactions,” *J. Chem. Phys.* **107**, 10691 (1997).

[30] S. W. Smith, B. D. Freeman, and C. K. Hall, “Discontinuous molecular dynamics for polymeric fluids.,” *J. Comput. Phys.* **134**, 16 (1997).

[31] A. J. Schultz, C. K. Hall, and J. Genzer, “Computer simulation of copolymer phase behavior,” *J. Chem. Phys.* **117**, 10329 (2002).

3.7 Figures

Page

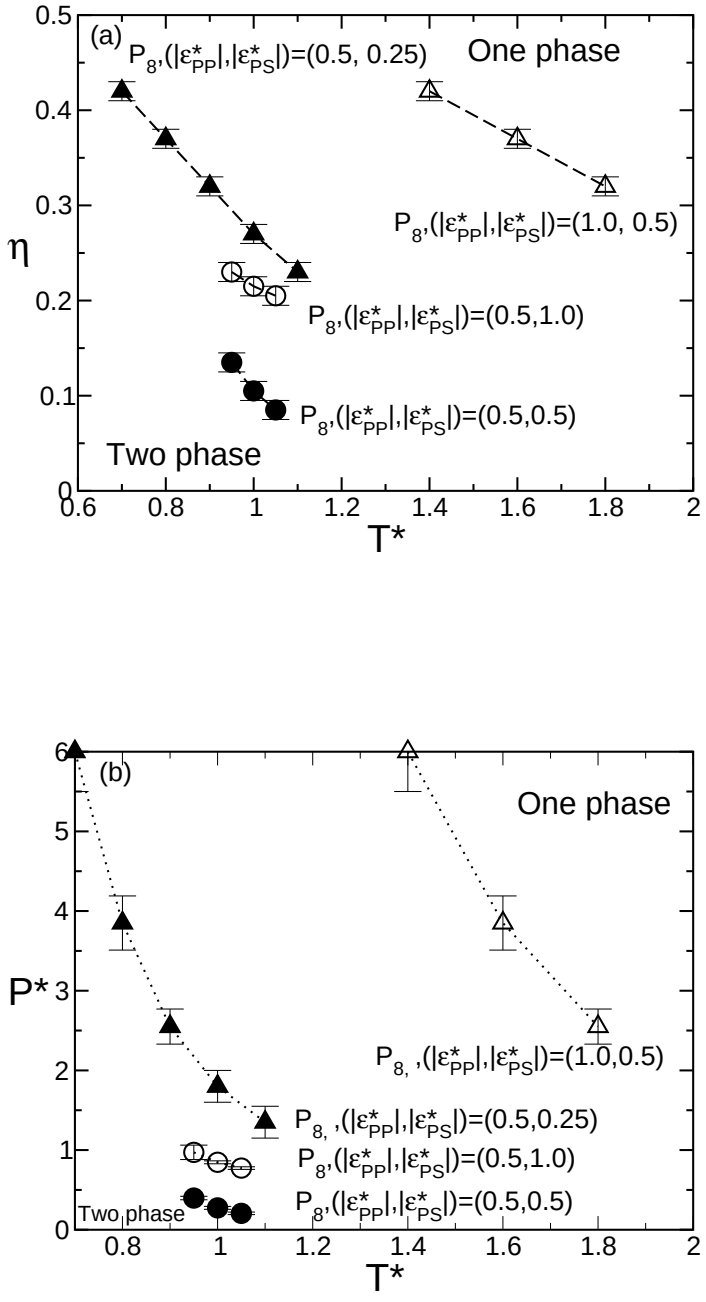

Figure 3.1: Phase transition in the (a) packing fraction (η) - reduced temperature (T^*) plane and (b) reduced pressure (P^*) - reduced temperature (T^*) plane for homopolymer P_8 with $(|\epsilon^*_{PP}|, |\epsilon^*_{PS}|) = (0.5, 0.25), (0.5, 0.5)$, (0.5, 1.0) and (1.0, 0.5) in hard-sphere solvents at $\phi_P = 0.067$.

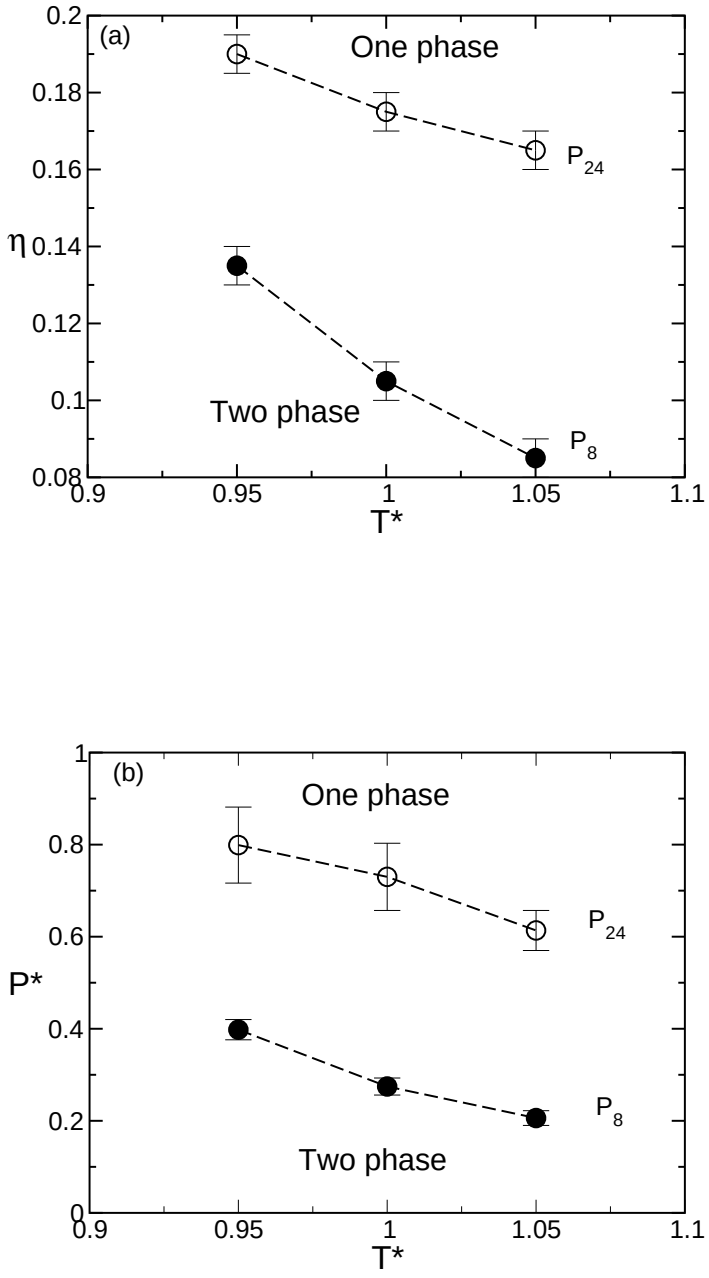

Figure 3.2: Phase transition in the (a) packing fraction (η) - reduced temperature (T^*) plane and (b) reduced pressure (P^*) - reduced temperature (T^*) plane for homopolymers P_8 and P_{24} with $(|\epsilon^*_{PP}|, |\epsilon^*_{PS}|) = (0.5, 0.5)$ in hard-sphere solvents at $\phi_P = 0.067$.

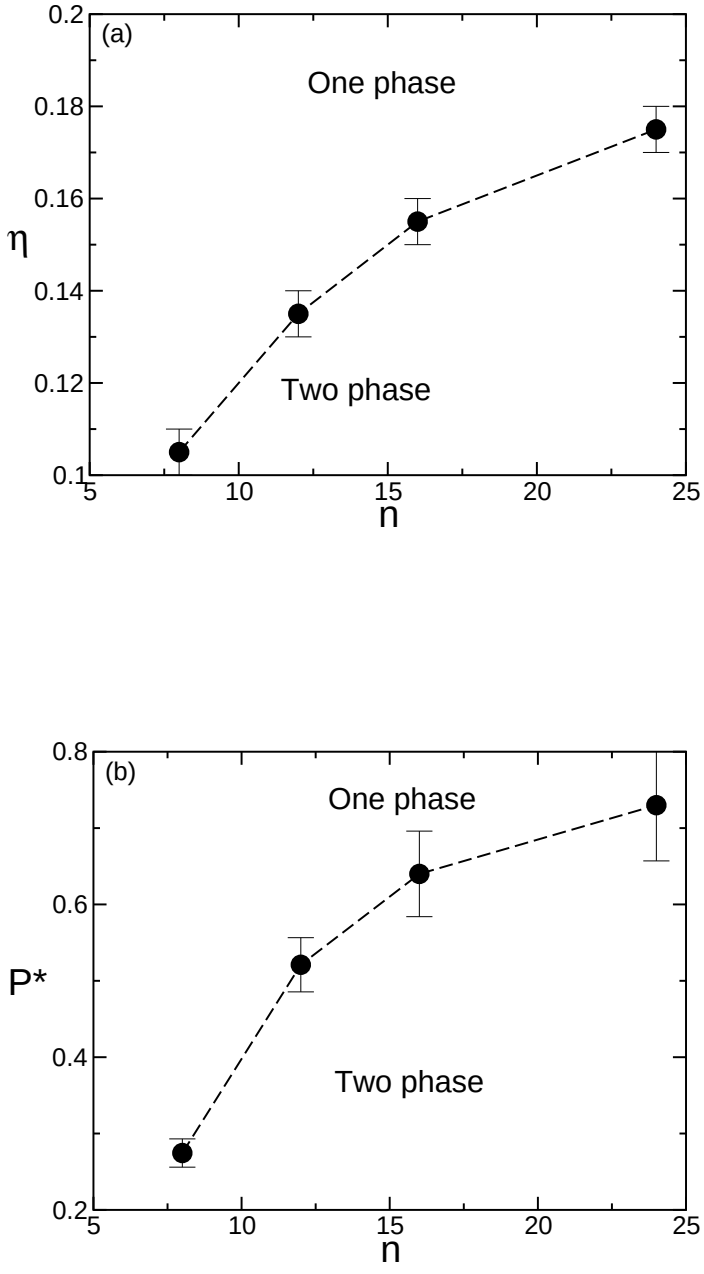

Figure 3.3: Phase transition in the (a) packing fraction (η) - chain length (n) plane and (b) reduced pressure (P^*) - chain length (n) plane for homopolymers P_8, P_{12}, P_{16} and P_{24} with $(|\epsilon^*_{PP}|, |\epsilon^*_{PS}|) = (0.5, 0.5)$ in hard-sphere solvents at $\phi_P = 0.067$ and $T^* = 1.0$.

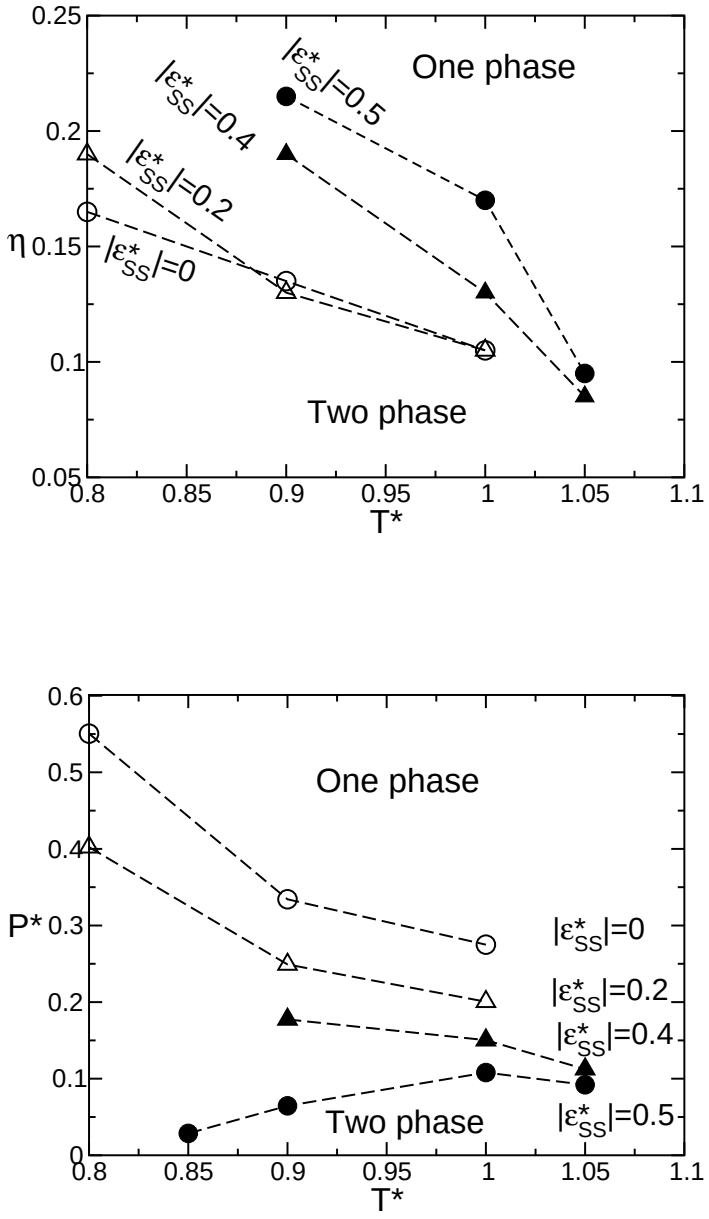

Figure 3.4: Phase transition in the (a) packing fraction (η) - reduced temperature (T^*) plane and (b) reduced pressure (P^*) - reduced temperature (T^*) plane for homopolymer P_8 in hard-sphere solvents and square-well solvents when $(|\epsilon^*_{\rm PP}|, |\epsilon^*_{\rm PS}|) = (0.5, 0.5)$, $|\epsilon^*_{\rm SS}| = 0.2, 0.4$ and 0.5, $\lambda_{\rm SS} = 0.75$ and $\phi_{\rm P} = 0.067$.

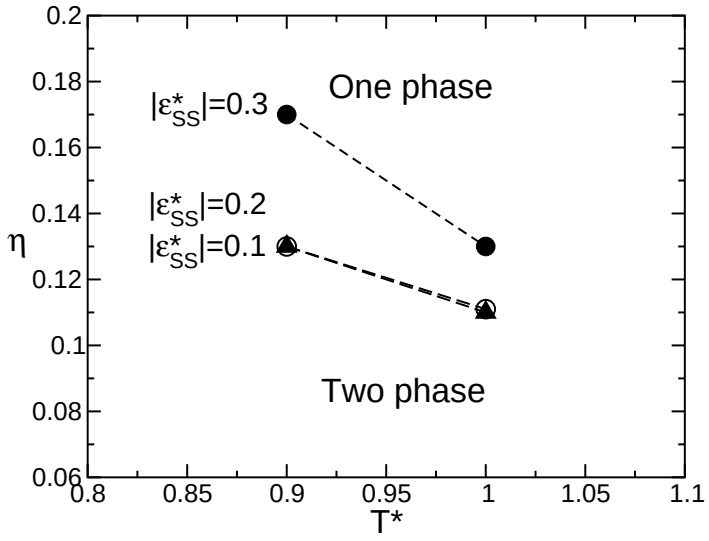

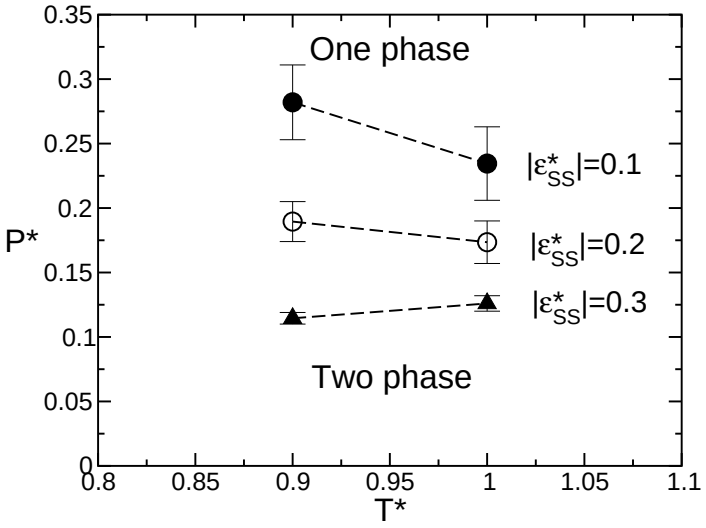

Figure 3.5: Phase transition in the (a) packing fraction (η) - reduced temperature (T^*) plane and (b) reduced pressure (P^*) - reduced temperature (T^*) plane for homopolymer P_8 in square-well solvents when $(|\epsilon^*_{\rm PP}|, |\epsilon^*_{\rm PS}|) = (0.5, 0.5)$, $|\epsilon^*_{\rm SS}| = 0.1, 0.2$ and 0.3, $\lambda_{\rm SS} = 1.0$ and $\phi_{\rm P} = 0.067$.

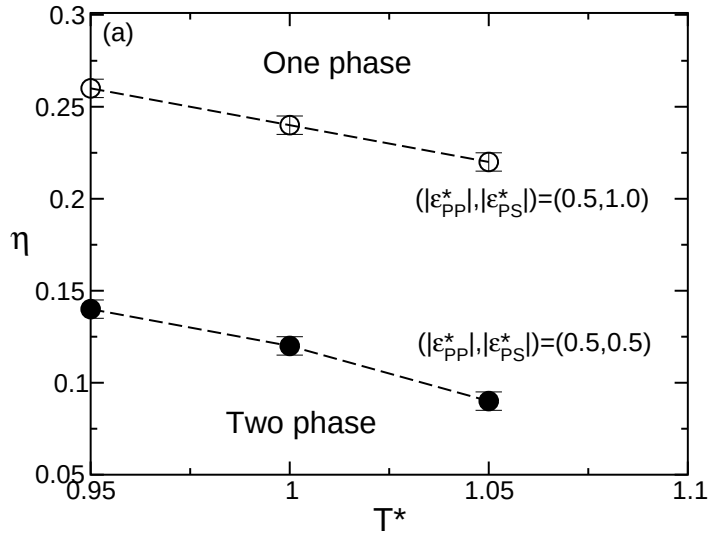

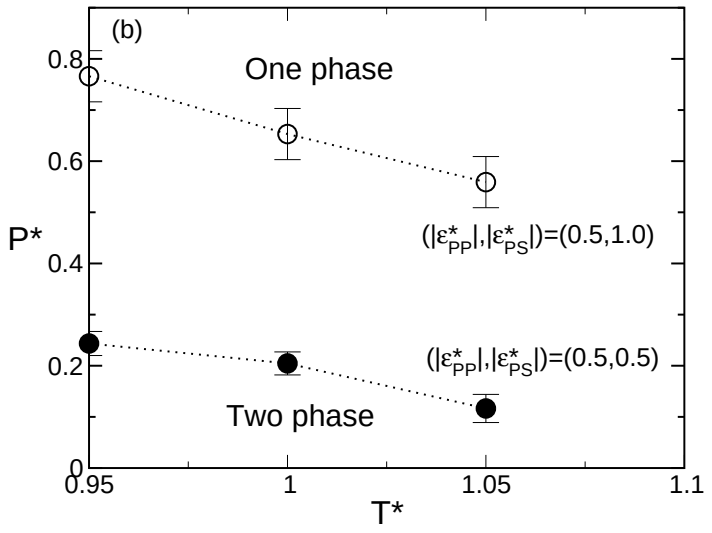

Figure 3.6: Phase transition in the (a) packing fraction (η) - reduced temperature (T^*) plane and (b) reduced pressure (P^*) - reduced temperature (T^*) plane for homopolymer P_8 in square-well solvents when $(|\epsilon^*_{\rm PP}|, |\epsilon^*_{\rm PS}|) = (0.5, 0.5)$ and (0.5, 1.0), $|\epsilon^*_{\rm SS}| = 0.15$, $\lambda_{\rm SS} = 1.0$ and $\phi_{\rm P} = 0.067$.

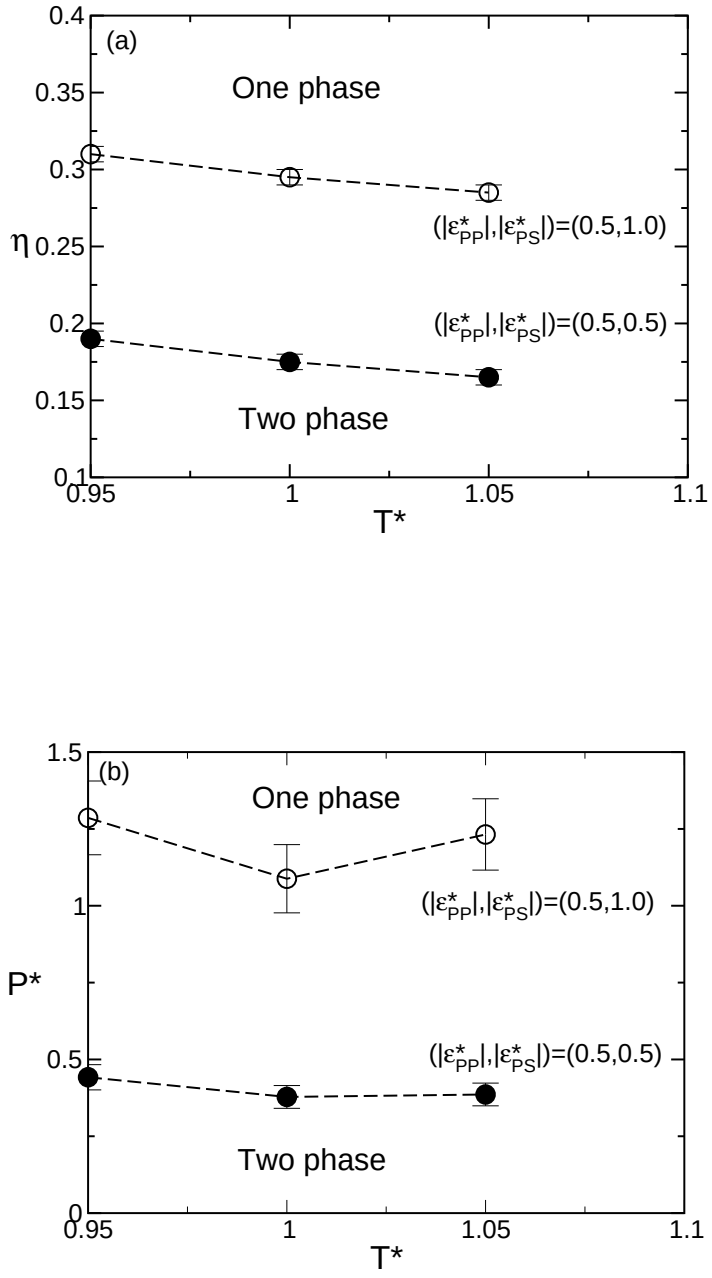

Figure 3.7: Phase transition in the (a) packing fraction (η) - reduced temperature (T^*) plane and (b) reduced pressure (P^*) - reduced temperature (T^*) plane for homopolymer P_{24} in square-well solvents when $(|\epsilon^*_{\rm PP}|, |\epsilon^*_{\rm PS}|) = (0.5, 0.5)$ and (0.5, 1.0), $|\epsilon^*_{\rm SS}| = 0.15$, $\lambda_{\rm SS} = 1.0$ and $\phi_{\rm P} = 0.067$.

CHAPTER 4

FUTURE WORK

We are currently working to extend our previous simulations on homopolymer/solvent and surfactant/solvent systems to longer chain lengths. We have found some important results for homopolymers P_n (n = 8 - 24). In hard-sphere solvents, homopolymers always exhibit UCST behavior for all chain lengths we have examined. By doing simulations on even longer homopolymer chains (P_{48} and P_{72}) in hard-sphere solvents, we will learn whether the findings in our previous simulations also apply to long chains. In square-well solvents, homopolymers exhibit UCST behavior at weak solvent-solvent interaction strengths and exhibit both UCST and LCST behavior at strong solvent-solvent interaction strengths. We will find how the solvent-solvent interaction parameters at the transition from UCST to LCST change with increasing chain length for homopolymers with various interaction parameter sets ($|\epsilon^*_{\rm PP}|, |\epsilon^*_{\rm PS}|$). Our simulation results on surfactant (H_4T_8)/solvent systems show that at strong head-solvent attractions the micelle $\rightarrow$ unimer transition occurs in the two-phase region, which is interesting but not observed experimentally. By doing simulations on longer surfactant chains (H_8T_{16} and $H_{16}T_{32}$) we will find out whether this phenomenon is just an artefact of the short chain lengths considered or whether it has a deeper physical meaning.

In addition to investigating longer chains in solvents, we would like to investigate how

the size of each unit (polymer segment and solvent molecule) affects the phase behavior of polymer/solvent systems. Thus far the polymer segments and solvent molecules in our model polymer/solvent systems have had the same diameter for simplificity. However, in reality, the size of a polymer segment is bigger than that of a CO_2 molecule. We will vary the ratio of the diameters of the homopolymer segment and solvent molecule to be $1.5:1$, $2:1$ and $3:1$ for homopolymer/solvent systems and the ratio of the diameters of the head bead, tail bead and solvent molecule to be $1.5:2:1$ and $2:3:1$ for surfactant/solvent systems. Motivation for these parameters is that polymer segments in $scCO_2$ systems are composed of a number of groups (i.e. CH_2, CF_2, etc.). We will perform simulations for polymer/solvent systems with these different unit sizes and construct phase diagrams in the $|\epsilon^*_{\rm PP}| - |\epsilon^*_{\rm PS}|$ plane for homopolymer P_8 at η = 0.2 and 0.4 and fixed $\phi_{\rm P}$ and T^*. We will also construct phase diagrams in the $\eta - |\epsilon^*_{\rm HS}|$ plane for surfactant H_4T_8 again holding $\phi_{\rm H_4T_8}$ and T^* fixed. Thus we can find out whether or not the effect of varying interaction strengths on phase transitions is sensitive to the relative size of polymer segments and solvent molecules.

Appendices

APPENDIX A

PHASE BEHAVIOR IN MODEL HOMOPOLYMER/CO_2 AND SURFACTANT/CO_2 SYSTEMS: DISCONTINUOUS MOLECULAR DYNAMICS SIMULATIONS

A.1 Introduction

Supercritical carbon dioxide ($scCO_2$) has received a great deal of scientific and industrial attention as a potential alternative to organic solvents because it is environmentally benign[1] and the temperature and pressure ranges for its operation are easily accessible ($T_c = 31^oC$, $P_c = 73.8$ bar). An additional attractive feature of $scCO_2$ as a solvent is that solute solubility can be controlled by varying pressure as well as temperature due to $scCO_2$'s high compressibility. However, $scCO_2$ is a poor solvent for nonvolatile polar molecules and polymers; the only polymers that readily dissolve in $scCO_2$ are fluorinated or silicon-based.[2–7] This makes it necessary to use surfactants to assist in the solvation process, prompting the need for a better theoretical understanding of the behavior of surfactants in compressible solvents. During the last decade, a great deal of experimental effort has been devoted to the study of surfactants in $scCO_2$.[8–14] In comparison, there have been relatively few attempts to use molecularly-based theory or computer simulation

to understand the solvation of surfactants in $scCO_2$.[15–21] This study is aimed at developing a simple model to use in exploring phase behavior and micellization in homopolymer/$scCO_2$ systems and surfactant/$scCO_2$ systems. The long-term goal of this study is to gain enough insight into how surfactant intermolecular forces and geometry affect the performance of surfactants in $scCO_2$ to provide a useful set of guidelines for the design of new surfactants for specific applications.

Buhler et al. used static and dynamic light scattering to explore the effect of varying the CO_2 density on the phase behavior of surfactant polyvinyl acetate-*b*-poly(1,1,2,2-tetrahydroperfluorooctyl acrylate) (PVAc-*b*-PTAN) in supercritical CO_2 while maintaining the temperature and the surfactant/$scCO_2$ molar ratio fixed.[14] They observed three different regions in the phase diagram when plotted in the surfactant concentration$-$$scCO_2$ density plane: a two-phase region at low CO_2 densities, a spherical micelles solution at intermediate densities, and a unimer solution at high densities. This was the first observation that a transition from micelles to unimers could be induced by increasing CO_2 density. They interpreted the transition from micelles to unimers (micelle $\rightarrow$ unimer transition) upon increasing the solvent density as being a result of an increase in solvent quality for both surfactant blocks. The $scCO_2$ density at which the micelle $\rightarrow$ unimer transition occurs is called the critical micelle density (CMD)[13]. The micelle $\rightarrow$ unimer transition line on the phase diagram as plotted in the surfactant concentration$-$$CO_2$ density plane is referred to as the CMD when viewed at fixed surfactant concentration and as the critical micelle concentration (CMC) when viewed at fixed CO_2 density. Buhler et al.[14] found that the critical micelle concentration (CMC) increases as the $scCO_2$ density increases, which means that more surfactant molecules can be dissolved as unimers at high $scCO_2$ densities than

at low $scCO_2$ densities.

Recently there have been studies of compressible surfactant/$scCO_2$ systems using lattice Monte Carlo simulations.[19,20] Lisal et al.[19] explored the self-assembly of surfactants in $scCO_2$ by introducing vacancies into Larson's lattice model[22], making the surfactant/solvent system compressible and hence the solvent density adjustable. They performed large-scale canonical Monte Carlo simulations on model surfactant $[F(CF_2)_n(CH_2CH_2O)_mH]/scCO_2$ systems to investigate the influence of surfactant structure (head and tail lengths), solvent density and surfactant concentration on the CMC, the micelle size distribution, and micelle size and shape. They obtained parameters for carbon dioxide and perfluoroalkylpoly(ethylene oxide) by using experimental values for critical parameters and solubility along with a modified Berthelot mixing rule. Pseudophase diagrams were constructed based on their simulation results and compared with those from experiments on surfactant [PVAc-*b*-PTAN]/$scCO_2$[14]. A major difference between the simulation phase diagram and experimental results was that the CMC decreased as density increased, in contrast with experimental observations that showed that the CMC increases with increasing density. The discrepancy between the simulations and experimental results could be traced to the decrease in the solubility of the CO_2-phobic block in their simulations as CO_2 density increased. In contrast the solubilities of both surfactant blocks (CO_2-philic PTAN and less CO_2-philic PVAc) in the experiments of Buhler et al.[14] increased as solvent density increased. Atomistic-level molecular dynamics simulation studies on compressible surfactant/$scCO_2$ systems have also been conducted.[17,18,23,24]

There have been numerous simulation studies of incompressible model surfactant systems using highly simplified models over the years.[22,25–31] Quite recently Panagiotopoulos et

al.[31] investigated the phase behavior of incompressible systems containing diblock and/or triblock surfactants in water using histogram-reweighting grand-canonical lattice Monte Carlo simulations[30]. The interactions were chosen to be short-ranged and temperature-independent for the systems they studied. The only interaction considered was the tail-tail attraction (the tail is the solvent-phobic block); the other interactions were all neglected. The surfactant volume fraction at which the micellization (unimer $\rightarrow$ micelle transition) occurs, ϕ_{cmc}, was found by calculating the osmotic pressure at different surfactant volume fractions.[30] They distinguished between micellization and phase separation by determining whether or not the resulting phase diagram depends on system size. The surfactant/solvent system displayed either phase separation or micellization in the simulations depending upon the surfactant head/tail ratios, but never both; in contrast, both phase separation and micellization are observed in experiments[32]. Panagiotopoulos et al. attributed the disagreement between their simulation results and experiments to the lack of temperature-dependence in the model interactions between the surfactant molecules and water; temperature dependence was thought to be necessary to reflect the unusual solvation properties of water. They also found that ϕ_{cmc} increases as the temperature increases.

In this paper, we describe discontinuous molecular dynamics (DMD) simulations on surfactant ($\mathrm{H}_m\mathrm{T}_n$) /scCO_2 systems modeled as a mixture of single-sphere solvent molecules (CO_2) and freely-jointed surfactant chains composed of m slightly solvent-philic head spheres (H) and n more solvent-philic tail spheres (T), all of the same size. We first simulate homopolymer (P_n)/scCO_2 systems of chain length $n = 4, 8, 12$ and 24 to help establish the appropriate interaction parameter set for a surfactant/scCO_2 system. Parameters were chosen to ensure that the packing fractions at which the two-phase $\rightarrow$ one phase transition and the micelle $\rightarrow$ unimer tran-

sition occur are in the desired range of $0.2 - 0.5$, which keeps the solvent density of our model systems near or above the critical density of CO_2 and less than the packing fraction at which any hard-sphere fluid would undergo a transition to a solid phase. We then perform simulations on model surfactant (H_4T_8)/scCO_2 systems and explore the effect of variations in the surfactant mole fraction, system packing fraction and temperature on the phase behavior. Finally we investigate the influence of the variation in the surfactant head and tail chain length on the location of the two-phase $\rightarrow$ one-phase transition and the micelle $\rightarrow$ unimer transition.

A.2 Molecular Models and Simulation Methods

The surfactant/solvent system is modeled as a mixture of single-sphere solvent molecules (S) and freely-jointed surfactant chains (H_mT_n) composed of m slightly-solvent-philic head spheres (H) and n solvent-philic tail spheres (T), all of the same size. We choose a hard-sphere potential for the solvent-solvent and head-tail interactions and a square-well potential for the head-head, head-solvent, tail-tail and tail-solvent interactions. The hard sphere ($U_{\rm hs}$) and square-well ($U_{\rm sw}$) potentials are:

$$U_{\rm hs}(r) = \begin{cases} \infty & \text{if } r < \sigma \\ 0 & \text{if } r > \sigma \end{cases} \tag{A.1}$$

$$U_{\rm sw}(r) = \begin{cases} \infty & \text{if } r < \sigma \\ \epsilon & \text{if } \sigma < r < (1+\lambda)\sigma \\ 0 & \text{if } r > (1+\lambda)\sigma \end{cases} \tag{A.2}$$

where r is the distance between two segments, σ is the segment diameter and ϵ is the interaction

strength between two segments with a square-well potential interaction; negative ϵ signifies an attraction. The well width parameter, λ, is set to 0.75, a reasonable approximation since there are no long-range segment-segment interactions in non-ionic surfactant/scCO_2 systems.

We choose a hard-sphere potential for the solvent-solvent interaction (ϵ_{SS}) because the simulations are much faster without attractions between solvent molecules than with attractions. Most of the collisions are between solvent molecules due to the low surfactant volume fraction and it is easier computationally to calculate the collision dynamics for a hard-sphere potential than for a square-well potential. In addition the interactions between CO_2 molecules are relatively weak (quadrupolar) compared to other interactions in the system, so the neglect of solvent-solvent attactions compared to other interactions is not unreasonable. As we will see, using a hard-sphere potential for the solvent-solvent interaction still permits us to capture the essential feature of scCO_2 density's effect on the phase behavior of polymer/solvent systems. The head-tail interaction is also modeled with a hard-sphere potential since the miscibility of real polymers comprised of the surfactant head segments and surfactant tail segments is generally low.

The variables in our simulations are defined as the following. The homopolymer P_n volume fraction is defined to be $\phi_{\mathrm{P}_n} \equiv nN_{\mathrm{P}_n}/(nN_{\mathrm{P}_n} + N_{\mathrm{CO}_2})$ and the surfactant $\mathrm{H}_m\mathrm{T}_n$ volume fraction is defined to be $\phi_{\mathrm{H}_m\mathrm{T}_n} \equiv (m+n)N_{\mathrm{H}_m\mathrm{T}_n}/[(m+n)N_{\mathrm{H}_m\mathrm{T}_n} + N_{\mathrm{CO}_2}]$, where N_i is the number of molecules of species i. The homopolymer P_n mole fraction is defined to be $X_{\mathrm{P}_n} \equiv N_{\mathrm{P}_n}/(N_{\mathrm{P}_n} + N_{\mathrm{CO}_2})$ and the surfactant $\mathrm{H}_m\mathrm{T}_n$ mole fraction is defined to be $X_{\mathrm{H}_m\mathrm{T}_n} \equiv N_{\mathrm{H}_m\mathrm{T}_n}/(N_{\mathrm{H}_m\mathrm{T}_n} + N_{\mathrm{CO}_2})$. The system packing fraction is defined to be $\eta \equiv \pi N_{\mathrm{b}}\sigma^3/6V$, where V is the box volume and N_{b} is the number of beads in the system. In this paper, $|\epsilon_{\mathrm{PP}}|$ and $|\epsilon_{\mathrm{PS}}|$ are the polymer-polymer and polymer-solvent attractions

in homopolymer/CO_2 system and $|\epsilon_{\rm HH}|$, $|\epsilon_{\rm HS}|$, $|\epsilon_{\rm TT}|$ and $|\epsilon_{\rm TS}|$ are the head-head, head-solvent, tail-tail and tail-solvent attractions in surfactant/CO_2 systems. We choose a reference interaction strength $|\epsilon^*|$ and will refer to reduced parameters for the interaction strengthes as $|\epsilon^*_{\rm HH}|$ = $|\epsilon_{\rm HH}|/|\epsilon^*|$, $|\epsilon^*_{\rm HS}|$ = $|\epsilon_{\rm HS}|/|\epsilon^*|$, $|\epsilon^*_{\rm TT}|$ = $|\epsilon_{\rm TT}|/|\epsilon^*|$, $|\epsilon^*_{\rm TS}|$ = $|\epsilon_{\rm TS}|/|\epsilon^*|$, $|\epsilon^*_{\rm PP}|$ = $|\epsilon_{\rm PP}|/|\epsilon^*|$ and $|\epsilon^*_{\rm PS}|$ = $|\epsilon_{\rm PS}|/|\epsilon^*|$. The reduced temperature is defined to be $T^* \equiv {\rm k_B T}/|\epsilon^*|$, where $\rm k_B$ is Boltzman's constant, T is the temperature.

We limit our study to packing fractions η between 0.2 and 0.5 so as to keep the solvent packing fraction greater than the critical packing fraction for a square-well fluid of width $\lambda = 0.75$ ($\eta_{\rm c} \approx 0.126$) and less than the packing fraction at which a hard-sphere fluid would undergo a transition to a solid phase. This serves to limit our study to model CO_2 densities that are in the supercritical or liquid regime. Since solvent, homopolymer segments and surfactant segments all have the same diameter in our model, the solvent reduced density in our simulations can be simply calculated from ${\rho_{\rm CO_2}}^* = \phi_{\rm CO_2}\rho^*$, where $\rho^* \equiv N_{\rm b}\sigma^3/V = 6\eta/\pi$ is the overall reduced density, and $\phi_{\rm CO_2}$, the solvent volume fraction, is obtained from $\phi_{\rm CO_2} = 1 - \phi_{\rm P_n}$ for homopolymer ($\rm P_n$)/solvent systems or $\phi_{\rm CO_2} = 1 - \phi_{\rm H_m T_n}$ for surfactant ($\rm H_m T_n$)/solvent systems. Since the number of surfactant molecules in our simulations is low compared to the number of CO_2 molecules, i.e. $\phi_{\rm CO_2}$ is between 0.755 and 0.965, the (total) packing fraction is a reasonable measure of CO_2 density. Thus setting the total packing fraction in our simulations to be $\eta > 0.20$ means that the model CO_2 density is effectively higher than its critical density would have been if we had modeled the CO_2 molecules in more detail as square-well molecules of width $\lambda = 0.75$.

In a discontinuous molecular dynamics (DMD) simulation, particles collide when they ar-

rive at a discontinuity in the potential, i.e. the hard-sphere diameter or the square-well width. Between collisions, particles move with linear trajectories, making DMD simulations much faster than traditional molecular dynamics simulations with continuous potentials which require a small integration time step. The post-collision velocities of particles in DMD are found by solving the collision dynamics equations analytically. To simulate chains of spheres effectively, Rapaport introduced bonds between spheres by limiting the distance between adjacent beads to be between σ and $\sigma(1+\delta)$, where δ is the bond extension parameter.[33] Later Bellemans modified this model so that the distance between adjacent spheres must lie between $\sigma(1-\delta/2)$ and $\sigma(1+\delta/2)$ which makes the average bond length equal to σ.[34] The value of δ in our simulations is 0.3.

Since we are interested in simulating at constant temperature, we use discontinuous canonical molecular dynamics (DCMD),[35–38] an adaptation of the standard microcanonical ensemble DMD technique. The DCMD technique is based on Anderson's stochastic collision method[36] and involves stochastic interaction of the system particles with imaginary constant-temperature heat bath particles. We assume that the system is immersed in a constant-temperature heat bath containing imaginary "ghost" particles. The ghost particles stabilize the system temperature by colliding with the system particles, resulting in the reassignment of particle velocities according to a Maxwell-Boltzmann distribution about the required temperature. Details of the DCMD method have been described by Gulati et al.[35] and by Zhou et al.[38]

Our DMD code was originally developed by Smith and coworkers[39] to treat entangled polymer melts. More recently, it was extended by Schultz et al.[40] to the treatment of any mixture of monomers, polymers, and/or copolymers and optimized to allow for the efficient simulation of large multicomponent systems.

The reduced pressure, P^*, in our simulations is calculated using the virial theorem

$$P^* \equiv \frac{P\sigma^3}{\mathrm{k_B}T} = \frac{N_\mathrm{b}\sigma^3}{V} - \frac{\sigma^3 m \sum_{\mathrm{coll}} \vec{r}_{ij}\Delta\vec{v}_j}{3V\mathrm{k_B}Tt} \tag{A.3}$$

where $\mathrm{k_B}$ is Boltzman's constant, T is the temperature, N_b is the number of beads, V is the volume, m is the mass of each segment, $\vec{r}_{ij}$ is the distance between colliding particles i and j, $\Delta\vec{v}_j = -\Delta\vec{v}_i$ is the velocity change for the particle j, $\sum_{\mathrm{coll}}$ refers to a sum over all collisions, and t is the elapsed simulation time.

Several different types of transitions occur in the homopolymer/solvent and surfactant/solvent systems considered here. As the packing fraction or temperature increases, a two-phase $\rightarrow$ one-phase transition occurs as a phase-separated homopolymer/solvent or surfactant/solvent system turns into a one-phase system. In the one-phase region for the homopolymer/solvent system, the chains are evenly distributed throughout the solvent either as homopolymer aggregates or as unimers. In the one-phase region for the surfactant/solvent system, the chains are evenly distributed throughout the solvent either as micelles or as unimers. If the surfactant/solvent system two-phase $\rightarrow$ one-phase transition results in the formation of micelles, then an additional transition, the micelle $\rightarrow$ unimer transition, can occur in which the micelles turn into unimers as the packing fraction or temperature increases. The surfactant chains are distributed evenly as unimers throughout the solvent in the unimer phase.

The two-phase $\rightarrow$ one-phase transition for the homopolymer/solvent and surfactant/solvent systems are located by calculating the contrast structure factor. The structure factor is the Fourier transform of the radial distribution function. Murat and coworkers[41] and McGreevy[42] evaluated the structure factor for any multicomponent system using different but equivalent equations.

We follow McGreevy[42] since his calculation is more computationally efficient and use the following equivalent formula

$$S(\vec{q}) = \frac{1}{N}\left|\sum_j b_j e^{i\vec{q}\cdot\vec{r}_j}\right|^2 \tag{A.4}$$

where $\vec{q}$ is the wave vector, b is a labelling variable for each component in the system, and $\vec{r}$ is the vector between particles. The value of b_j for the different components can be either 1, -1 or 0. If b_j equals zero for particle j of component A, then component A is ignored in the structure factor calculation. If only one of the components has a non-zero b_j, we obtain the single component structure factor. A contrast structure factor (showing the difference between the distribution of components A and B) can be obtained by setting $b_j = 1$ if particle j is component A and $b_j = -1$ if particle j is component B. If a solute structure factor is desired (which is sensitive only to variations in the solute density), then one can set $b_j = 1$ for solutes A or B and $b_j = 0$ for solvent particles (or vacancies in a lattice simulation). In our work we focus on the contrast structure factors (S_{P-S} and S_{H+T-S}) which highlight the contrast between the distribution of polymer (P) beads and solvent molecules (S) in the homopolymer/CO_2 system and the contrast between the distribution of head (H) and tail (T) beads and solvent molecules (S) in the surfactant/CO_2 system. These contrast structure factors can be obtained by setting $b_j = 1$ for homopolymer beads and for surfactant head and tail beads and $b_j = -1$ for solvent beads in Equation A.4.

To illustrate how the calculated structure factor is used to locate the two-phase $\rightarrow$ one-phase transition, consider the snapshots of the configuration of an equilibrated system shown in figure A.1 for a surfactant (H_4T_8)/solvent system at (a) η = 0.24 and (b) η = 0.27. The solvent

molecules are not shown for the sake of clarity. At η=0.24, almost all of the surfactant molecules cluster tightly in the center of the simulation box signaling phase separation. At η=0.27, the surfactant molecules form micelles that are distributed evenly throughout the system, with the head block as the core and the tail block as the corona. In the snapshots for the systems at η = 0.25 and 0.26 (not shown), the clusters formed by the surfactants in the system are loose compared with those for η = 0.24 and the tail corona of different aggregates are connected, making it difficult to determine whether this is in the two-phase region or the micelle phase. To help make this decision we calculate the contrast structure factors for the H_4T_8/solvent system shown in figure A.2 for η = 0.25 and 0.26. In the figure, which plots the contrast structure factor $(S(|\vec{q}|\sigma))$ versus the reduced wave vector ($|\vec{q}|\sigma$), the lowest wave vector corresponds to the box length, which is the maximum possible wave length. A sharp peak occuring at the lowest wave vector indicates that the system is phase separated. We see that the contrast structure factor at η = 0.25 has a sharp peak at the lowest wave vector ($|\vec{q}|\sigma$ = 0.2) but that no sharp peak occurs at the lowest wave vector at η=0.26. In order to determine if the peak is sharp enough to signal a phase transition, we plot the slope of the structure factor at the lowest wave vector versus the packing fraction (η) as in figure A.3. It can be seen that the slope of the structure factor is large and negative (indicating a very sharp peak at the lowest wave vector) at η = 0.23 and 0.24, then increases quickly as η increases from 0.24 to 0.25 and is negative and close to zero (indicating a very shallow peak at the lowest wave vector) at $\eta = 0.26 - 0.30$. Based on this we conclude that the packing fraction at which the transition from the two-phase region to the one-phase region occurs, $\eta_{2\phi \rightarrow 1\phi}$, lies between 0.25 and 0.26 (the packing fraction at which the sharp peak disappears). We record $\eta_{2\phi \rightarrow 1\phi} = 0.255$ with an error bar of ± 0.01 for this condition.

To locate the micelle $\rightarrow$ unimer transition, we calculate the aggregate size distribution at different η (chosen to be higher than $\eta_{2\phi\rightarrow 1\phi}$). The aggregate size distribution is represented by a plot of the volume fraction of aggregates containing M surfactant molecules (an aggregate with $M = 1$ is a unimer), ϕ_{M}, versus M, where the aggregate volume fraction is defined to be the volume occupied by aggregates containing M surfactant molecules divided by the total volume occupied by all the "aggregates" (including unimers) in the system. We calculate the number of surfactants in an aggregate as follows. If the distance between a head bead on chain A and a head bead on chain B, $d_{\mathrm{H_A H_B}}$, is smaller than the square-well width, $(1 + \lambda)\sigma$, we then define chain A and chain B to be in the same aggregate, say M_i. If we also find chains B and C in the same aggregate, we then consider chains A, B and C to be in the same aggregate; i.e. chains A, B and C are all part of aggregate M_i. Since we calculate the distance between the head beads of two chains to determine whether they are in the same aggregate, two aggregates in near contact via tail beads would not be counted in the same aggregate. Doing this for all chains in the system, we obtain a list of the surfactants in each aggregate M_i. The number of surfactants in each aggregate is obtained from the list; this is the aggregate size. We can then calculate the number of micelles in the system with a given aggregate size to obtain the aggregate size distribution.

To illustrate how the micelle $\rightarrow$ unimer transition is calculated, consider the aggregate size distributions shown in figure A.4 for a surfactant $\mathrm{H_4T_8}$/solvent system in the $\phi_{\mathrm{M}} - M$ plane at packing fractions, η = 0.29, 0.30 and 0.31. For η = 0.31, the aggregate size distribution exhibits only one peak at very small M, which represents unimers. At η = 0.30, the peak at very small M is lowered and a small bump occurs at a higher value of M, indicating that small aggregates begin to form in the system. For η = 0.29, the first peak is lower still and a second (micellar)

peak occurs, indicating that spherical micelles are formed in the system. In this study, we choose the location of the micelle $\rightarrow$ unimer transition $\eta_{\mathrm{m}\rightarrow\mathrm{u}}$ to be the packing fraction at which the second peak just disappears in the aggregate size distribution. In figure A.4 the packing fraction at which the $\mathrm{H_4T_8}$/solvent system undergoes a micelle $\rightarrow$ unimer transition is 0.30. A similiar method in which the size distribution was calculated at different surfactant concentrations was used to determine the CMC in non-compressible surfactant/solvent systems.[31] Another method for detemining the CMC is to plot the mole fraction of free unimer vs surfactant mole fraction and define the CMC as the surfactant mole fraction at which the number of surfactants aggregated in micelles is equal to the number of free unimers.[43] Panagiotopoulos found that these two methods agree with each other quite well.[31]

For the homopolymer/solvent systems, the two-phase $\rightarrow$ one-phase transition can be located by comparing the configurational snapshots and contrast structure factors at different conditions. The homing-in procedure used to locate the two-phase $\rightarrow$ one-phase transition for homopolymer/solvent systems is similiar to that used for surfactant/solvent systems.

Discontinuous molecular dynamics simulations aree performed in the canonical ensemble (constant N, V, T) on the homopolymer/solvent or surfactant/solvent systems. In order to investigate phase separation it is necessary to consider large systems. In the interests of computational efficiency, we begin by equilibrating a small system with a random initial configuration and then enlarge the now-equilibrated small system to re-equilibrate. The simulations are started in a small cell at the desired packing fraction, reduced temperature and polymer volume fraction. The small cell contains either 500 solvent molecules and $6-12$ chains or 2000 solvent molecules and $18-54$ chains. We first run the simulation for $20-30$ minutes (CPU time) to calculate

the initial aggregate or micelle size distribution; we then continue running the simulation and re-calculating the size distribution several times. Once the system is equilibrated, as indicated by a lack of variation in the peak positions of the aggregate or micelle size distribution, the simulation box is replicated three times (for systems containing 500 solvent molecules) or two times (for systems containing 2000 solvent molecules) in every direction yielding 13500 solvent molecules and $162 - 324$ chains or 16000 solvent molecules and $144 - 432$ chains. The simulation is then continued on the large system until equilibrium is reached, as indicated by a lack of variation in the peak position for the contrast structure factor and the aggregate or micelle size distribution. The size distribution and the contrast structure factor calculated for the large system are used to determine the phase transitions. (The small system size distribution only serves to indicate whether the small system is equilibrated.) Since the systems containing 500 solvent molecules and $6 - 12$ chains were not as helpful as those containing 2000 solvent molecules and $18 - 54$ chains in establishing equilibrium, the latter systems were chosen as the initial small cells in most of our simulations. In addition, to investigate the influence of the system size on the calculated structure factor, we double the size of the large system and run simulations. The idea here is to see whether or not the structure factor of the systems in the two-phase region and in the one-phase region change as the system size increases. We find that the location of the phase transition stays the same as the size of the large system is doubled, indicating that the system is big enough for the calculation of phase transitions.

The average CPU time needed on our 600 MHz Alpha 21164 for each state point included 2h for equilibration of the small systems containing 500 solvent molecules and $6 - 12$ chains or those containing 2000 solvent molecules and $18 - 54$ chains and 30h for equilibration of the large

systems containing 13500 solvent molecules and $162 - 324$ chains or those containing 16000 solvent molecules and $144 - 432$ chains. At the end of this process, a snapshot of the large system displaying the distribution of chains in the solvent was taken, and the contrast structure factor or aggregate size distribution is calculated to determine which phase the system was in. Phase transitions are assumed to be located at the mid-point between two different phases and are determined as a function of homopolymer or surfactant volume fraction or mole fraction, system packing fraction and reduced temperature. The error bars in these calculations are based on the closest state points in the two different regions.

A.3 Results and Discussion

A.3.1 Homopolymer

In order to establish appropriate polymer-polymer and polymer-solvent interaction parameters and to ensure that $\eta_{2\phi\rightarrow 1\phi}$ and $\eta_{\mathrm{m}\rightarrow\mathrm{u}}$ are in the desired range of $0.2 - 0.5$ for the surfactant/solvent systems, we first simulated homopolymer/scCO_2 systems. The two-phase $\rightarrow$ one-phase transition for the homopolymer/solvent system was located by monitoring the configurational snapshots and calculating the contrast structure factors at different η as described in Section A.2.

Figure A.5 shows the transitions for homopolymers of length 4, P_4, from the two-phase region to the one-phase region in the polymer volume fraction (ϕ_{P})$-$total packing fraction (η) plane for three different parameter sets $(\epsilon^*_{\mathrm{PP}},\ \epsilon^*_{\mathrm{PS}}) = (-0.9, -0.6), (-1.0, -0.6)$ and $(-1.0, -0.55)$. This figure shows that the amount of homopolymer that can dissolve in the solvent is larger at higher η. This trend is in agreement with experimental observations on PVAc,

whose solubility increases as $scCO_2$ density increases[14]. The polymer dissolves in the solvent as η increases at fixed homopolymer volume fraction because the solvent density around each homopolymer molecule increases, establishing more attractions between the polymer molecule and solvent and screening the attractive polymer-polymer interaction.

Figure A.5 shows that homopolymers with stronger polymer-polymer attractions or weaker polymer-solvent attractions need higher packing fractions to dissolve. This is because homopolymer molecules with strong $|\epsilon^*_{\rm PP}|$ or weak $|\epsilon^*_{\rm PS}|$ are more likely to attract other polymer molecules than to attract solvent molecules, and hence to form aggregates.

To compose the surfactant we choose a homopolymer that dissolves at high η as the surfactant head block and a homopolymer that dissolves at low η as the surfactant tail block. Figure A.6 shows two-phase $\rightarrow$ one-phase transitions in the polymer mole fraction ($X_{\rm P}$)$-$total packing fraction (η) plane for homopolymer P_4 with $(\epsilon^*_{\rm PP}, \epsilon^*_{\rm PS}) = (-1.0, -0.525)$ and homopolymer P_8 with $(\epsilon^*_{\rm PP}, \epsilon^*_{\rm PS}) = (-0.45, -0.4)$. We choose to plot polymer mole fraction instead of polymer volume fraction to make it easier to compare the values of $\eta_{2\phi\rightarrow 1\phi}$ for homopolymers with different chain lengths. Figure A.6 shows that homopolymer P_4 with $(\epsilon^*_{\rm PP}, \epsilon^*_{\rm PS}) = (-1.0, -0.525)$ dissolves in the solvent at high η and homopolymer P_8 with $(\epsilon^*_{\rm PP}, \epsilon^*_{\rm PS}) = (-0.45, -0.4)$ dissolves in the solvent at low η, which makes them suitable as surfactant head and tail block, respectively.

Figure A.7 shows the transition from the two-phase region to the one-phase region in the total packing fraction (η) $-$ chain length (n) plane for homopolymer P_n with parameter sets $(\epsilon^*_{\rm PP}, \epsilon^*_{\rm PS}) = (-1.0, -0.525)$, $(-0.45, -0.4)$ and $(-0.9, -0.6)$ at polymer volume fraction $\phi_{\rm p} = 0.0672$. We find that the packing fraction at which the two-phase $\rightarrow$ one-phase transition occurs is higher for long chains than for short chains, in qualitative agreement with exper-

imental results[14] on PVAc that show that the solubility decreases as the chain length increases. The packing fraction of the two-phase $\rightarrow$ one-phase transition increases fairly sharply as chain length increases from 4 to 12 and much more slowly as chain length increases from 12 to 24. The dependence of the two-phase $\rightarrow$ one-phase transition on chain length in our simulations in consistent with experimental results that the cloud-point pressure increases rapidly with increasing molecular weight below a certain value and then much more slowly at high molecular weights for PVAc[44] and fluorinated polybutadienes(FPBD)[45] in scCO$_2$. The solubility of long chains is lower than that of short chains for the following reasons. Homopolymer solubility represents the ability of homopolymer chains to "escape" from the polymer-rich phase to the solvent-rich phase by exchanging polymer-polymer attractive interactions for polymer-solvent attractive interactions. A long chain has more opportunities for attractions with itself and/or other chains in a polymer-rich phase than a short chain. There are comparatively less opportunities for attractions between the chain and the solvent since the solvent is a single molecule.

Figure A.8 displays the transition from the two-phase region to the one-phase region in the homopolymer volume fraction (ϕ_{P})$-$reduced temperature (T^*) plane for homopolymer P_4 with the parameter set $(\epsilon^*_{\mathrm{PP}}, \epsilon^*_{\mathrm{PS}}) = (-1.0, -0.525)$ at packing fraction η = 0.40 and homopolymer P_8 with $(\epsilon^*_{\mathrm{PP}}, \epsilon^*_{\mathrm{PS}}) = (-0.45, -0.4)$ at packing fraction η = 0.20. We find that more homopolymer molecules dissolve in the solvent as T^* increases at fixed packing fraction. This means that the homopolymer solubility in our model increases as temperature increases at fixed solvent density. Increasing the reduced temperature increases the importance of the entropy (S) term in the free energy (A) according to its definition $\Delta A = \Delta U - T\Delta S$ since the mixing entropy (ΔS) is positive. Thus increasing the temperature increases the miscibility between polymer chains and

solvent molecules.

Figure A.9 displays the two-phase $\rightarrow$ one-phase transition in the (a) packing fraction (η) $-$ reduced temperature (T^*) plane and (b) reduced pressure (P*) $-$ reduced temperature (T^*) plane at $\phi_{\mathrm{P}} = 0.067$ for homopolymer P_4 with $(\epsilon^*_{\mathrm{PP}}, \epsilon^*_{\mathrm{PS}}) = (-1.0, -0.525)$ and for P_8 with $(\epsilon^*_{\mathrm{PP}}, \epsilon^*_{\mathrm{PS}}) = (-0.45, -0.4)$. Figures A.9a and A.9b show, respectively, that the packing fraction and reduced pressure at which the two-phase $\rightarrow$ one-phase transition occur decrease with increasing temperature. Figure A.9b further shows that homopolymers P_4 and P_8 exhibit upper critical solution temperature behavior (UCST) since a single phase is obtained as the temperature increases isobarically. CF_2-modified polybutadiene and polyisoprene exhibit UCST behavior in $scCO_2$ at very high pressures.[45] We observe UCST behavior for both the CO_2-phobic and CO_2-philic homopolymers examined in our simulations. In contrast however, many substances (such as PVAc) dissolved in $scCO_2$ exhibit lower critical solution temperature behavior (LCST).[44] This disrepancy is likely due to the lack of solvent-solvent attractions in our model, thus the PVT behavior of the solvent in our simulations is different from that in experiments. We hope to further explore UCST/LCST behavior in polymer/CO_2 systems in a future modeling effort which takes solvent-solvent attractions into account and considers the effect of variation in chain length and interaction strengths.

A.3.2 Surfactant

As described earlier, our $\mathrm{H}_4\mathrm{T}_8$ surfactant molecules are modeled by covalently connecting homopolymer P_4 with $(\epsilon^*_{\mathrm{PP}}, \epsilon^*_{\mathrm{PS}}) = (-1.0, -0.525)$, which becomes our slightly CO_2-philic head block, to homopolymer P_8 with $(\epsilon^*_{\mathrm{PP}}, \epsilon^*_{\mathrm{PS}}) = (-0.45, -0.4)$ which becomes our more

CO_2-philic tail block. This choice of parameter values is motivated by the following considerations. Many surfactants used in $scCO_2$ are composed of a CO_2-phobic block which is polar (such as PVAc) and a CO_2-philic block which is non-polar (such as PFOA). In these surfactant/$scCO_2$ systems, the attraction between the polar blocks (our ϵ^*_{HH}) is strong and the attraction between the non-polar blocks (our ϵ^*_{TT}) is weak. In addition, due to the CO_2 quadrupole moment the attraction between the polar block and the solvent molecule (ϵ^*_{HS}) may be stronger than the attraction between the non-polar block and the solvent molecule (ϵ^*_{TS}) and both of them are weaker than the attraction between polar blocks (ϵ^*_{HH}) and stronger than the attraction between non-polar blocks (ϵ^*_{TT}). The location of the transition from the two-phase region to the one-phase region for surfactant $\mathrm{H_4T_8}$ was determined by monitoring the contrast structure factors and the configurational snapshots, and the location of the micelle $\rightarrow$ unimer transition was determined by monitoring the aggregate size distribution as described in Section A.2.

Figure A.10, which plots the surfactant volume fraction versus packing fraction for $\mathrm{H_4T_8}$ at $T^* = 1.0$, shows that the surfactant/solvent system goes from a two-phase region at low η to a micelle phase at intermediate η and finally to a unimer phase at high η. The three regions (two-phase region, micelle phase and unimer phase) are separated by the $2\phi \rightarrow 1\phi$ transition line and the micelle $\rightarrow$ unimer transition line. We also find that the packing fractions at which the $2\phi \rightarrow 1\phi$ transition and the micelle $\rightarrow$ unimer transition occur increase as surfactant volume fraction increases. The observed trend in our simulations that the packing fraction at which the micelle $\rightarrow$ unimer transition occurs increases as surfactant volume fraction increases is in qualitative agreement with the trend that the CMC increases as $scCO_2$ density increases in experiments on PVAc-*b*-PTAN[14]. The trends in the density dependence of the $2\phi \rightarrow 1\phi$ transition and the

micelle $\rightarrow$ unimer transition can be understood by recalling that the solubilities of the head and tail block in the solvent increase with increasing packing fraction as shown in Figure A.6.

It is of interest to relate the phase behavior of a surfactant/solvent system to the phase behavior (i.e., the solubilities) of the homopolymers that make up the surfactant head or tail block. Figure A.11 shows the $2\phi \rightarrow 1\phi$ transition and the micelle $\rightarrow$ unimer transition for H_4T_8 on the same diagram as the $2\phi \rightarrow 1\phi$ transitions for the slightly CO_2-philic homopolymer, P_4, and for the more CO_2-philic homopolymer, P_8, in the polymer mole fraction (X_P)$-$packing fraction (η) plane. The four transitions occur in the following order as η increases: (1) the $2\phi \rightarrow 1\phi$ transition of P_8, (2) the $2\phi \rightarrow 1\phi$ transition of H_4T_8, (3) the micelle $\rightarrow$ unimer transition of H_4T_8 and (4) the $2\phi \rightarrow 1\phi$ transition of P_4. The value of $\eta_{2\phi\rightarrow 1\phi}$ is higher for H_4T_8 than for P_8 since adding the slightly CO_2-philic P_4 to the much more CO_2-philic P_8 decreases the solubility in scCO_2 and since solubility decreases in general with increasing chain length. The value of $\eta_{m\rightarrow u}$ for H_4T_8 is lower than the value of $\eta_{2\phi\rightarrow 1\phi}$ for P_4 since adding the much more CO_2-philic P_8 to the slightly CO_2-philic P_4 makes it easier for H_4T_8 to dissolve as single chains in the solvent than for P_4 to dissolve in the solvent. It is apparent that the phase behavior of a surfactant/solvent system is directly related to the solubilities of the corresponding homopolymers that serve as the surfactant's head and tail block. In effect $\eta_{2\phi\rightarrow 1\phi}$ for the homopolymer that serves as head block and $\eta_{2\phi\rightarrow 1\phi}$ for the homopolymer that serves as tail block bracket $\eta_{2\phi\rightarrow 1\phi}$ and $\eta_{m\rightarrow u}$ for the surfactant system.

Figure A.12 shows the phase behavior of the H_4T_8/solvent system in the $\phi_{H_4T_8} - T^*$ plane at η = 0.30. The surfactant/solvent system goes from a two-phase region at low T^* to a micelle phase at intermediate T^* and then to a unimer phase at even higher T^*. This is because the

solubilities of the head and tail block increase as T^* increases as indicated in Figure A.8. We find both a two-phase $\rightarrow$ one-phase transition and a micelle $\rightarrow$ unimer transition in our simulations as is found in most experiments.[32] This is in contrast to the simulation results on an incompressible model surfactant/solvent system by Panagiotopoulos et al.[31], who found either micellization or phase separation in their simulations upon decreasing temperature for copolymers with different head and tail lengths, but never both. We also find that the surfactant volume fraction at which the micelle $\rightarrow$ unimer transition occurs increases as T^* increases, in agreement with the trend observed by Panagiotopoulos et al.[31]

The discrepancy between our simulation results and the simulation results of Panagiotopoulos et al.[31] is due to the difference in the models employed in the simulations. In our model the head-head (solvent-phobic block), head-solvent, tail-tail (solvent-philic block) and tail-solvent attractions are considered; whereas in their model the only attraction considered is between the solvent-phobic segments. In our model, temperature influences the solvent affinities of both solvent-philic and solvent-phobic blocks while in their model temperature can only influence the solvent affinity of the solvent-phobic block. Panagiotopoulos et al.[31] hypothesized that the disagreement between their simulation results and experimental observations that both the $1\phi \rightarrow 2\phi$ and unimer $\rightarrow$ micelle transition are present was due to their neglect of the unusual solvation properties of water, in particular that water's solvation power decreases with increasing temperature. Instead, our results suggest that the most likely explanation is their neglect of the interactions experienced by the solvent-philic block.

To explore the influence of surfactant architecture on the solubility of surfactant in $scCO_2$, we performed simulations on three different surfactants H_4T_8, H_3T_9 and H_3T_6 thereby varying

the head length/tail length ratio (f) and the total chain length ($m+n$). Figure A.13 compares the location of the two-phase $\rightarrow$ one-phase transition in the $\phi_{\mathrm{H}_m\mathrm{T}_n} - \eta$ plane for different surfactant architectures: (a) $\mathrm{H_4T_8}$ and $\mathrm{H_3T_9}$ ($f = 1/2$ and $1/3$ with $m + n = 12$) and (b) $\mathrm{H_3T_6}$ and $\mathrm{H_4T_8}$ ($m + n = 9$ and 12 with $f = 1/2$). The packing fraction at which the two-phase $\rightarrow$ one-phase transition occurs for $\mathrm{H_4T_8}$ is higher than those for $\mathrm{H_3T_9}$ and $\mathrm{H_3T_6}$. The surfactant solubility decreases as f increases at fixed $m + n$ and decreases as $m + n$ increases at fixed f. The effect of f on the two-phase $\rightarrow$ one-phase transition is in agreement with experimental results on the effect of varying the ratio f of the segment numbers on the solubility of the copolymer $\mathrm{C_{12}H_{25}}$-O-$(\mathrm{EO})_m(\mathrm{PO})_n$.[46] Increasing f at fixed $m + n$ for a surfactant decreases the solvent affinity of the surfactants since the solvent-philic block becomes shorter and the slightly solvent-philic block becomes longer. Increasing $m + n$ at fixed f yields a surfactant with longer head and tail blocks which, since homopolymer solubility decreases with increasing chain length, decreases the solvent affinities of both the head and tail block. Thus the entire surfactant molecule has lower solvent affinity than a short-chain surfactant with the same f.

A.4 Summary and Discussion

In this study we developed a simple model for homopolymer/solvent and surfactant/solvent systems and explored the phase behavior using fast DMD simulation. We performed simulations on model homopolymer/solvent systems with varying interaction strengths and chain lengths and on model surfactant/solvent systems with varying surfactant head length/tail length ratio and overall chain length at different polymer volume fractions, packing fractions and reduced temperatures. The phase diagrams constructed for the surfactant/solvent systems in the surfactant

volume fraction−packing fraction plane are consistent with the experimentally observed phase diagram for the PVAc-PTAN/scCO$_2$ system in the surfactant concentration−CO$_2$ density plane[14] indicating that the essential features of scCO$_2$ density's effect on the phase behavior are captured with our model. We show that the phase behavior for a surfactant/solvent system is directly related to the solubilities of the corresponding homopolymers that serve as the head and tail block for the surfactant.

The solubilities of homopolymers and surfactants increase as packing fraction increases at fixed temperature and as temperature increases at fixed packing fraction, in agreement with experiments on the effect of solvent density on non-inonic surfactant solubility in scCO$_2$ at fixed temperature and the effect of temperature on its solubility at fixed density.[47] Both micellization and phase separation are found in our simulations upon decreasing temperature in contrast to the simulations of Panagiotopoulos et al.[31] This indicates that including interactions for both solvent-phobic and solvent-philic blocks of a surfactant might be important in describing the phase behavior of a surfactant/solvent system with varying temperature.

The packing fraction η at which the two-phase $\rightarrow$ one-phase transition occurs increases as the surfactant head/tail ratio increases at fixed surfactant chain length and as the surfactant chain length increases at fixed surfactant head/tail ratio, in qualitative agreement with experimental observations on the effect of head/tail ratio and molecular weight on surfactant solubility in scCO$_2$.[46]

One limitation of our model for homopolymer/CO$_2$ and surfactant/CO$_2$ systems is that we only observe UCST behavior in our simulations while many substances exhibit LCST behavior in scCO$_2$. We attribute this limitation to our treatment of CO$_2$ molecules as hard-sphere molecules.

Although it would have been more realistic to model ϵ_{SS} with a square-well potential rather than a hard-sphere potential, we wanted to see whether such a simplified model would be able to represent polymer/scCO_2 systems and to take advantage of the computational efficiency afforded by using the hard-sphere potential. Efforts are under way to model the solvent-solvent interaction with a square-well potential so as to better capture the behavior of real surfactant/scCO_2 systems.

A.5 Acknowledgements

The material is based upon work supported by the STC Program of the National Science Foundation under Agreement No. CHE-9876674. Acknowledgment is made to the Office of Energy Research, Basic Sciences, Chemical Science Division of the U. S. Department of Energy under Contract No. DE-FG05-91ER14181 for partial support of this work. Z. Li thanks A. J. Schultz for fruitful discussions and many valuable suggestions.

A.6 References

[1] C. A. Eckert, B. L. Knutson, and P. G. Debenedetti, "Supercritical fluids as solvents for chemical and materials processing," *Nature* **383**, 313 (1996).

[2] M. K. McHugh and V. J. Krukonis, *Supercritical fluid extraction: principles and practice.* (Butterworth-Heinemann, Boston, MA, 1994).

[3] T. Hoefling, D. Stofesky, M. Reid, E. Beckman, and R. M. Enick, "The incorporation of a fluorinated ether functionalty into a polymer or surfactant to enhance CO_2-solubility," *J. Supercrit. Fluids* **5**, 237 (1992).

[4] J. M. Desimone, Z. Guan, and C. S. Elsbernd, "Synthesis of fluoropolymers in supercritical carbon-dioxide," *Science* **257**, 945 (1992).

[5] T. A. Hoefling, D. A. Newman, R. M. Enick, and E. J. Beckman, "Effect of structure on the cloud-point curves of silicone-based amphiphilies in supercritical carbon-dioxide," *J. Supercrit. Fluids* **6**, 165 (1993).

[6] Y. L. Hsiao, E. E. Maury, J. M. DeSimone, S. Mawson, and K. P. Johnston, "Dispersion polymerization of methyl-methacrylate stablized with poly(1,1-dihydroperfluorooctyl acrylate) in supercritical carbon-dioxide," *Macromolecules* **28**, 8159 (1995).

[7] Y. Xiong and E. Kiran, "Miscibility, density and viscosity of poly(dimethylsiloxane) in supercritical carbon-dioxide," *Polymer* **36**, 4817 (1995).

[8] D. ChilluraMartino, R. Triolo, J. B. McClain, J. R. Combes, D. E. Betts, D. A. Canelas, J. M. DeSimone, E. T. Samulski, H. D. Cochran, and J. D. Londono, "Neutron scatter-

ing characterization of homopolymers and graft-copolymer micelles in supercritical carbon dioxide," *J. Mol. Struct.* **383**, 3 (1996).

[9] A. Dardin, J. B. Cain, J. M. DeSimone, and C. S. Johnson, "High-pressure NMR of polymers dissolved in supercritical carbon dioxide," *Macromolecules* **30**, 3593 (1997).

[10] J. B. McClain, D. E. Betts, D. A. Canelas, E. T. S. J. M. DeSimone, J. D. Londono, H. D. Cochran, G. D. Wignall, D. ChilluraMartino, and R. Triolo, "Design of nonionic surfactants for supercritical carbon dioxide," *Science* **274**, 2049 (1996).

[11] F. Triolo, A. Triolo, R. Triolo, J. D. Londono, G. D. Wignall, J. B. McClain, D. E. Betts, S. Wells, E. T. Samulski, and J. M. DeSimone, "Critical micelle density for the self-assembly of block copolymer surfactants in supercritical carbon dioxide," *Langmuir* **16**, 416 (2000).

[12] R. Triolo, A. Triolo, F. Triolo, D. C. Steytler, C. A. Lewis, R. K. Heenan, G. D. Wignall, and J. M. DeSimone, "Structure of diblock copolymers in supercritical carbon dioxide and critical micellization pressure," *Phys. Rev. E* **61**, 4640 (2000).

[13] A. Triolo, F. Triolo, F. L. Celso, D. E. Betts, J. B. McClain, J. M. DeSimone, G. D. Wignall, and R. Triolo, "Critical micellization density: A small-angle-scattering structural study of the monomer-aggregate transition of block copolymers in supercritical CO_2," *Phys. Rev. E* **62**, 5839 (2000).

[14] E. Buhler, A. V. Dobrynin, J. M. DeSimone, and M. Rubinstein, "Light-scattering study of diblock copolymers in supercritical carbon dioxide: CO_2 density-induced micellization transition," *Macromolecules* **31**, 7347 (1998).

[15] D. G. Gromov, J. J. de Pablo, G. Luna-Barcenas, I. C. Sanchez, and K. P. Johnston, "Simulation of phase equilibria for polymer-supercritical solvent mixtures," *J. Chem. Phys.* **108**, 4647 (1998).

[16] C. M. Colina, C. K. Hall, and K. E. Gubbins, "Phase behavior of PVAC-PTAN block copolymer in supercritical carbon dioxide using SAFT," *Fluid Phase Equilib.* **194**, 553 (2002).

[17] S. Salaniwal, S. T. Cui, H. D. Cochran, and P. T. Cummings, "Molecular simulation of a dichain surfactant water carbon dioxide system. 1. Structural properties of aggregates," *Langmuir* **17**, 1773 (2001).

[18] S. Salaniwal, S. T. Cui, H. D. Cochran, and P. T. Cummings, "Molecular simulation of a dichain surfactant water carbon dioxide system. 2. Self-assembly and aggregation dynamics," *Langmuir* **17**, 1784 (2001).

[19] M. Lisal, C. K. Hall, K. E. Gubbins, and A. Z. Panagiotopoulos, "Self-assembly of surfactants in a supercritical solvent from lattice Monte Carlo simulations," *J. Chem. Phys.* **116**, 1171 (2002).

[20] L. F. Scanu, K. E. Gubbins, and C. K. Hall, "Lattice Monte Carlo simulations of phase separation and micellization in supercritical CO_2/surfactant systems: Effect of CO_2 density," *Langmuir* **20**, 514 (2004).

[21] M. Lisal, C. K. Hall, K. E. Gubbins, and A. Z. Panagiotopoulos, "Micellar behavior in supercritical solvent-surfactant systems from lattice Monte Carlo simulations," *Fluid Phase Equilib.* **194**, 233 (2002).

[22] R. G. Larson, L. E. Scriven, and H. T. Davis, "Monte-Carlo simulation of model amphiphilic oil-water systems," *J. Chem. Phys.* **83**, 2411 (1985).

[23] S. Salaniwal, S. T. Cui, H. D. Cochran, and P. T. Cummings, "Molecular dynamics simulation of reverse micelles in supercritical carbon dioxide," *Ind. Eng. Chem. Res.* **39**, 4543 (2000).

[24] S. Senapati, J. S. Keiper, J. M. DeSimone, G. D. Wignall, Y. B. Melnichenko, H. Frielinghaus, and M. L. Berkowitz, "Structure of phosphate fluorosurfactant based reverse micelles in supercritical carbon dioxide," *Langmuir* **18**, 7371 (2002).

[25] R. G. Larson, "Simulations of self-assembly," *Curr. Opin. Colloid. In.* **2**, 361 (1997).

[26] A. Bhattacharya, S. D. Mahanti, and A. Chakrabarti, "Self-assembly of neutral and ionic surfactants: An off-lattice Monte Carlo approach," *J. Chem. Phys.* **108**, 10281 (1998).

[27] A. Bhattacharya and S. D. Mahanti, "Critical micelle concentration in three-dimensional lattice models of amphiphiles," *J. Phys.: Condens. Matter* **13**, 861 (2001).

[28] R. Rajagopalan, L. A. Rodriguez-Guadarrama, and S. K. Talsania, *Handbook of microemulsion science and technology* (Marcel Dekker, New York, 1999), p. 105.

[29] S. K. Talsania, L. A. Rodriguez-Guadarrama, K. K. Mohanty, and R. Rajagopalan, "Phase behavior and solubilization in surfactant-solute-solvent systems by Monte Carlo simulations," *Langmuir* **14**, 2648 (1998).

[30] M. A. Floriano, E. Caponetti, and A. Z. Panagiotopoulos, "Micellization in model surfactant systems," *Langmuir* **15**, 3143 (1999).

[31] A. Z. Panagiotopoulos, M. A. Floriano, and S. K. Kumar, “Micellization and phase separation of diblock and triblock model surfactants,” *Langmuir* **18**, 2940 (2002).

[32] J. Israelachvili, *Intermolecular and surface forces, 2nd ed.* (Wiley, New York, 1989).

[33] D. C. Rapaport, “Molecular dynamics study of a polymer chain,” *J. Chem. Phys.* **71**, 3299 (1979).

[34] A. Bellemans, J. Orban, and D. V. Belle, “Molecular dynamics of rigid and non-rigid necklaces of hard disks,” *Mol. Phys.* **39**, 781 (1980).

[35] H. S. Gulati and C. K. Hall, “Fluids and fluid mixtures containing square-well diatomics: Equations of state and canonical molecular dynamics simulation,” *J. Chem. Phys.* **107**, 3930 (1997).

[36] H. C. Anderson, “Molecular-dynamics simulations at constant pressure and-or temperature,” *J. Chem. Phys.* **72**, 2384 (1980).

[37] Y. Zhou, C. K. Hall, and M. Karplus, “First-order disorder-to-order transition in an isolated homopolymer model,” *Phys. Rev. Lett.* **77**, 2822 (1996).

[38] Y. Zhou, M. Karplus, J. M. Wichert, and C. K. Hall, “Equilibrium thermodynamics of homopolymers and clusters: Molecular dynamics and Monte Carlo simulations of systems with square-well interactions,” *J. Chem. Phys.* **107**, 10691 (1997).

[39] S. W. Smith, B. D. Freeman, and C. K. Hall, “Discontinuous molecular dynamics for polymeric fluids.,” *J. Comput. Phys.* **134**, 16 (1997).

[40] A. J. Schultz, C. K. Hall, and J. Genzer, "Computer simulation of copolymer phase behavior," *J. Chem. Phys.* **117**, 10329 (2002).

[41] M. Murat, G. S. Grest, and K. Kremer, "Statics and dynamics of symmetric diblock copolymers: A molecular dynamics study," *Macromolecules* **32**, 595 (1999).

[42] R. L. McGreevy, in *Computer modelling in inorganic crystallography.*, edited by C. R. A. Catlow (Academic Press, San Diego, 1997).

[43] J. N. Israelachvili, D. J. Mitchell, and B. W. Ninham, "Theory of self-assembly of hydrocarbon amphiphiles into micelles and bilayers," *J. Chem. Soc., Frarday Trans.2* **72**, 1525 (1976).

[44] Z. Shen, M. A. McHugh, J. Xu, J. Belardi, S. Kilic, A. Mesiano, S. Bane, C. Karnikas, E. Beckman, and R. Enick, "CO_2-solubility of oligomers and polymers that contain the carbonyl group," *Polymer* **44**, 1491 (2003).

[45] M. A. McHugh, I. H. Park, J. J. Reisinger, Y. Ren, T. P. Lodge, and M. A. Hillmyer, "Solubility of CF_2-modified polybutadiene and polyisoprene in supercritical carbon dioxide," *Macromolecules* **35**, 4653 (2002).

[46] J. C. Liu, B. X. Han, Z. W. Wang, J. L. Zhang, G. Z. Li, and G. Y. Yang, "Solubility of Ls-36 and Ls-45 surfactants in supercritical CO_2 and loading water in the CO_2/water/surfactant systems," *Langmuir* **18**, 3086 (2002).

[47] J. C. Liu, B. X. Han, G. Z. Li, Z. M. Liu, J. He, and G. Yang, "Solubility of non-inonic

surfacant Tetraethylene Glycol n-laurel ether in supercrtical Ls-36 and Ls-45 surfactants in supercritical CO_2 with n-pentanol," *Fluid Phase Equilib.* **187**, 247 (2001).

A.7 Figures

Page

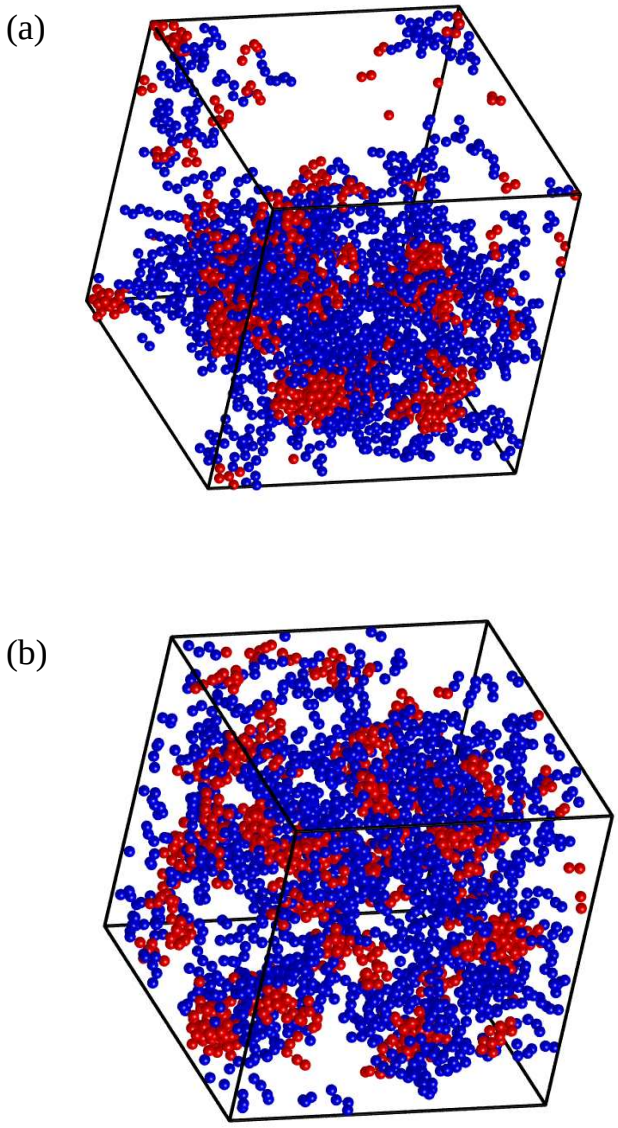

Figure A.1: Snapshot of the H_4T_8/solvent system at $\eta = (a)\ 0.24$ and $(b)\ 0.27$ with $X_{H_4T_8} = 0.0177$ and $T^* = 1.0$ for the parameter set $(\epsilon^*_{HH}, \epsilon^*_{HS}, \epsilon^*_{TT}, \epsilon^*_{TS}) = (-1.0, -0.525, -0.45, -0.4)$. Head beads in red, tail beads in blue, solvent beads not shown.

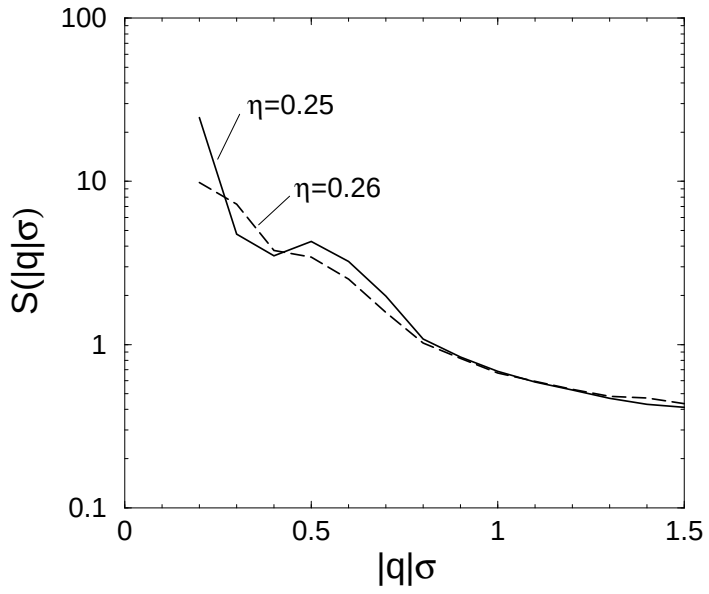

Figure A.2: Contrast structure factor for the H_4T_8/solvent system at $\eta = 0.25$ and 0.26 for the same surfactant concentration, temperature, system size and interaction parameters as in figure A.1.

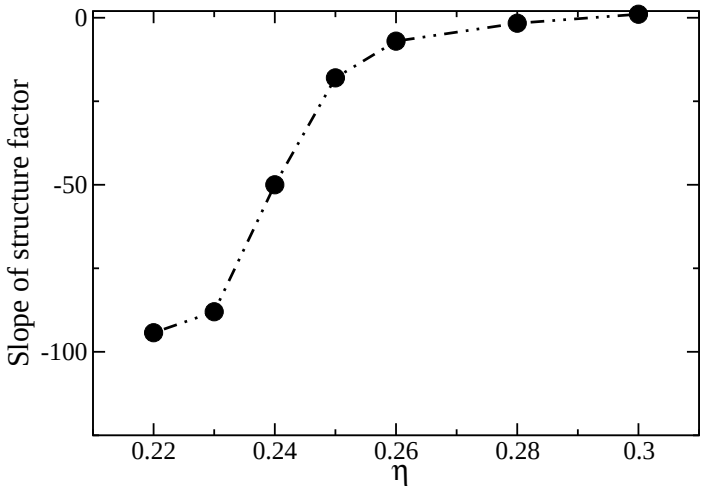

Figure A.3: Slope of structure factor vs. packing fraction for the H_4T_8/solvent system at $\eta = 0.22 - 0.30$ for the same surfactant concentration, temperature, system size and interaction parameters as in figure A.1.

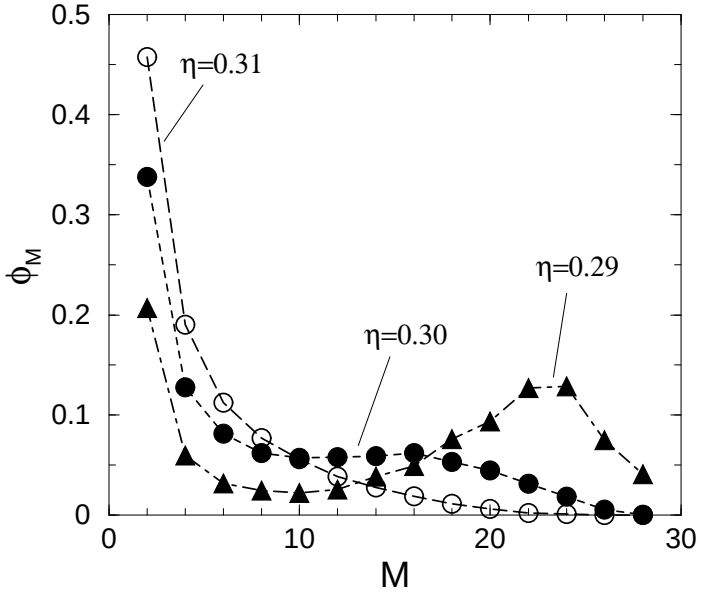

Figure A.4: Aggregate (micelle) size distribution at $\eta = 0.29, 0.30, 0.31$ for H_4T_8 at $X_{H_4T_8} = 0.0119$ and $T^* = 1.0$ for the parameter set ($\epsilon^*_{HH}, \epsilon^*_{HS}, \epsilon^*_{TT}, \epsilon^*_{TS}$) = $(-1.0, -0.525, -0.45, -0.4)$.

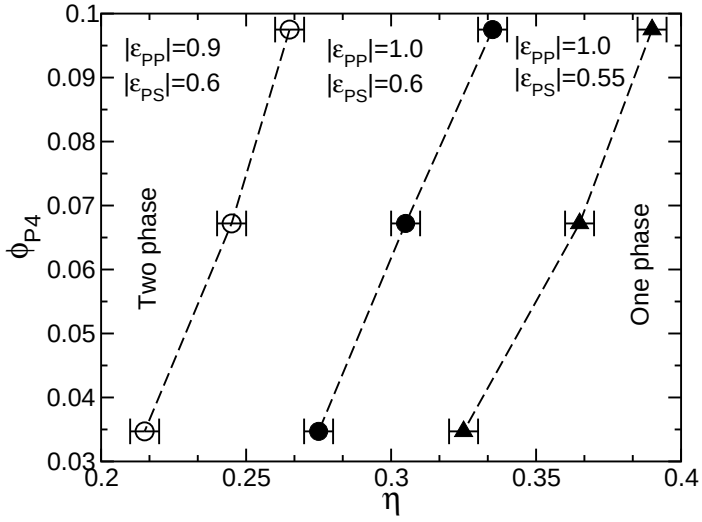

Figure A.5: Two-phase $\rightarrow$ one-phase transition at $T^* = 1.0$ for homopolymer P_4 in the homopolymer volume fraction (ϕ_{P_4}) $-$ packing fraction (η) plane for $(\epsilon^*_{PP}, \epsilon^*_{PS}) = (-0.9, -0.6), (-1.0, -0.6)$ and $(-1.0, -0.55)$.

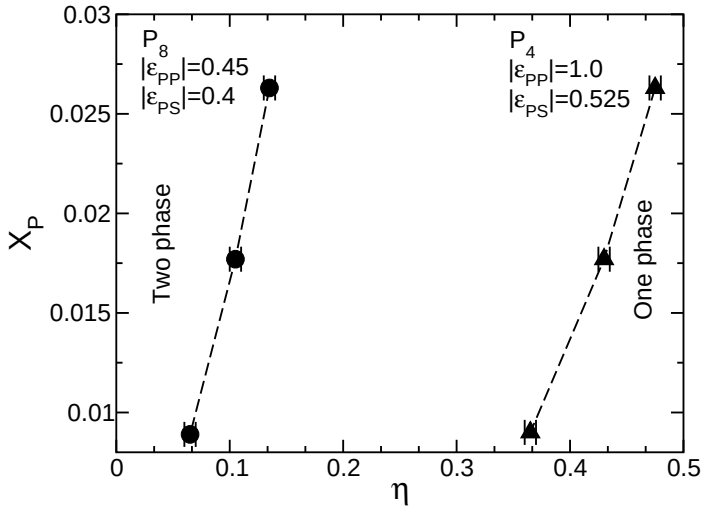

Figure A.6: Two phase $\rightarrow$ one phase transition at $T^* = 1.0$ in the homopolymer mole fraction (X_{P_4}) $-$ packing fraction (η) plane for homopolymer P_4 with $(\epsilon^*_{\mathrm{PP}}, \epsilon^*_{\mathrm{PS}}) = (-1.0, -0.525)$ and homopolymer P_8 with $(\epsilon^*_{\mathrm{PP}}, \epsilon^*_{\mathrm{PS}}) = (-0.45, -0.4)$.

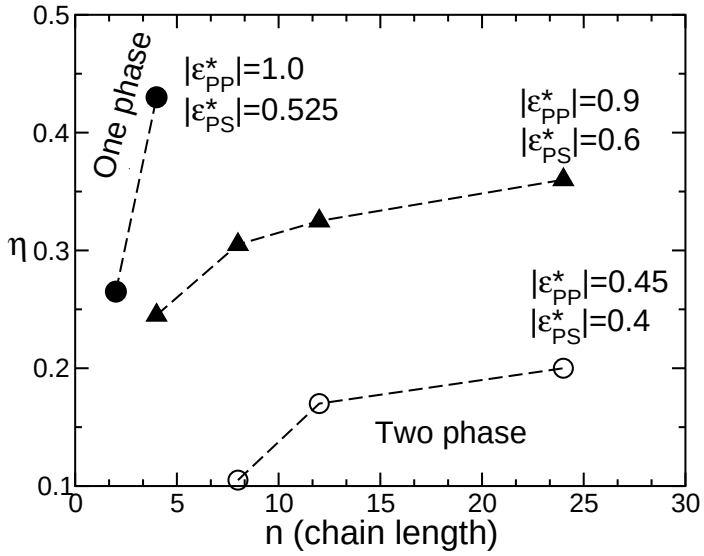

Figure A.7: Two-phase $\rightarrow$ one-phase transition in the packing fraction (η)$-$chain length (n) plane for homopolymer P$_n$ with $(\epsilon^*_{\rm PP}, \epsilon^*_{\rm PS}) = (-1.0, -0.525), (-0.45, -0.4)$ and $(-0.9, -0.6)$ at $\phi_{\rm P} = 0.0672$.

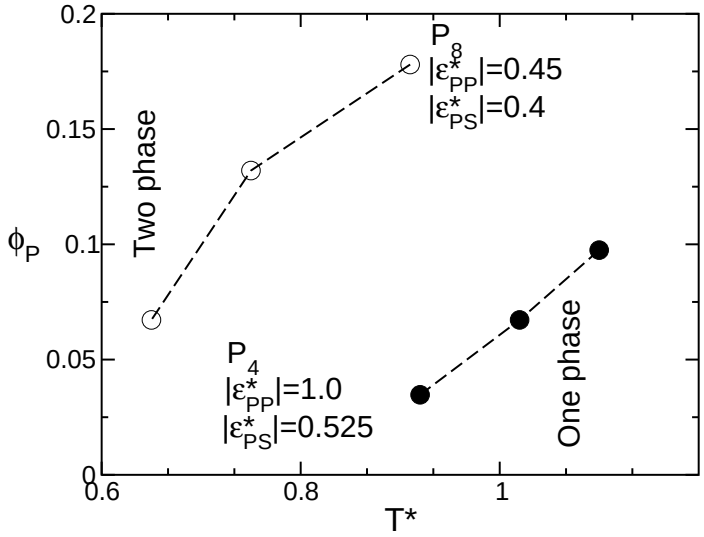

Figure A.8: Two-phase $\rightarrow$ one-phase transition in the polymer volume fraction (ϕ_{P}) $-$ reduced temerature (T^*) plane for homopolymer P_4 with $(\epsilon^*_{\mathrm{PP}}, \epsilon^*_{\mathrm{PS}}) = (-1.0, -0.525)$ at $\eta = 0.4$ and homopolymer P_8 with $(\epsilon^*_{\mathrm{PP}}, \epsilon^*_{\mathrm{PS}}) = (-0.45, -0.4)$ at $\eta = 0.2$.

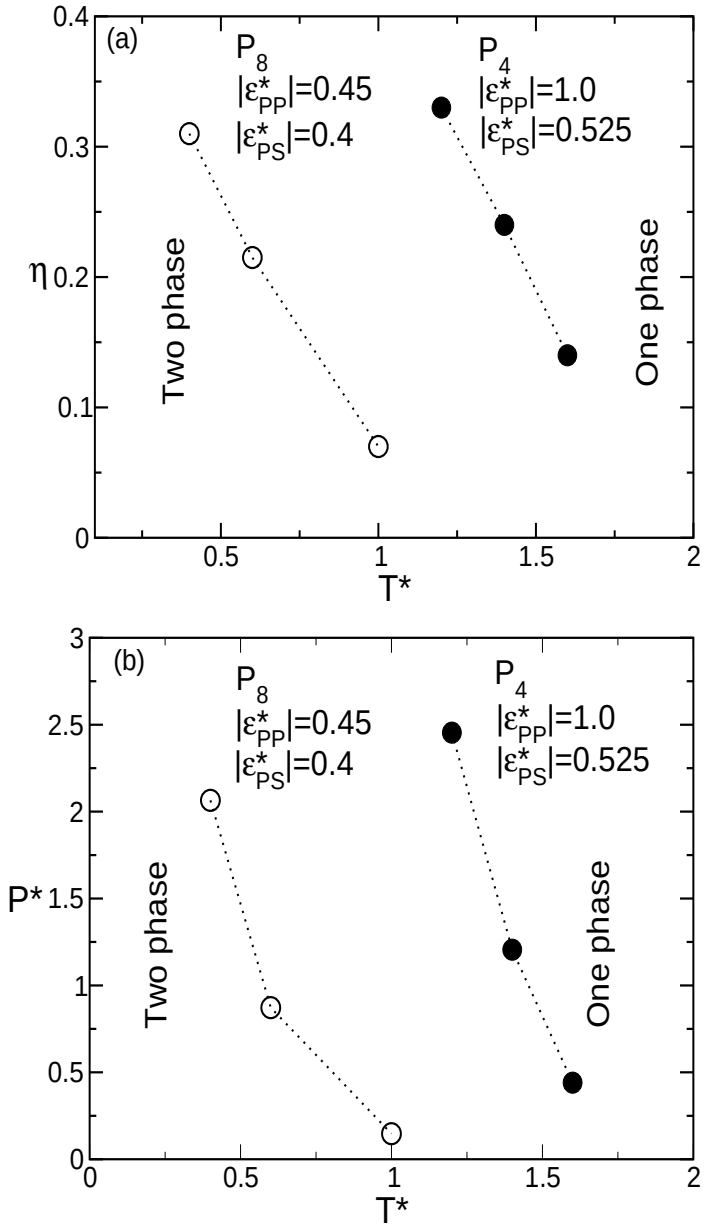

Figure A.9: Two-phase $\rightarrow$ one-phase transition in the (a) packing fraction (η) $-$ reduced temperature (T^*) plane and (b) reduced pressure (P*) $-$ reduced temperature (T^*) plane at $\phi_{\rm P} = 0.067$ for homopolymer P_4 with $(\epsilon^*_{\rm PP}, \epsilon^*_{\rm PS}) = (-1.0, -0.525)$ and for P_8 with $(\epsilon^*_{\rm PP}, \epsilon^*_{\rm PS}) = (-0.45, -0.4)$.

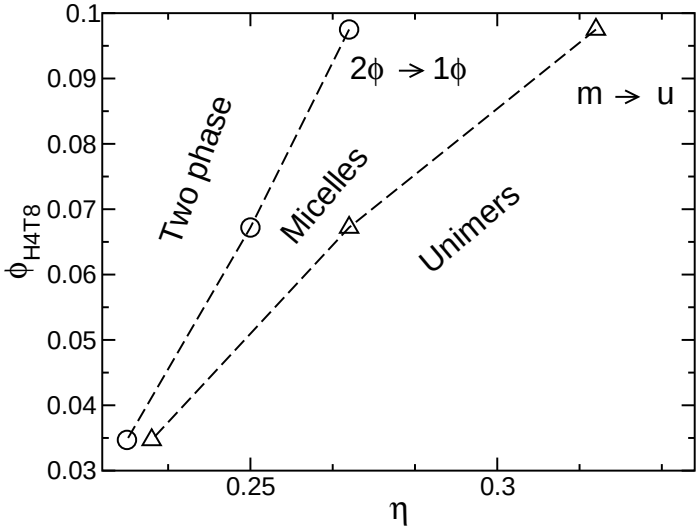

Figure A.10: Phase diagram in the surfactant volume fraction ($\phi_{\mathrm{H_4T_8}}$) $-$ packing fraction (η) plane for surfactant $\mathrm{H_4T_8}$ at $T^* = 1.0$ for the parameter set ($\epsilon^*_{\mathrm{HH}}, \epsilon^*_{\mathrm{HS}}, \epsilon^*_{\mathrm{TT}}, \epsilon^*_{\mathrm{TS}}$) = ($-1.0, -0.525, -0.45, -0.4$).

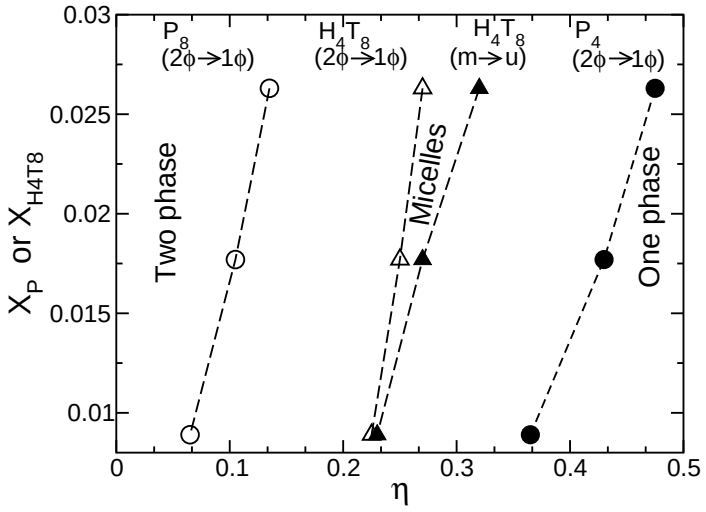

Figure A.11: Phase diagram in the polymer mole fraction ($X_{\rm P}$ or $X_{\rm H_4T_8}$) $-$ packing fraction (η) plane at $T^* = 1.0$ for homopolymer P_4 with $(\epsilon^*_{\rm PP}, \epsilon^*_{\rm PS}) = (-1.0, -0.525)$, homopolymer P_8 with $(\epsilon^*_{\rm PP}, \epsilon^*_{\rm PS}) = (-0.45, -0.4)$ and surfactant H_4T_8 with ($\epsilon^*_{\rm HH}, \epsilon^*_{\rm HS}, \epsilon^*_{\rm TT}, \epsilon^*_{\rm TS}$) = $(-1.0, -0.525, -0.45, -0.4)$.

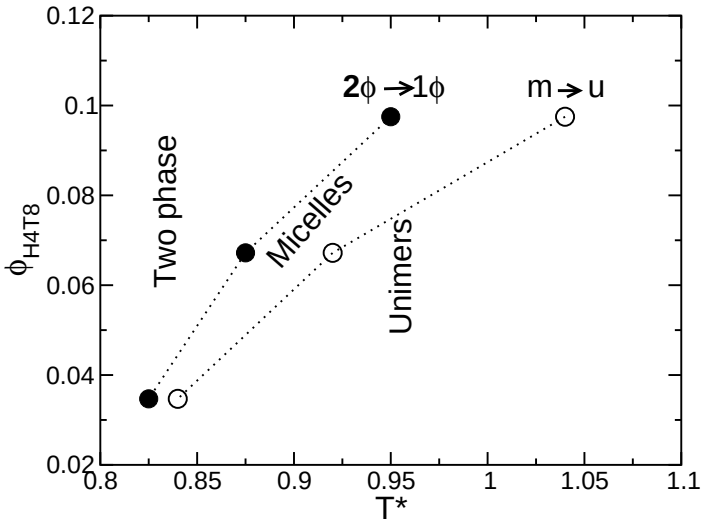

Figure A.12: Phase diagram for surfactant H_4T_8 in the surfactant mole fraction ($\phi_{H_4T_8}$) − reduced temperature (T^*) plane at $\eta = 0.30$ for $(\epsilon^*_{HH}, \epsilon^*_{HS}, \epsilon^*_{TT}, \epsilon^*_{TS})$ = $(-1.0, -0.525, -0.45, -0.4)$.

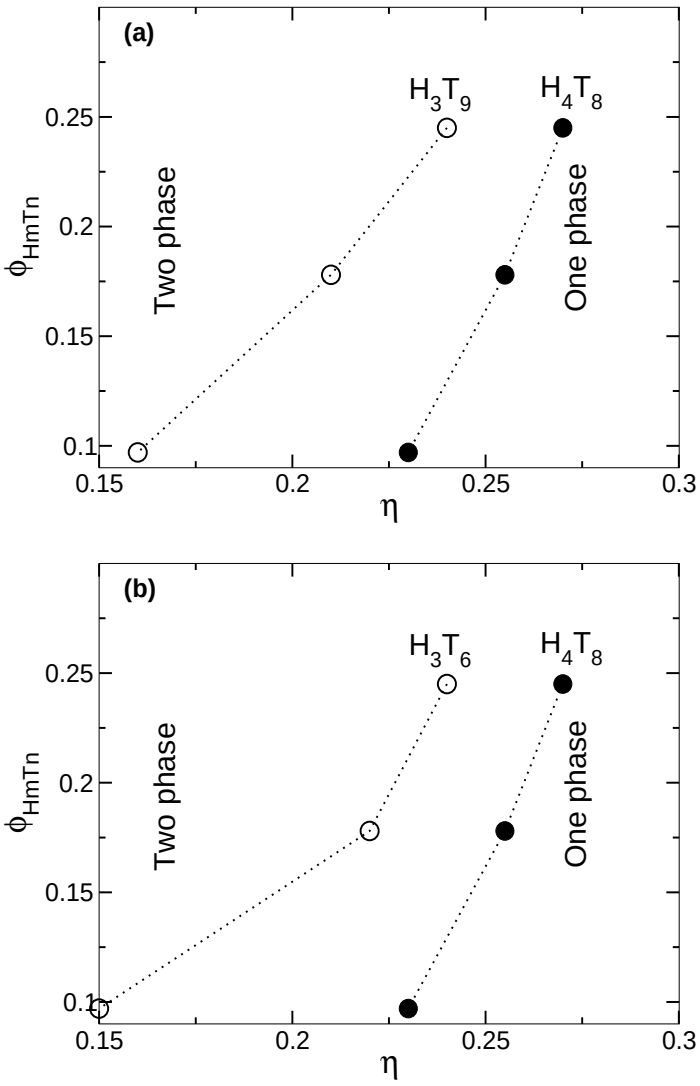

Figure A.13: Micelle → unimer transition at $T^* = 1.0$ in the surfactant volume fraction ($\phi_{\mathrm{H_nT_m}}$) − packing fraction (η) plane for surfactants: (a) H_4T_8 and H_3T_9, and (b) H_4T_8 and H_3T_6 at ($\epsilon^*_{\mathrm{HH}}, \epsilon^*_{\mathrm{HS}}, \epsilon^*_{\mathrm{TT}}, \epsilon^*_{\mathrm{TS}}$) = ($-1.0, -0.525, -0.45, -0.4$).